ERS-1
Interferometric Baseline
Algorithm Verification

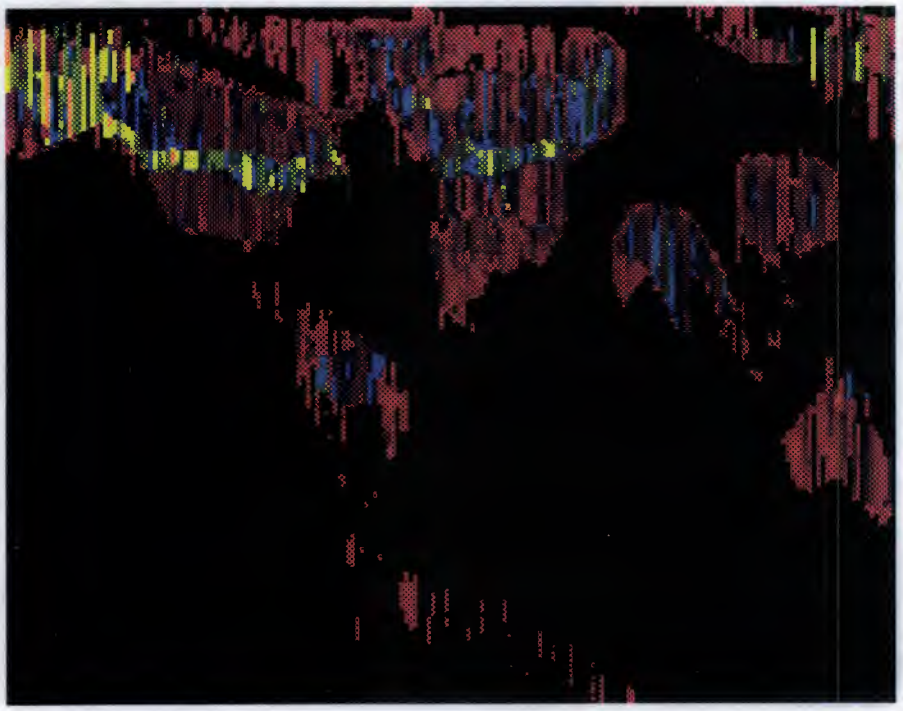

Gaute Aarbakke SOLAAS

ESA Fellow
ESA - ESRIN
Project Engineering Department
ERS Missions Section

ES-TN-DPE-OM-GS02, version 2.0 **August 1994**

Front Page.

ERS-1 plot of repeated acquisition occurrences for the Multidisciplinary phase. This plot is a distorted latitude / longitude map with the axis defined as follows:

The vertical axis is sampled in frames (15 seconds intervals) along the orbit, starting at the top from the north pole (frame 1791), passing by equator (frame 3591) and ending with the south pole (frame 5391).

The horizontal axis is sampled in ERS-1 orbit track sequence with adjacent tracks corresponding to adjacent geographic location (i.e. adjacent tracks are not sequential track numbers).

This projection with tracks as columns gives an indication of the geographical location of INSAR acquisitions which is accurate at equator, but which gives large distortions towards the poles. To correct for these distortions and to translate into actual geographic coverage, one has to compare with plots similar to the DESC screen outputs shown in chapter 5.0, figure 20 to 24.

The advantage of frame-tied baseline measurements comes from the geographically fixed position of the measurements. The baseline data can be directly tied to specific products and their locations. The change from UTC minute to frame based baselines was done to facilitate a flexible identification of suitable repeated acquisitions for interferometric use.

Acknowledgements.

I want to thank friends and colleagues that have helped me in my work as ESA-Fellow at ESRIN.

In particular I want to thank ESA-ESRIN-DPE-OM staff member S. N. Coulson for his help during the development and verification of the INSAR Baseline Listing.

In addition I want to thank ESA-ESOC-FCSD-OAD-STB staff member M. Rosengren and FRINGE members: Zebker of JPL (USA) and Wärner / Small of University of Zürich (Switzerland), Rocca / Prati / Parizzi of POLIMI (Italy), Ulander / Hagberg at CTH (Sweden) and Massonnet of CNES (France). All of these persons have given me valuable help in the validation of the INSAR Baseline Listing.

Contents:

Acronyms:

ESA	European Space Agency
ESRIN	European Space Research INstitute
SAR	Synthetic Aperture Radar
ERS	Earth Remote sensing Satellite
INSAR	INterferometric SAR
DTM	Digital Terrain Models
CUS	Customers User Service
TBD	To Be Defined
OCM	Orbit Control Manoeuvre
UTC	Universal Time Coordinates
DESC	Display ERS-1 SAR Coverage
ERSORB	ERS Orbit Propagator
ECC	Earth Centered Coordinate system
SCC	Satellite Centered Coordinate system
ESOC	European Space Operations Centre
RSL	Remote Sensing Laboratories, University of Zürich
JPL	Jet Propulsion Laboratories
POLIMI	POLItecnico di MIlano
CNES	Centre National de la Recherche Scientifique
CTH	Chalmers University of Technology

1.0 Introduction.

1.1 Scope.

The scope of this report is to determine the accuracy of the Interferometric Baseline Algorithm used in the generation of the ERS-1 INSAR Baseline Listing.

This is obtained by the use of several verification methods.

This second version of the report was judged necessary because of the change from UTC minute to frame based baselines. This leads in particular to a more accurate estimation of the internal consistency of the algorithm.

Besides the verification itself we present an **updated description of the algorithm** and a **frame based analysis** of the interferometric potential of the ERS-1 mission.

1.2 Purpose of ERS-1 INSAR Baseline Listing.

Recently it has been demonstrated that ERS SAR interferometry (INSAR) is a potential major application area of ERS SAR data (see i.e. ref. 1). Therefore it is important to assess the number and the location of ERS SAR acquisitions which are suitable for interferometric processing.

To address this subject the restituted orbit files created for each day of the ERS-1 phases have been used to create an INSAR Baseline Listing for ERS-1. This listing currently includes the whole Commissioning phase, 1st Ice phase, the Multidisciplinary phase, the 2nd Ice phase the repeats between the 1st and the 2nd Ice phase and finally the repeats between any of the earlier phases and the four first months of the Geodetic phase.

The purpose of the generated INSAR Baseline Listing is:

- To supply a guide to the users to identify suitable interferometric pairs for INSAR applications.
- The investigation of global interferometric coverage.
- The investigation and evaluation of ERS orbit maintenance strategy for interferometry applications.

1.3 INSAR Orbit Constraints.

In spaceborne repeat-pass INSAR (as the case for ERS-1), the interferometer baseline B, is defined as the cross-track orbit separation; i.e. the distance perpendicular to the satellite flight direction between two repeat orbits (see fig. 1).

For INSAR the critical parameter is the component of the baseline perpendicular to the SAR slant range direction (see ref. 1). We denote this parameter B_{perp} (see fig.2).

For INSAR to be possible, the absolute value of B_{perp} has to satisfy a condition determined by the radar characteristics and the imaging geometry. For ERS-1, the theoretical upper limit is 1100m, however for practical applications of INSAR with ERS-1, experience shows that $|B_{perp}|$ should be less than 600m for flat terrain.

As reported in the second ERS-1 symposium (Hamburg 1993), there are emerging three major domains of INSAR applications use. Each has its own requirements for optimal values of $|B_{perp}|$. Approximate values for these baseline domains are given in table 1 below.

TABLE 1. INSAR application baseline domains.

Application		$\|B_{perp}\|$
1.	Digital Terrain Models:	150m to 300m
2.	Surface Change Detection:	30m to 70m
3.	Surface Feature Movement:	0m to 5m

Note, however, that the overall Baseline criterion ($|B_{perp}|<600$m) is not a sufficient condition for the INSAR technique to be possible. Other factors, in particular the surface conditions at the time of the two SAR acquisitions, affect the complex image scene phase coherence and thus the quality of the interferometric fringes. This is especially true for vegetation, snow covered regions or surfaces subject to moisture content changes. For INSAR applications 1. and 3. listed above in regions subject to surface change, the time interval between acquisitions should be as little as possible (i.e. the basic repeat cycle period of the mission phase).

Consequently, ESA takes no commitment that users ordering products based upon the ERS-1 INSAR Baseline Listing will obtain interferometric fringes.

1.4 Some Explanations and Definitions.

ERS-1 Mission:

The ERS-1 mission is split up into several operational phases. They are named A, B, C, D and E and occur in the sequence as described in table 2.

TABLE 2. ERS-1 operational phases.

Phase	Phase Name	Date range*		Orbit range*		Repeat cycle**	
A	Commissioning	910726	911210	140	2103	3 days	43 orbits
B	1st Ice	911228	920330	2354	3695	3 days	43 orbits
C	Multidisciplinary	920414	931220	3901	12707	35 days	501 orbits
D	2nd Ice	931224	940410	12758	14300	3 days	43 orbits
E	Geodetic	940410	TBD	14302	TBD	168 days	2411 orbits
F	Geodetic	TBD	TBD	TBD	TBD	168 days	2411 orbits**

* The date and orbit ranges are here defined by the first and last SAR acquisition marked as available in the CUS catalogue.

** The Geodetic phase is split into two cycles due to a 8 km shift of the tracks at equator between cycle 1 and cycle 2 (This is done to get a tighter geodetic grid of measurements from the mission). The cycle relevant for interferometric purposes then becomes twice the basic repeat cycle.

Orbit:

The satellite trajectory around the earth beginning over the equator heading northward (ascending node). The satellite is at the shadow side of the earth when this happens.

The night side of the orbit (south pole to north pole) is therefore called by the name 'ascending pass'.

Similarly the day side of the orbit is called 'descending pass'.

Because of the limited amount of energy that can be stored in the on-board batteries, the amount of SAR scenes taken during ascending pass is nominally limited to 4 minutes. In the descending pass, 6 minutes of SAR operation are possible.

Repeat Cycle:

The repeat cycle for a mission phase is the time between one pass over a fixed location on earth and the subsequent pass over the same location. The repeat cycle is identified by the number of orbits between the two repeated passes. More practically, but less accurate it is identified by the number of days between repeats.

See table 2 for the repeat cycles of ERS-1 operational phases.

For the 3 day repeat cycles the SAR coverage leaves big gaps between geographically neighbouring tracks of SAR products. The gaps are biggest at equator and narrows off to zero at the poles.

For the 35 day repeat cycle the standard SAR product give complete global coverage since the products cover 100 km and the distance between neighbouring tracks at equator is 80 km.

In the 168 day repeat cycle a very narrow grid of orbits exist with only 16 kilometres between each neighbouring ground tracks at equator. The 8 km shift between cycle 1 and cycle 2 halves this value and increases the real repeat cycle to 2*168 days.

Track:

The 43, 501 or 2411 orbits in a repeat cycle are all having different trajectories in space. The track number of an orbit is dependant of where the orbit is placed in the repeat cycle. Two following orbits within a repeat cycle have subsequent track numbers. This means that for two neighbouring ground tracks the track numbers are not subsequent numbers, but a product on the repeat pattern of the orbit cycle.

OCM:

Orbit Control Manoeuvre. To maintain the specified accuracy in the orbit repeat pattern, the satellite has to correct its position at regular intervals.

Two different phenomena displaces the orbit in space: Air drag and gravitational forces.

Air drag effects:

The air drag leads to a loss of speed and altitude. With the shorter orbit caused by the altitude loss the satellite will be in advance of its nominal track, which leads to a pass to the east of the nominal track. To correct this 'easting' a 'in plane' OCM has to be performed to boost the satellite altitude (see ref. 2).

It is the sunspot activity that is the decisive factor for the atmosphere conditions which affect the trajectory of ERS-1. The sunspot activity is following a 13 year cycle and is currently decreasing. In the beginning of the ERS-1 life cycle the 'in plane' OCM's had to be performed at 2 to 4 week intervals while it is now sufficient to perform this kind of corrections at 6 to 8 week intervals.

Gravitational effects:

The gravitational influence of the sun upon the satellite depends on the angle between the sun direction and the orbital plane. The angle varies from a minimum of 16.7° in the beginning of June to a maximum of 27.3° in the beginning of February. The gravitational force is therefore seasonal, with its maximum during the first winter months. The corresponding force results in an inclination change of the orbit over time, known as inclination drift. The inclination of an orbit is the angle between the orbital plane and equator, for ERS-1 the inclination is about 98°.

The inclination drift results in an across track drift at high to middle latitudes. To maintain the ERS-1 ground track within the specified limits, an 'out of plane' OCM has to be performed about twice a year to correct the orbit inclination (see ref. 1).

The moon is also resulting in a perturbation of the ERS-1 orbit inclination. However the moon cycle is monthly and does not give any bias after a complete cycle. The effect on the OCM planning is therefore dependent on the phasing of the moon cycle in relation to the sun cycle and varies from year to year.

2.0 The INSAR Baseline Algorithm.

The INSAR Baseline Algorithm is based upon use of restituted orbits generated within a period of 48 hours after each orbit at ESOC.

2.1 Algorithm Overview.

The algorithm consists of the following steps:

1. The algorithm looks backward in time for orbit and acquisition repeats.
2. Each orbit in a mission phase is used as a reference orbit to identify previous repeats within the same phase or cross mission phases. Repeat orbit is defined by the physical nearness of two orbits with the additional criterion of being nearly parallel, i.e. not orbits with high crossing angles.
3. The reference orbits and their associated repeats are split up into monthly files for each mission phase.
4. For all repeated orbits we identify those acquisitions which overlap with the reference orbit acquisitions. This is done using the acquisition files available in the ESA DESC software.
5. The restituted orbit files are used as input to the algorithm. In these files the orbit arcs are given by the satellite position and velocity vectors at integer UTC minutes.
6. For each orbit an 'INSARORB' file is generated. This file contains of a header with information needed by the algorithm followed by propagated state vectors for each frame in the orbit (see fig. 1).
   The computations are done in a Satellite Centred Coordinate system (SCC):
   -Along track axis (Z) defined by the velocity vector of the reference orbit.
   -Across track axis (X) defined by the normal vector of the plane formed by the Z axis and the radial from the earth centre to the satellite position (positive direction to the instrument side).
   -Radial axis (Y) defined as the normal vector of the two proceeding axis (positive side away from the earth).
7. For each frame of the reference orbit for which there exists an overlapping acquisition with the repeat orbit, the interferometric baseline between the two orbits is computed by propagation of the repeat orbit frame to the shortest point of approach to the reference frame. The computations are done in SCC as described above.
8. The orbit propagations are done by using the ESA orbit propagator, ERSORB.
9. A Satellite coordinate frame rotation of the reference coordinate system (of point 6 above) through the nominal mid-swath depression angle (69.645 °) about the satellite velocity vector (Z-axis) is performed to estimate the components of the baseline perpendicular to slant range (B_{perp}) and parallel to slant range (B_{para}) (see fig. 2). At the applied nominal depression angle the incidence angle for flat terrain equal to 23°.

10. The resulting baseline components are written to file together with the frame number.

2.2 Algorithm Details.

The details concerning the use of repeat orbit propagation are important for the accuracy of the resulting baseline estimates. Therefore these details (relating to point 6 and 7 given in the overview) are presented below.

2.2.1 Orbit Propagation.

The restituted orbit files give the position and the velocity vectors of the satellite in Earth a Centred Coordinate (ECC) system at each UTC minute.

For the baseline computation and the orbit propagation time estimation we use the velocity vectors to establish a satellite centred reference system with the following axis orientation:

- One axis pointing in the satellite heading direction (Along Track, Z),
- One axis perpendicular to the plane defined by the first axis and the radial vector from the earth centre to the satellite. The positive pointing direction of this axis is in the AMI look direction (Across Track, X).
- The last axis is perpendicular to the two first and is pointing radially out into space away from the earth (Radial, Y).

The described coordinate system is drawn in dotted lines in figure 1.

INSARORB:

Two orbit propagations (forward and backward in time) are performed at ascending node (beginning of the orbit) to establish the orbit start time.

A frame is defined as a fixed time offset from ascending node dependent on the Mean Nodal Period (MNP) of the mission phase.

Each frame is then found by performing two orbit propagations from the nearest UTC minutes to the frame time, one forward in time and one backward in time.

Baseline Generation:

Three orbit propagation exercises are performed for each repeated frame at which the baseline is to be calculated. Two propagations using zero along track component as the stop criterion and a third propagation using the shortest point of approach as the stop criterion. The first two propagate in opposite directions along track, one forward in time and one backwards in time. The shortest propagation of the two (normally under 5.5 km along track = 1 node) is used as input to the third propagation method.

1. Forward propagation.

The repeat orbit is propagated iteratively forward in time from the previous nearest repeat frame until the along track component of the propagated position intersects the radial/across-track (Y/X) plane of the reference frame centred on the reference orbit frame timing mark. The propagation is stopped when the along track component is less than one meter.

In each iteration an time error estimate is calculated using the along track length and velocity (time = length / velocity). This time error estimate is used to correct the input propagation time for the next iteration of the orbit propagation. This method of propagating the repeat orbit leads to the required along track accuracy within 2 to 3 iterations.

2. **Backward Propagation.**

As for forward in time, but the post nearest repeat frame is used as the starting point of the orbit propagation backwards in time.

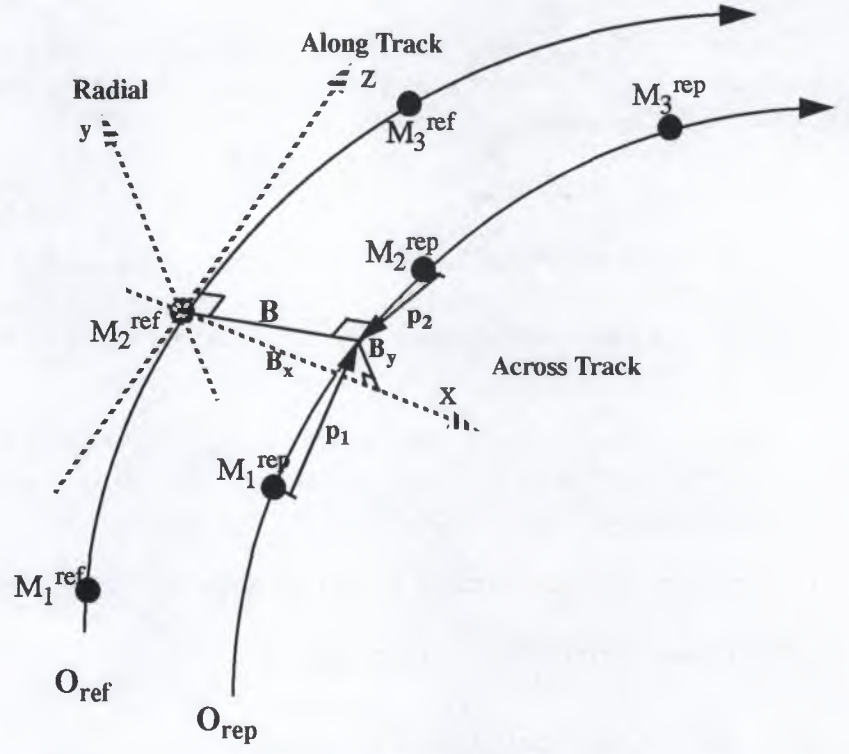

FIGURE 1. Orbit propagation of a UTC minute timing mark at the repeated orbit to align with the Across-track/Radial plane defined at a UTC minute timing mark at the reference orbit.

- O_{ref} Reference orbit.
- O_{rep} Repeated orbit.
- M_i^{ref} ith UTC minute mark for the reference orbit.
- M_i^{rep} ith UTC minute mark for the repeated orbit (different along track position to the reference orbit).

- B Baseline, shortest distance between the two orbits (i.e. perpendicular to both orbits) at the reference orbit UTC minute node.
- B_x Across Track component of the Baseline.
- B_y Across Track component of the Baseline.
- Across Track - X, Radial -Y and Along Track - Z: The reference system established for the two iterative orbit propagations. The Z component of the repeated orbit is propagated to be less than 1 meter.
- p_1 Forward in time propagation of the repeated orbit.
- p_2 Backward in time propagation of the repeated orbit.

3. Propagation to Shortest Point of Approach.

The propagation time is varied by small amounts around the point found by the shortest propagation (measured in prop. time) of the two prior orbit propagations (see 1 and 2 above). The absolute baseline length from the reference orbit UTC node is calculated and the propagation time resulting in minimum orbit separation length is found (closest point of approach).

The result of the shortest distance baseline results in a configuration corresponding to a cross-track interferometer. The cross-track perpendicular separation B, forms the INSAR baseline.

Propagation error checking:

If the absolute difference between the results of propagation 1 and 2 is greater than 2m the execution of the program is halted. This have only occurred at about 20 day changes (and therefore restituted orbit file change) where inconsistencies of up to 7m have been observed.

Similarly the execution is halted if the difference in absolute baseline length is more than 2m between propagation method 3 and the shortest propagation (in propagation time) of the two preceding propagations.

The result of propagation method 3 is saved in the INSAR Baseline Listing.

The orbit propagation is illustrated in figure 1.

2.2.2 Satellite Coordinate Frame Rotation.

After the nearest point of approach has been found the radial and across track components of the baseline are projected through a rotation about the along track axis, Z, of 69.645° (the ERS-1 SAR depression angle in normal operation, **not** roll tilt mode).

We then have a reference system with one axis parallel and one perpendicular to the mid-swath look direction also called slant range, see figure 2.

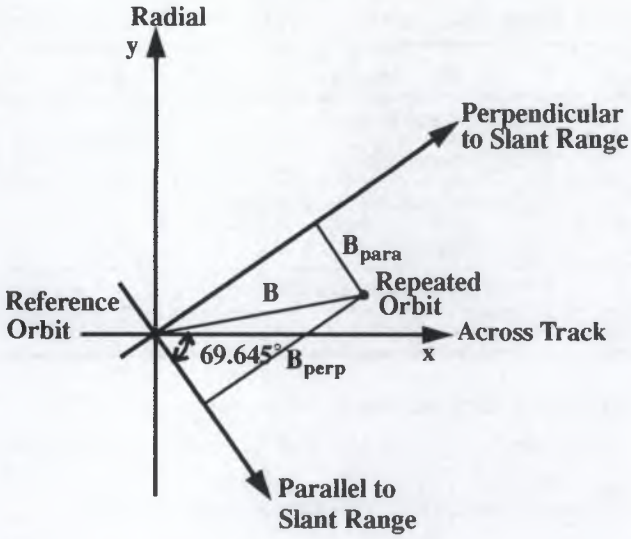

FIGURE 2. The rotation of the reference system performed after the orbit propagation to find the interferometric baseline component |Bperp|. The flight direction is into the paper on both orbits.

The component of the baseline perpendicular to slant range in this reference system, B_{perp}, is decisive for the applicability of interferometry on the image pairs acquired at this part of the orbit.

Because of the limited accuracy of the restituted orbit files and the ERSORB orbit propagator and the existence of only one baseline sampling point per frame it is not possible to use the INSAR Baseline Listing for removal of baseline induced fringes in the interferogram. However the sampling interval and accuracy of the baselines is good enough to satisfy the use defined in the primary goals of the INSAR Baseline Listing.

2.3 Theoretical Accuracy of INSAR Baseline Algorithm.

The worst case accuracy of the INSAR Baseline Listing is calculated by:

1. Finding the combined rms error of the two restituted orbits: $\sigma_{orb} = \sqrt{\sigma_{ref}^2 + \sigma_{rep}^2}$.
2. Finding the total rms error of the orbits and the propagation: $\sigma_{tot} = \sqrt{\sigma_{orb}^2 + \sigma_{prop}^2}$ where σ_{tot} is the rms error in either the radial or across track baseline component.
3. Finding the total baseline rms error: $\sigma_B = \sqrt{\sigma_{rad}^2 + \sigma_{acr}^2}$

4. The worst case baseline error is then taken as the 3-sigma bound (similarly for radial and across track baseline components).

TABLE 3. Theoretical rms errors of the INSAR Baselines components [m]

Step no.	Description	σ_B	σ_{rad}	σ_{acr}
	One restituted orbit:		2	5
	Orbit propagation:*		3	1
1	Reference plus repeated orbit: σ_{orb}		2.8	7.1
2	Orbits plus propagation: σ_{tot}		4.1	7.2
3	Radial and across combined: σ_B	8.3		
4	The worst case: 3σ	**24.9**	12.4	21.6

* maximum error of the orbit propagation is 7m radial and 3m across track for propagation over 3 minutes. We assume that the two step propagation does not result in additional errors.

The 3-sigma rms error estimate is then:

$$|\Delta B| = 25 \text{ m (worst case)}$$

Where $|\Delta B|$ is the maximum error for the absolute baseline value.

We shall see later in this report that the observed absolute accuracy is better than this estimate. This may be caused by the random errors from all sources not being statistically independent (e.g. correlated errors between the two restituted orbits).

3.0 Verification of the Algorithm.

Verification has been carried out on five levels:

- Internal Consistency of the Algorithm.
- External Consistency with Precision Orbit Propagator used at ESOC.
- External Consistency by study of inclination orbit drift velocities.
- Checks with specific baseline values derived by users.
- Checking of consistency of the restituted orbits.

3.1 Internal Consistency of the Algorithm.

The internal consistency of the algorithm has been checked by the following procedure:

1. Baselines are computed at each fourth frame in the reference orbit (i.e. independent of acquisition). This gives 100 sampling points for ERS-1.
2. Limit the calculation burden by choosing a specific track number in a particular phase. I.e. track 29 in the commissioning phase.
3. Use all orbits with more than one previous repeat as reference orbit.
4. We now have an over-determined set of baselines where it should be possible to check at any minute node if vector summation of the baselines between three orbits A, B, and C gives consistent results (i.e. AC = AB + BC). This is done by shifting out the different origins to a chosen reference.

We expect to observe discrepancies in the above vector summation ($AC = AB + BC + \Delta_{radial} + \Delta_{across\ track}$) due to errors (combined error of the restituted orbits and the orbit propagation) and along track displacement of the frames (max 1 node = 5.5 km) used in the orbit propagation. The along track baseline change should be observable as a sine curve with eventually a minimum at the minute node where the along track baseline change is smallest. With only 5.5 km maximum displacement between the frames for the frame based algorithm this effect should be negligible.

Since the orbit propagator has no systematic errors (e.g latitude dependant accuracy) the internal accuracy of the algorithm can be estimated to be better than the minima of the sine function.

In figure 3 and 4 we have plotted the different values before and after the shift operation for a specific frame in all orbits on track 249 in the Multidisciplinary phase (i.e. all orbits with subsequent repeats have been used as reference orbits and one of the hundred minute nodes have been plotted for all repeats).

We see that the shifted plot has a much tighter concentration of the points as the reference systems are shifted into the same position.

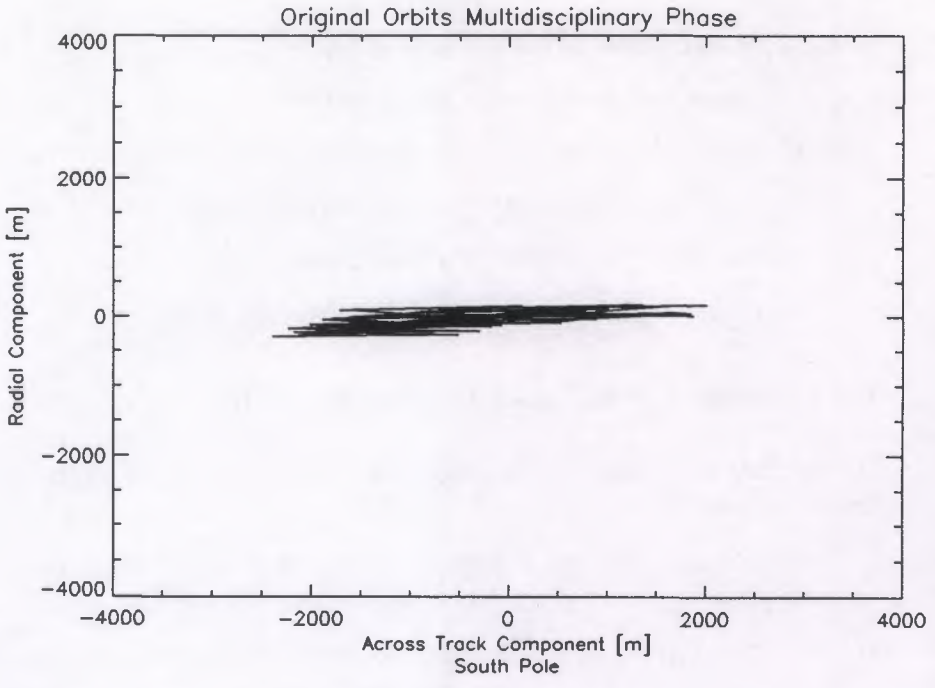

FIGURE 3. Across track plotted against radial baseline component for look-ahead repeats between orbits at track 249 in the Multidisciplinary phase. The different origins makes the baseline spread much larger than the biggest individual baseline.

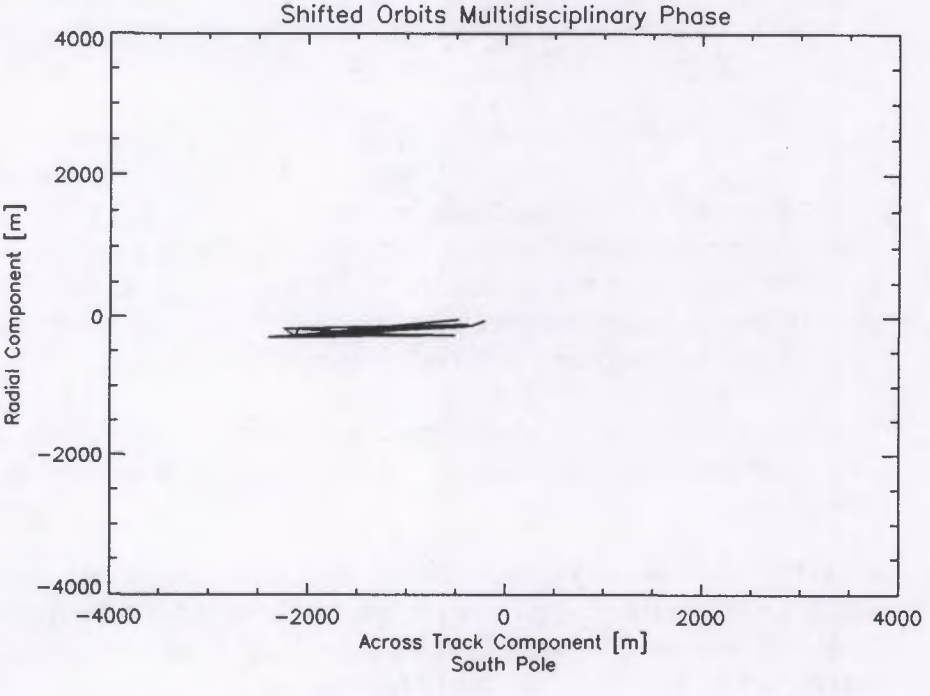

FIGURE 4. Across track plotted against radial baseline component for look-ahead repeats between orbits a track 249 in the Multidisciplinary phase. The different origins have been shifted out and only the real spread between the passes remains. Notice that the spread is much narrower than in the preceding figure.

Figure 6, 7 and 8 represents the absolute maximum shifted differences at frames along the orbit for each of the three first operational phases of ERS-1. No systematic variation of the errors can be discerned along the orbit.

Figure 5 is the equivalent of figure 6 (commissioning phase), but the applied algorithm is based on UTC minutes. The sine error variation along the orbit of the across track baseline can clearly be observed. That the tendency is only discernable in the radial component is expected since the along track radial change between orbits is very small.

The frame based algorithm does not have sufficient along track variation of the measure points to show similar behaviour (only up to 5.5 km). The internal error estimate of the INSAR Baseline Algorithm for the three first mission phases can be found in table 4 below.

TABLE 4. Absolute error estimate of the INSAR Baseline Algorithm based on internal consistency.

Mission Phase	Radial [m]*	Across [m]*	B_{para} [m]*	B_{perp} [m]*
Commissioning	5 (5)	4 (14)	4 (5)	5 (14)
1st Ice	4 (4)	4 (6)	4 (4)	4 (6)
Multidisciplinary	4 (4)	4 (11)	4 (4)	4 (11)

* Numbers in parenthesis give the results of the UTC minute based algorithm. These are not valid estimates of the accuracy.

Conclusion:

The internal consistency test of the frame based algorithm gives an upper bound of 5m absolute error for the INSAR Baseline Algorithm accuracy.

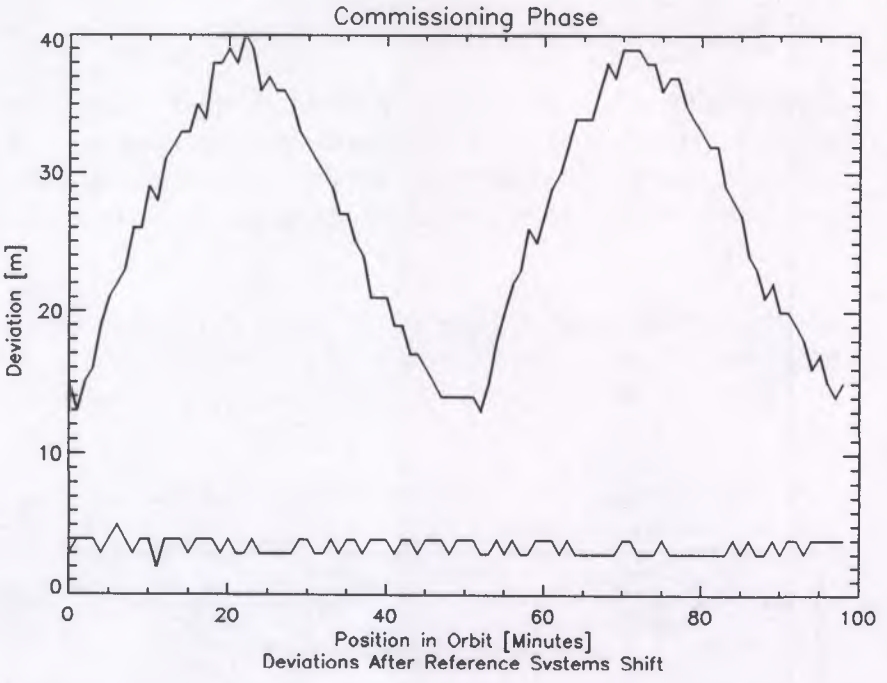

FIGURE 5. The maximum differences between the shifted values of the UTC minute based algorithm throughout the orbit for repeat cycle on track 29 in the Commissioning phase. Across track (sine curve) and radial (flat curve) components of the baseline are plotted.

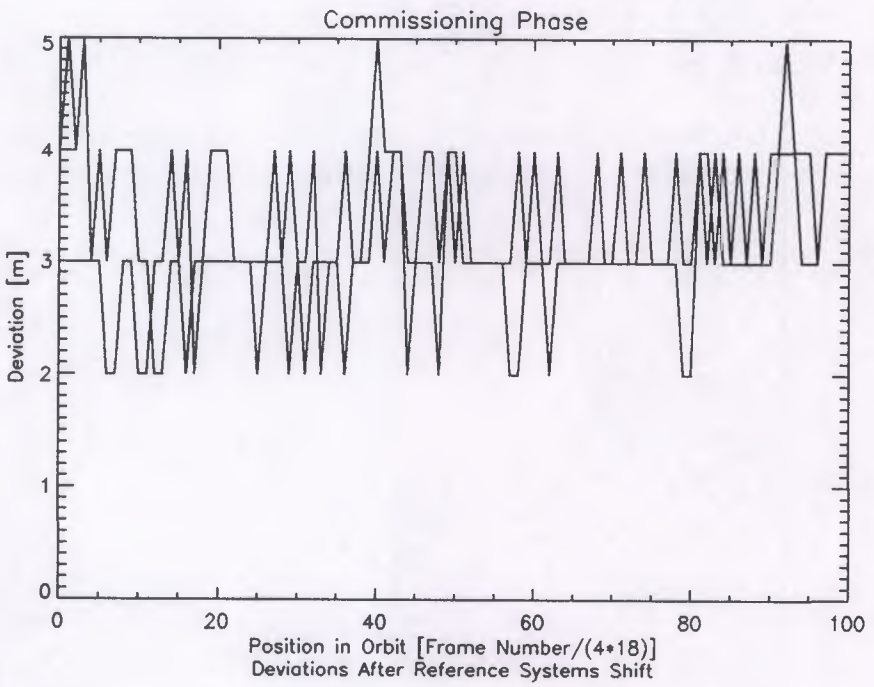

FIGURE 6. The maximum differences between the shifted values of the frame based algorithm throughout the orbit for repeat cycle on track 29 in the Commissioning phase. Across track and radial components of the baseline are plotted.

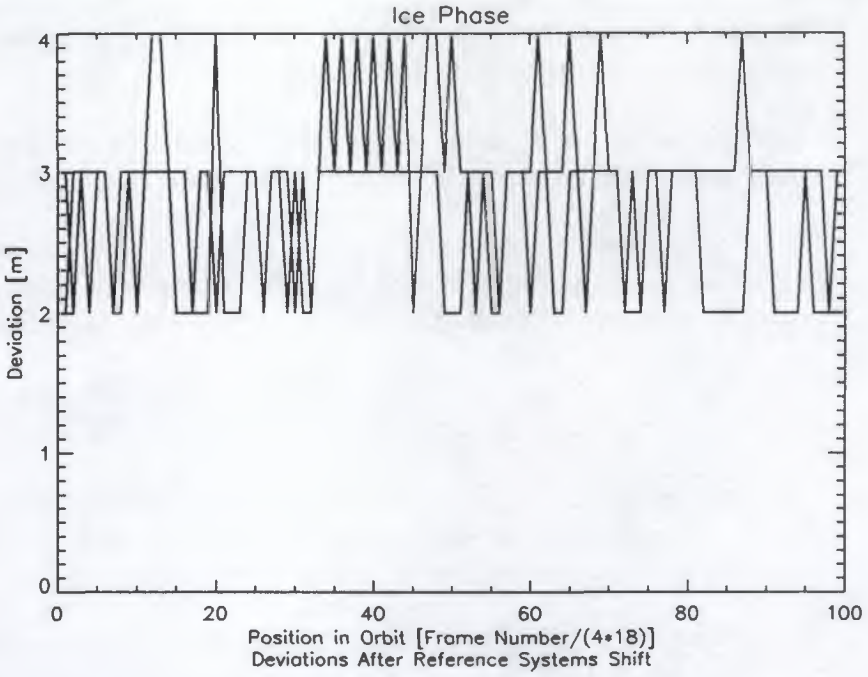

FIGURE 7. The maximum differences between the shifted values throughout the orbit for repeat cycle on track 21 in the 1st Ice phase. Across track and radial components of the baseline are plotted.

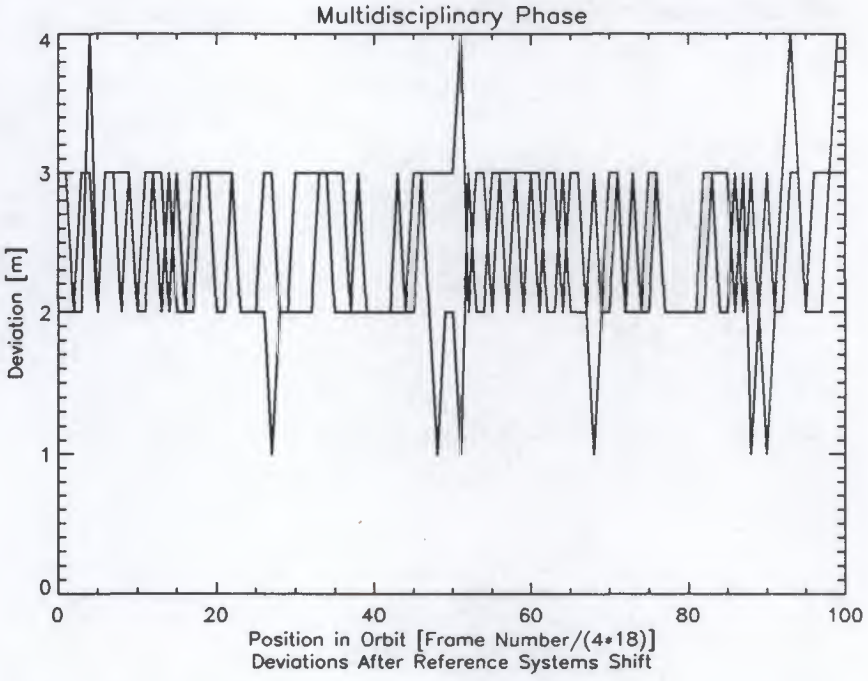

FIGURE 8. The maximum differences between the shifted values throughout the orbit for repeat cycle on track 249 in the Multidisciplinary phase. Across track and radial components of the baseline are plotted.

3.2 External Consistency with Precision Orbit Propagator.

The Baseline algorithm verification has been checked by comparing results obtained with precision orbit propagation performed by ESOC.

The test is performed by comparing propagated satellite positions at minute intervals over a quarter orbit with up to 9 month look ahead in the Multidisciplinary phase.

The reference system positions used by ESOC are different from those used by the INSAR Baseline algorithm. Therefore, there exists a varying time offset between the data calculated by ESOC and the data calculated by the INSAR Baseline Algorithm.

These time shift results in errors that should be removed before the accuracy of the INSAR Baseline Listing is estimated.

This has been done in figure 9 where the baseline absolute error is estimated to be less than 6m. The estimate has been done by extrapolating (to zero time offset) the extreme points of the trend observed in the comparison of data.

The 6m baseline error estimate contains components resulting from the error component in the restituted orbit as well as errors in the orbit propagation performed by the ESA orbit propagator and to a lesser degree errors from the precision orbit propagator used at ESOC.

The amount of data in the test is not significant enough to use the error estimate as an absolute upper bound, but the result can be used as an indication of the accuracy.

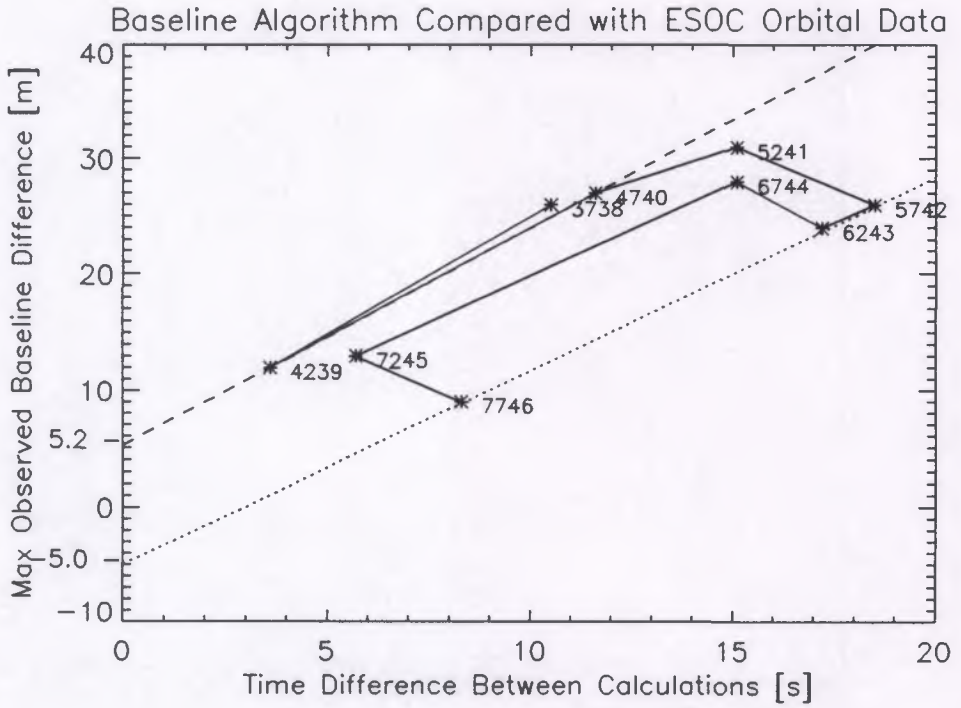

FIGURE 9. Comparison between the INSAR Baseline algorithm and orbital data calculated by ESOC. (ref. M. Rosengren ESA-ESOC-FCSD-OAD-STB)

Conclusion:

The comparison with data from the ESOC precision orbit propagator indicates that the INSAR Baseline Algorithm has an accuracy of about 6m absolute error (order of magnitude).

3.3 External Consistency by Study of Orbit Inclination Drift.

As explained in chapter 1.4 the inclination drift causes an across track baseline drift with time at the extreme latitudes of the ERS-1 orbit.

Extracting the across track component of the baseline at minute 25 (North pole) and 75 (South pole) of the orbit and plotting it against the time between repetition will result in graphs representing measurements of the inclination drift. To avoid problems in the interpretation one should not extend the time span to include inclination manoeuvres.

In figure 10 and 11 this has been done for repeats from the beginning to the end of the Commissioning phase and the 1st Ice phase. We observe that the mean baseline drift is stable, but that it is oscillating around the average drift velocity. We also observe that the average baseline drift velocity 12m and 21m for the Commissioning and 1st Ice phase respectively over a 24 hour period.

This result is verified by a extraction of data from a graph in reference 1 where the average baseline drifts are found to be 11m and 19m over a 24 hour period for the two mission phases.

As explained in section 1.4 the inclination drift varies throughout the year (see ref. 2 and 3). The two mission phases, occurred at different periods of the year (respectively autumn and winter). A difference in the inclination drift for these two phases is observed in accordance with known gravitational theory (see ref. 2 and 3).

The oscillation around the average drift is caused by the lunar gravitational influence on the satellite, and the monthly lunar cycle can be seen from the oscillating period.

Conclusion:

We observe that the INSAR Baseline algorithm is identifying and measuring the satellite inclination drift with an accuracy of a couple of meters, but no error bound on the INSAR baseline values can be found from this exercise.

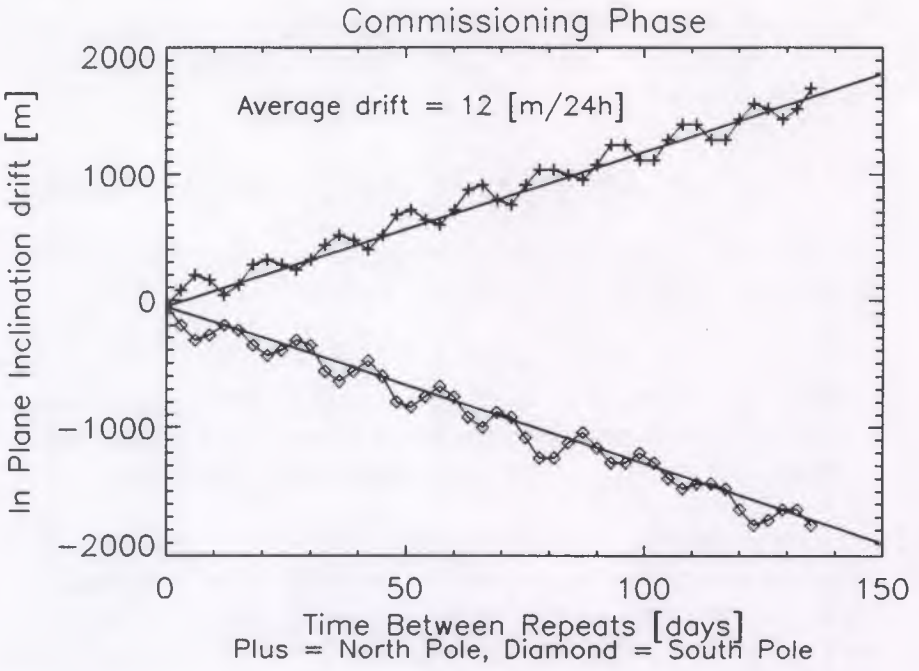

FIGURE 10. Baseline drift due to inclination change for track 29 in Commissioning phase, measured at the north and south pole.

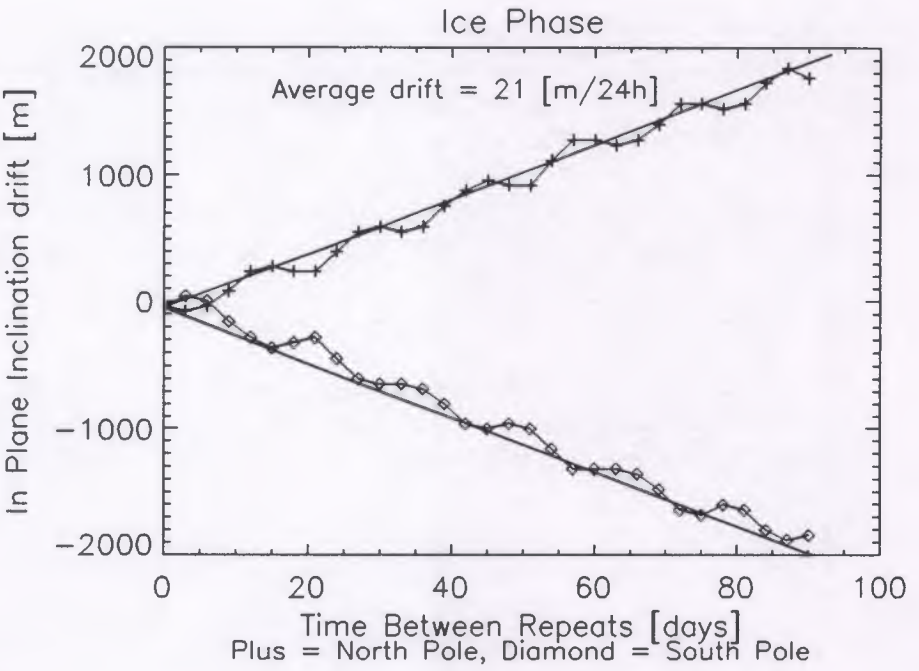

FIGURE 11. Baseline drift due to inclination change for track 21 in 1st Ice phase, measured at the north and south pole.

3.4 Checks with Baseline Values Derived by INSAR Scientists.

The INSAR user community make use of two methods for baseline estimation.

Method 1:

Analysis of orbital data by orbit propagation techniques similar to the ones used for the INSAR Baseline Listing.

Method 2:

Measurement of the frequency spectrum shift of the two complex SAR images used to create the interferogram. The shift can be related to the baseline through a known formula (see equation 1).

3.4.1 Method 1.

We have made comparisons with baselines derived by Zebker of JPL (USA) and Wärner / Small of University of Zürich (Switzerland).

The comparisons show a good fit with mostly small baseline differences and a maximum absolute error of 10m, occurring at a high latitude only where the along track positioning of the measuring point is uncertain (rapidly changing longitude and small variations in latitude).

3.4.2 Method 2.

We have made comparisons with baselines derived by Rocca / Prati / Parizzi of POLIMI (Italy), Ulander / Hagberg at CTH (Sweden) and Massonnet of CNES (France). The results of the comparisons fits with varying accuracy (0 to 50m absolute error in the baseline).

In the conversion from frequency shift to meters nominal values of several parameters are used. This leads to errors in the estimated baselines that need correction before comparisons with other data sources can be performed.

Formula 1 shows the relationship as Mr. Parizzi of POLIMI (Italy) has supplied through a private communication.

$$r = 4 \cdot f \cdot |Bperp| \cdot s / (k \cdot c \cdot h \cdot \tan(\alpha)) \qquad \textbf{(EQ 1)}$$

Where:

- r is the frequency shift
- f is the carrier frequency
- |Bperp| is the perpendicular to slant range component of the baseline
- s is the slant range sampling interval
- k is a constant equal to 1

- c is the light velocity
- h is the normal to ground satellite height
- α is the off-nadir look angle

In the calculation of the image derived baselines several of the parameters in this formula are set to nominal values due to lack of actual values. This means that both scaling errors and random errors occurs in the conversion. These errors come in addition to the errors of the INSAR Baseline Algorithm and the along track measurement inaccuracy.

It is possible to a certain extent to correct the scaling errors by changing **k** in equation 1 to minimize the error span of the data. This correction will remove the constant error due to the use of nominal values of parameters and any systematic bias in the errors from the INSAR Baseline algorithm. However the errors of both the restituted orbits and the orbit propagator are expected to be random, and therefore remain.

Data calculated by the team of Rocca and Prati of POLIMI on data used in the Bonn Interferometric Experiment is scaled using different scaling factors. The span of the resulting differences between the modified data and the INSAR Baseline Listing is plotted against the scaling factor in figure 12. As the scaling factor changes we observe a parabola with a minimum at k=1.189 for UTC and 1.194 for the frame based algorithm. The parabolic function arises due to the fact that we are looking at the maximum of the differences between a set of baselines, not absolute values. When the scaling factor changes some differences increase while other decrease. The minimum is occurring when the largest increasing error and the largest decreasing error is of the same size.

The resulting errors between the two methods with this scaling factor applied is plotted in figure 13. There appears to be a general trend in the remaining errors where they are dependant on the sign and size of the baseline value. The trend can be explained by the satellite drift within the ground track deadband at the latitude of the measurement (see reference 2 and 3), but the trend is not clear enough to draw conclusions.

The absolute values of the baseline errors is within 11m for UTC and 9m for the frame based algorithm. This estimate should be regarded as an estimate of the expected absolute error due to random effects. However the size of it could possibly be reduced by correcting for the along track displacement in a way similar to the one applied in section 3.3 One should note that the Bonn data start time has only 1 second offset to the nearest UTC minute. This means that it is unclear which of the two methods have the best sampling points. The total error changed from 131m to 121m when the new method was applied.

A similar test has been applied to the data supplied by the team of Ulander at Chalmers University of Technology, Sweden. The found minimum span was found with a scaling factor of 1.083 for the UTC and 1.104 for the frame based algorithm. The maximal absolute random error was within 10m for UTC and 8m for the frame based method. The original data and the minimized error data values can be found in Annex I. The total error changed from 51m to 45m when the new method was applied.

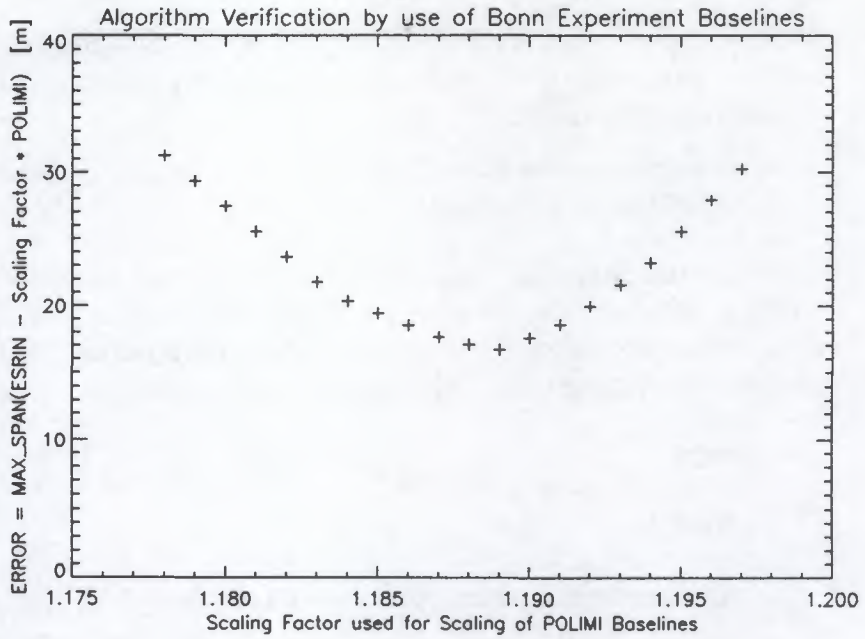

FIGURE 12. The scaling factor that minimises the error span of the test data is here found at the minimum of the parabola. Use of this scaling factor gives an estimate of the lower limit of the accuracy in the comparison.

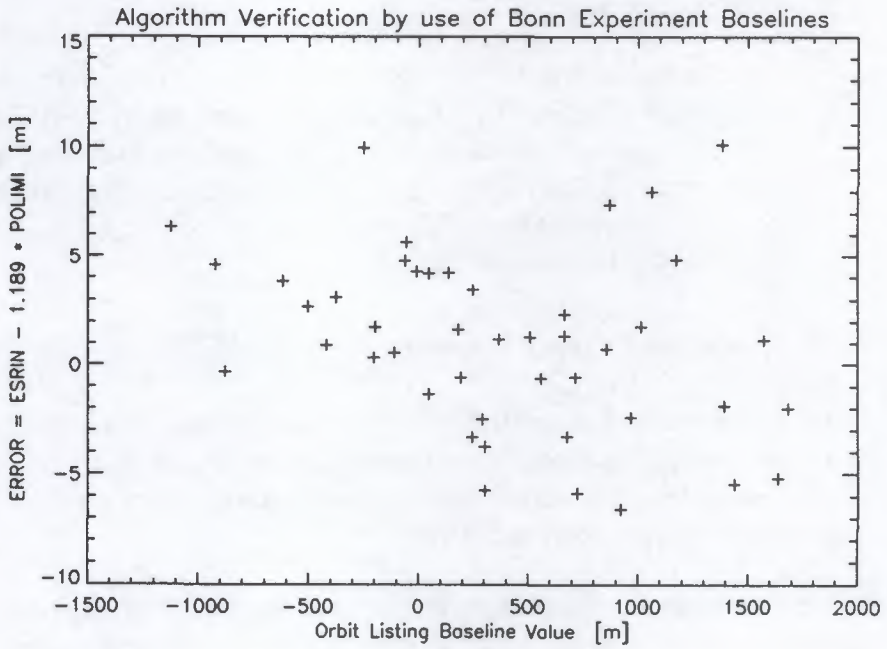

FIGURE 13. The resulting baseline errors between the two methods are here plotted against the INSAR Baseline Listing value.

The comparisons done with the baselines supplied by Massonnet CNES are inconclusive since several factors are unknown.

- Baselines over Spitsberg (Svalbard) are rapidly changing, which means that the along track uncertainty of the measuring point gives room for doubt about the observed differences.
- Baseline estimations from image data over Etna (Sicily) can be questionable since up to 300 raw data lines are missing.

Only few data points has been available, and the baseline derivation technique of CNES is different from the one used by POLIMI and Chalmers. It is therefore not possible to draw any definitive conclusions about the accuracy. We only observe that the baseline comparisons over Ukraine gives good agreement.

Conclusion:

Method 1:

Comparisons between baseline errors derived from orbit propagation give consistent results with an absolute error bound better than 10m.

Method 2:

Comparisons with baselines derived from the image spectrum give an absolute error bound of 9m, mostly due to random effects. Given the limited amount of data analysed this error bound can only be used as an indication of the accuracy.

The error bound (random and systematic effects) from the self-consistency test of the algorithm (section 3.1) is about half of the observed baseline errors seen with method 2 (random effects only). This may indicate that there is no significant systematic error in the baseline algorithm. In addition one may suspect that part of the errors found with method 2 are due to along track displacement of the sampling points used in the comparison.

3.5 Restituted Orbit Accuracy

During the creation of the INSARORB files all frames of the ERS-mission phases have been found by a combined forward and backward propagation. At about 20 dayshifts have been observed to have inconsistencies greater than 2m. The maximum inconsistency ever observed is 7m.

These errors at the file-change at midnight are due to the way backlog processing of restituted orbits is done (1 day delayed to the nominal restituted processing).

Conclusion:

The restituted orbit files have an observed error bound of maximum 7m.

4.0 Interferometric Opportunity with the ERS-1 Mission.

In figure 14 to 18 we present acquisition independent INSAR baseline statistics from phase A, B, C, D and the cross phase BD. The data is in the parallel / perpendicular to slant range reference system and represents baseline values independently of acquisitions (i.e. baselines computed along the complete orbit).

It should be noted that the symmetry and the zero centring of the acquisition independent histograms is lost when acquisitions are counted for. This is because of the high proportion of acquisitions made over the northern hemisphere.

In the figures it can be noted a dip at the peak of the distribution (especially pronounced in the Commissioning phase, fig. 14. This is caused by the inclination drift which leads to a lower probability of very small baselines at high latitudes and consequently to a higher probability of medium range baselines.

At the end of the Commissioning phase the nominal ± 1000m ground-track deadband was relaxed. This leads to a wider range of the measured Baseline distribution. In phase B and C the use of the nominal ground-track deadband resulted in a narrowing of the baseline distribution, while in phase D a further narrowing of the baseline distribution is occurring as a result of a change in the orbit maintenance strategy.

TABLE 5. Interferometric opportunity in percent of total mission phase time.

Mission Phase	B_{perp} < 1100m		B_{perp} < 600m	
	No	%	No	%
Commissioning Phase	302.128	67	182.975	41
1st Ice Phase	163.380	77	100.650	48
Multidisciplinary Phase	46.717	73	29.442	46
2nd Ice phase	257.399	98	229.069	88
1st to 2nd Ice Phase	432.425	88	270.190	55

This new strategy in phase D results in a narrowed deadband especially at mid to high latitudes and is a result of a mid-phase inclination manoeuvre, as well as an increased in-plane orbit manoeuvre frequency. The inclination manoeuvre is necessary to ensure a possibility of short baselines at long time between repeat at high and mid latitudes.

Conclusion:

We have observed that the orbit maintenance strategy in phase A, B and C will lead to from 40% to 50% of repeat orbit combinations that satisfy the INSAR baseline condition for the ERS-1 mission when acquisitions are not considered.

The increased inclination manoeuvre frequency applied in the 2nd Ice phase increased the INSAR opportunity to between 85% to 90%.

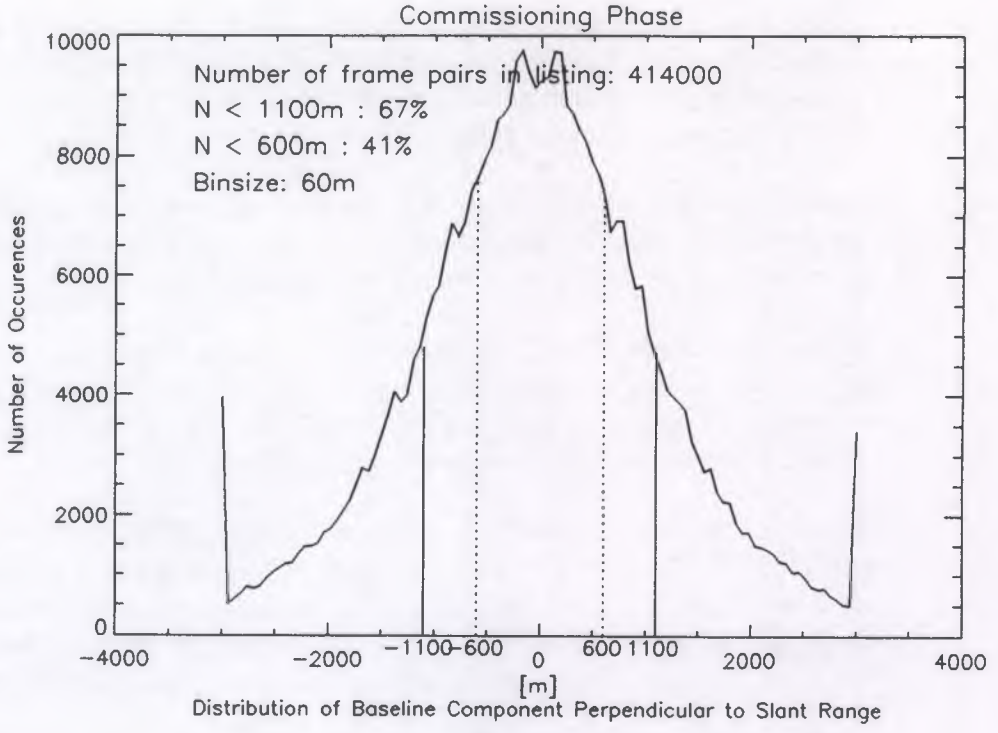

FIGURE 14. Baseline distribution for Commissioning phase, track 29.

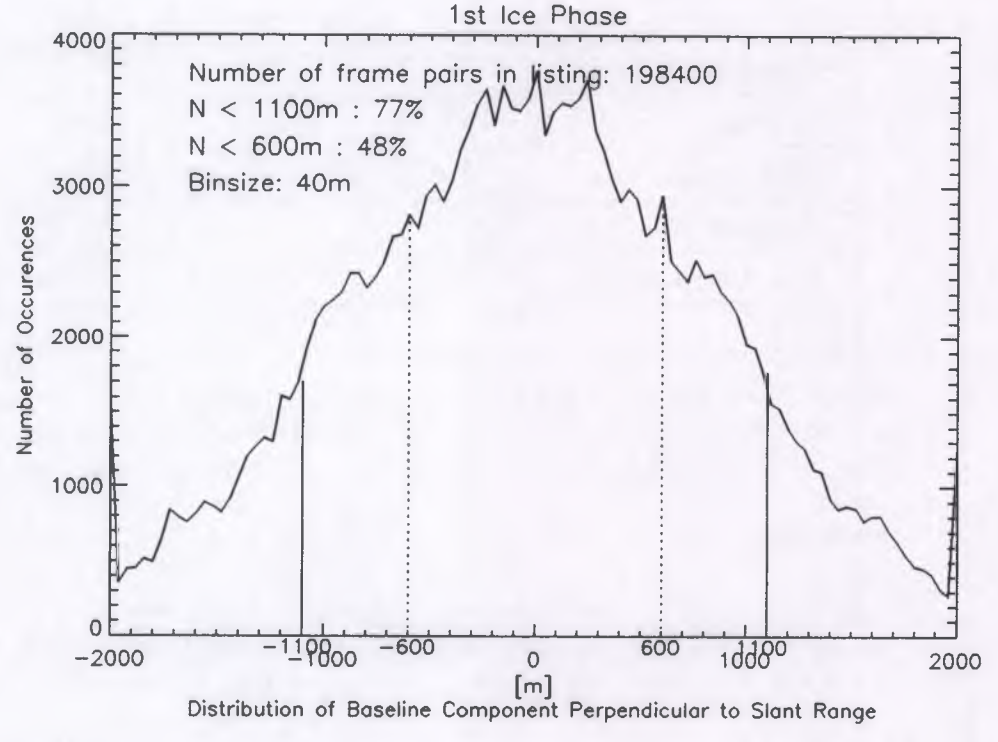

FIGURE 15. Baseline distribution for 1st Ice phase, track 21.

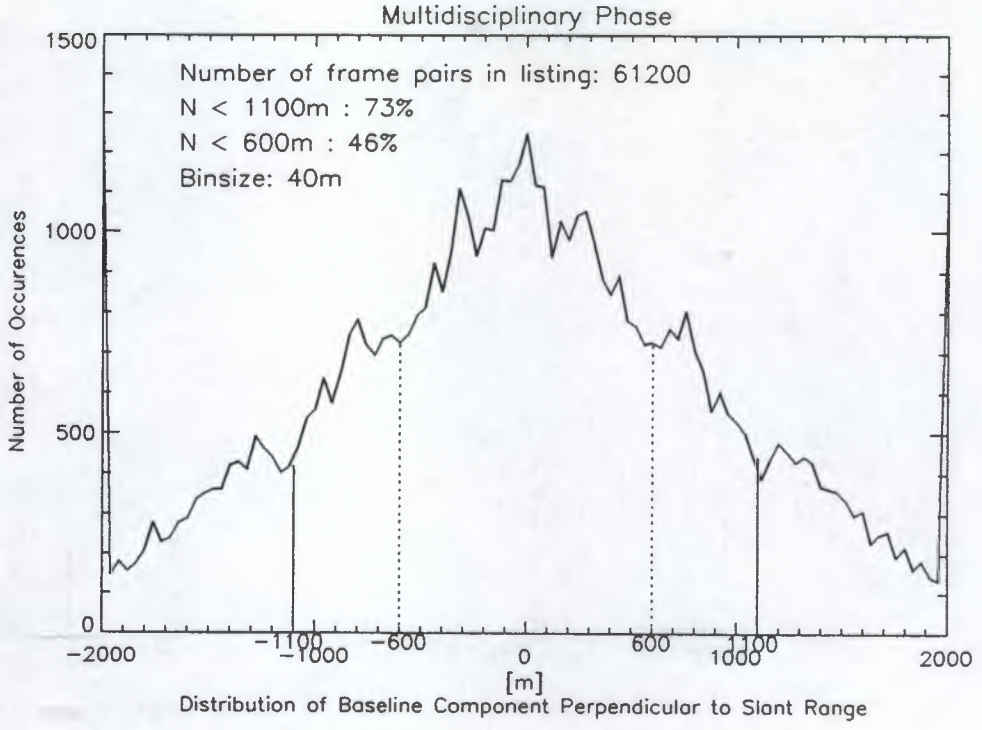

FIGURE 16. Baseline distribution for Multidisciplinary phase, track 249.

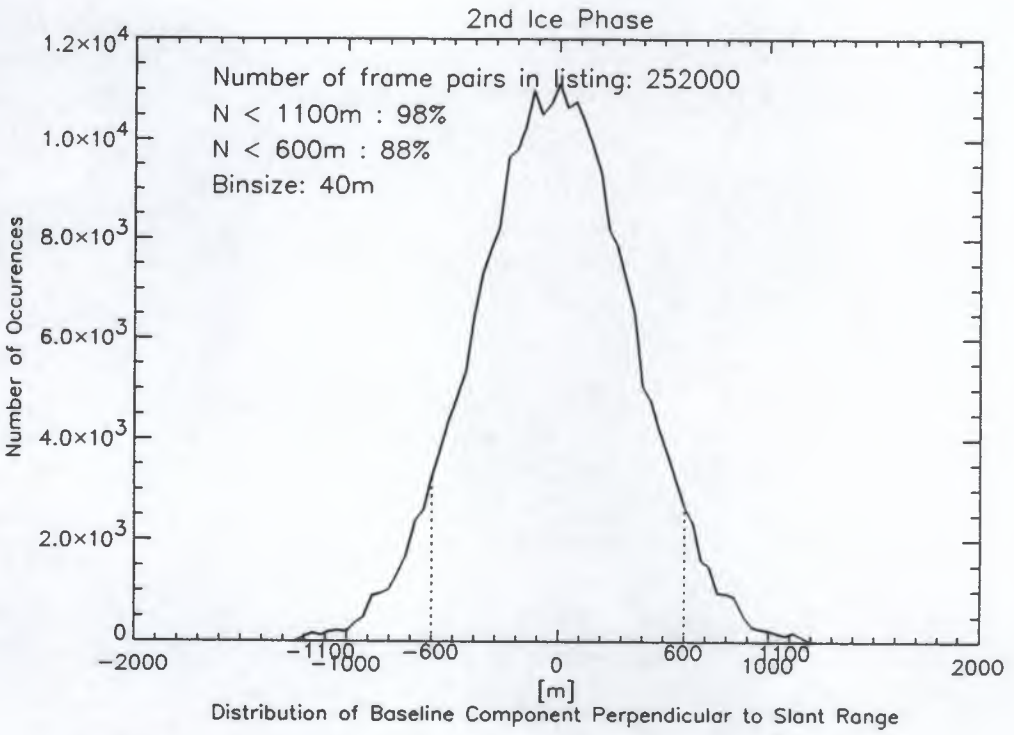

FIGURE 17. Baseline distribution for 2nd Ice phase, track 31.

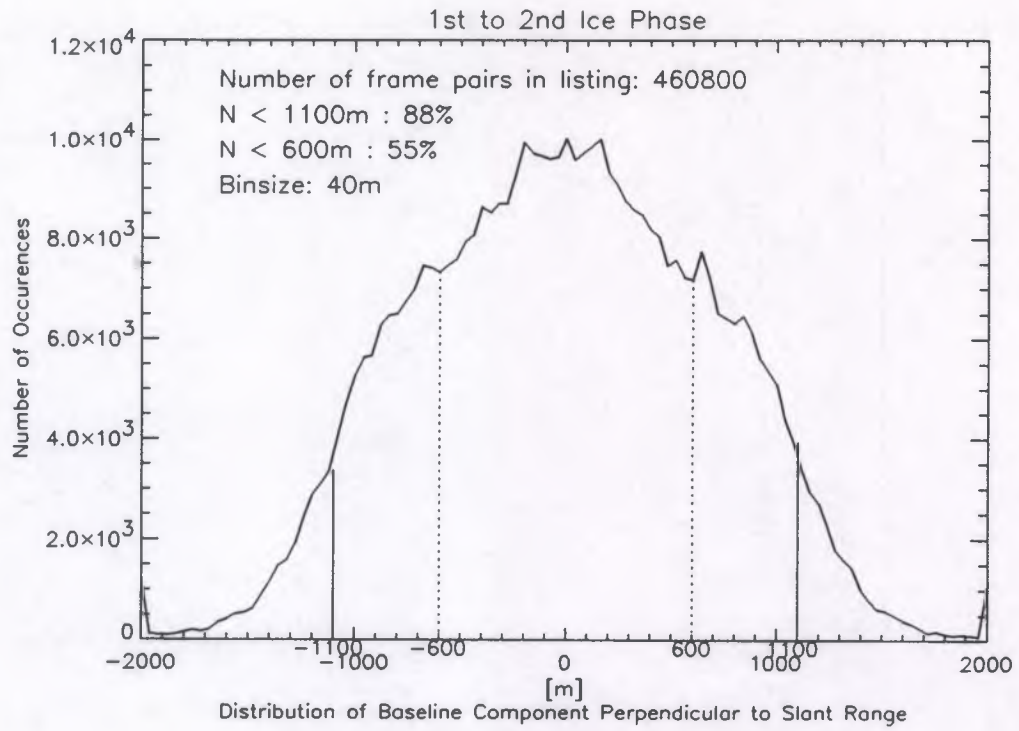

FIGURE 18. Baseline distribution for 1st to 2nd Ice phase, track 21.

5.0 Geographical Location of INSAR Acquisitions.

In this section we present four types of plots.

1. World map with ERS-1 acquisition stations (figure 19 and table 12) which serve to identify the theoretical coverage that can be obtained with current and planned acquisition stations.
2. DESC acquisition plots for the first four mission phases (figures 20 to 24). These plots shows where the actual acquisitions have been done and are presented to help the interpretation of the track plots described in point 4 further down.
3. INSAR baseline acquisition distributions for each of the current ERS-1 mission phases (A, B, C, D, BD, and the four first months of phase E).
4. Colour coded 'maps' made up of geographically interlaced tracks for each of these mission phases.

   The vertical axis is sampled in frames along the orbit, starting at the top from the north pole (frame 1791), passing by equator (frame 3591) and ending with the south pole (frame 5391).

   The horizontal axis is sampled in ERS-1 orbit track sequence with adjacent tracks corresponding to adjacent geographic location (i.e. adjacent tracks are not sequential track numbers).

   Such a 'map of tracks' gives an indication of the geographic location of the INSAR acquisition, it does not represent geographical coverage. This is so because of the gradual increase of overlap between neighbouring tracks as one moves towards the poles. The real geographical coverage is obtained by making comparisons between the track plots and e.g. the DESC acquisition plots (point 2) where the SAR image swaths are plotted on a world map.

The last two types of plots (3 and 4) are sorted by mission phase with two baseline distribution plots followed by 6 track plots for different baseline regimes for each mission phase as explained below.

The track plots represent the quantity of image pairs at all frames in the descending pass of each phase by the use of colour coding with the following scale:

Seven plots / graphs are given for each mission phase:

1. Distribution of acquisitions with $|B_{perp}| < 2000$ m, binsize 40m.
2. Distribution of acquisitions with |Bperp| < 400 m, binsize 8m.
3. Track plot without limitations on the length of |Bperp| (all repeated acquisitions).
4. Track plot with a 1100m bound on |Bperp| (all repeated acquisitions within the theoretical INSAR limit).

5. Track plot with a 600m bound on $|B_{perp}|$ (all repeated acquisitions with INSAR potential).
6. $|B_{perp}|$, between 300m and 150m (for topography mapping).
7. $|B_{perp}|$, between 70m to 30m (for surface change detection).
8. $|B_{perp}|$, less than 20m (surface movement detection).

We observe that the regions covered by the unlimited baseline plots show recognisable gross geographic features (taking into account the distortion in the track plots i.e. SAR acquisition over all major continental land masses). The geographic features observed in the baseline track plots are consistent with the DESC acquisition maps of actual geographic coverage. We note that there are at least two acquisitions over most parts of the acquisition area.

In the baseline plots where the baseline span is restricted, several regions of the acquisition areas are missing. This is due to the baseline values over regions systematically being out of range. E.g. acquisitions over Antarctica disappear when constraints are set on $|B_{perp}|$. This can be explained by the combination of the following factors:

- Few acquisitions (often only two).
- Long time between acquisitions.
- Inclination drift which systematically puts |Bperp| out of range between the acquisitions.

The results are summarised in table 6to 11.

The columns in the table are:

- A header column identifying the baseline span of the data in each row.
- Maximum number of repeated acquisition minute nodes in any 2-D bin of the track plots that satisfy the conditions imposed on |Bperp|
- The average number of repeated acquisition frames per 2-D bin of the track plots in the active acquisition area. Which is defined by the presence of at least two acquisitions.
- The percentage of the acquisition area that remains covered after the baseline filter has been applied to the INSAR Baseline Listing.
- The percentage of the total number of minute nodes in the INSAR Baseline listing that satisfy the conditions imposed on $|B_{perp}|$.
- The total number of repeated acquisition minute nodes over the whole acquisition area that satisfy the conditions imposed on $|B_{perp}|$.

TABLE 6. Commissioning Phase.

Baseline Spans	Max Repeats	Average Repeats	Acquisition Area %	Repeated Frames %	Repeated Frames
No limit on $\|B_{perp}\|$	903	10.19	100 *	100	442.271
$\|B_{perp}\|$<1100m	678	7.34	97.50	74.63	330.087
$\|B_{perp}\|$<600m	417	4.99	94.67	50.47	223.195
150m<$\|B_{perp}\|$<300m	106	1.36	82.01	13.83	61.163
30m<$\|B_{perp}\|$<70m	43	0.42	66.63	4.06	17.953
$\|B_{perp}\|$<20m	24	0.21	54.56	1.99	8.780

TABLE 7. 1st Ice Phase.

Baseline Spans	Max Repeats	Average Repeats	Acquisition Area %	Repeated Frames %	Repeated Frames
No limit on $\|B_{perp}\|$	496	34.94	100 *	100	457.083
$\|B_{perp}\|$<1100m	407	29.89	96.21	84.14	384.611
$\|B_{perp}\|$<600m	297	19.78	91.22	56.96	260.367
150m<$\|B_{perp}\|$<300m	81	5.10	80.73	14.66	67.013
30m<$\|B_{perp}\|$<70m	37	1.69	69.03	4.83	22.095
$\|B_{perp}\|$<20m	25	0.91	62.15	2.60	11.869

TABLE 8. Multidisciplinary Phase.

Baseline Spans	Max Repeats	Average Repeats	Acquisition Area %	Repeated Frames %	Repeated Frames
No limit on $\|B_{perp}\|$	153	3.23	100 *	100	1.093.974
$\|B_{perp}\|$<1100m	142	2.53	95.02	80.21	877.429
$\|B_{perp}\|$<600m	115	1.62	88.34	52.55	574.878
150m<$\|B_{perp}\|$<300m	36	0.41	65.14	13.35	146.064
30m<$\|B_{perp}\|$<70m	15	0.13	44.15	4.27	46.676
$\|B_{perp}\|$<20m	12	0.07	33.53	2.22	24.301

TABLE 9. 2nd Ice Phase.

Baseline Spans	Max Repeats	Average Repeats	Acquisition Area %	Repeated Frames %	Repeated Frames
No limit on $\|B_{perp}\|$	561	31.75	100 *	100	542.674
$\|B_{perp}\|$<1100m	561	31.48	98.14	98.07	532.222
$\|B_{perp}\|$<600m	530	26.72	97.57	85.02	461.359
150m<$\|B_{perp}\|$<300m	170	8.22	84.72	25.86	140.323
30m<$\|B_{perp}\|$<70m	63	2.58	76.39	8.68	47.096
$\|B_{perp}\|$<20m	35	1.45	69.81	4.45	24.154

TABLE 10. 1st to 2nd Ice Phase.

Baseline Spans	Max Repeats	Average Repeats	Acquisition Area %	Repeated Frames %	Repeated Frames
No limit on $\|B_{perp}\|$	589	23.27	100 *	100	364.655
$\|B_{perp}\|$<1100m	527	21.50	99.82	91.03	331.950
$\|B_{perp}\|$<600m	386	14.47	98.04	60.70	221.359
150m<$\|B_{perp}\|$<300m	118	3.52	83.13	14.94	54.497
30m<$\|B_{perp}\|$<70m	45	1.26	66.23	4.93	17.985
$\|B_{perp}\|$<20m	25	0.67	57.22	2.62	9.571

TABLE 11. Geodetic Phase (4 first months) to all previous phases.

Baseline Spans	Max Repeats	Average Repeats[1]	Acquisition Area %	Repeated Frames %	Repeated Frames
$\|B_{perp}\|$<2000m	49	No data	100 **	100	42.296
$\|B_{perp}\|$<1100m	37	No data	78.81	60.63	25.642
$\|B_{perp}\|$<600m	23	No data	61.01	34.92	14.768
150m<$\|B_{perp}\|$<300m	9	No data	34.72	8.98	3.800
30m<$\|B_{perp}\|$<70m	5	No data	15.61	2.76	1168
$\|B_{perp}\|$<20m	4	No data	8.90	1.40	594

* acquisition area is defined as those frames for which there are at least two acquisitions.

** acquisition area is defined as those frames for which there are at least one cross phase repeat. The 2411 tracks have been regrouped in bins of 10 tracks each.

1) The number of repeats for phase E baselines is dependent on the number of repeated acquisitions in the cross phase. This information is not presently extracted from the baseline data files.

It is clear that the repetition frequency of the short repeat cycles makes INSAR acquisitions of any combination accessible over large parts of the acquisition area.

In the 35 day cycle the INSAR potential drops significantly as a consequence of the increase in time between repeats. For such medium time repeat cycle it is important to optimise the probability of obtaining suitable baselines for INSAR applications. The experiment of the 2nd Ice phase with a narrowed ground track deadband through increased OCM frequency (in particular the introduction of an extra inclination OCM) should be adopted for future 35 day repeat cycles.

For Surface Feature Movement and Digital Terrain Models INSAR applications the numbers in Table 6 to 11 have to be used with caution. For these applications, depending on the site imaged, the time between repeats has to be limited to minimize loss of phase coherence.

There has not been applied any repeat time filtering in the statistics presented in this document.

For the Geodetic phase the INSAR potential will drop by an order of magnitude, due to no internal repeats in the mission phase (second cycle is shifted by 8 km at equator to tighten the geodetic sampling grid.

As a rule there will be a low probability of obtaining suitable INSAR image pairs for any specific site.

Because of the small separation between neighbouring tracks it may be possible to form interferogrammes with shorter time between repeat than the total repeat cycle in the Geodetic phase (37 and 131 days).

This application is limited to extreme latitudes at LAT>80 degrees. Which includes the southern part of the Ronne Ice shelf and the northern parts of Greenland and Svalbard.

At 80 degree latitude the reference orbits are separated by 2720 m. In a configuration where one have an inclination OCM between the take of two images (the satellite is moved from -1000m to +1000m across track) the across track distance is reduced to 720m. The combination of the moon cycle and any air-drag OCM might lead to even a smaller distance between the orbits, but will (due to deadband restrictions and OCM strategy) be more likely to increase this number.

Cross mission phase repeats is possible where the perpendicular to slant range displacement between the orbits is small even if the radial component is as large as 6 km to 12 km.

For this kind of repeats the baseline variation from frame to frame will tend to be larger than the normal in phase repeat baseline variation. Typical values being around 100 m to 200 m per frame.

This relatively rapid variation may result in decorrelation due to difficulties in the image co-registration process.

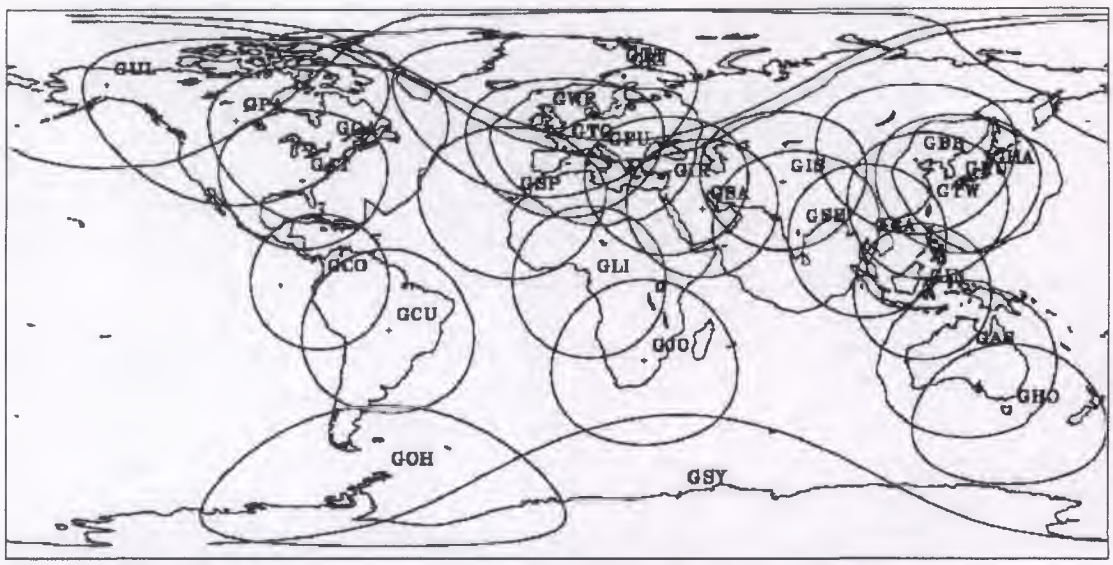

FIGURE 19. Coverage zones for operational and planned ERS-1 ground stations.

TABLE 12. Short codes for operational and planned reception stations.

Key	Name	Key	Name
GUL	Fairbanks, USA	GJO	Johannesburg, South-Africa
GPA	Prince Albert, Canada	GSY	Syowa, Antarctica, (Japan)
GCA	Gatineau, Canada	GIR	Tel Aviv, Israel
GAT	Atlanta Test Site, USA	GSA	Riyadh, Saudi Arabia
GCO	Cotopaxi, Equador	GIS	Islamabad, Pakistan
GCU	Cuiaba, Brazil	GSE	Hyderabad, India
GOH	O'Higgins, Antarctica, (Germany)	GBA	Bangkok, Thailand
GTT	Tromsø, Norway	GIN	Parepare, Indonesia
GKI	Kiruna, Sweeden	GAS	Alice Springs, Australia
GWF	West Freugh, UK	GHO	Hobart, Australia
GTO	Aussaguel, France	GBE	Beijing, China
GFU	Fucino, Italy	GHA	Hatoyama, Japan
GSP	Maspalomas, Spain	GKU	Kumamoto, Japan
GLI	Libreville, Gabon, (Germany)	GTW	Chung-Li, Taiwan

FIGURE 20. DESC ERS-1 cover map for Commissioning phase.

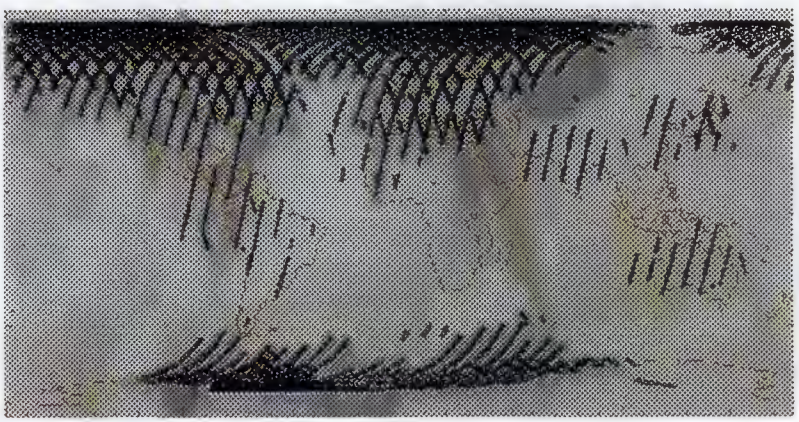

FIGURE 21. DESC ERS-1 cover map for 1st Ice phase.

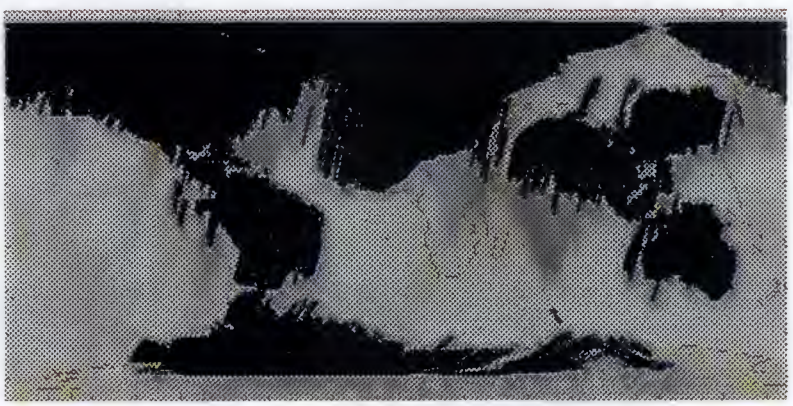

FIGURE 22. DESC ERS-1 cover map for Multidisciplinary phase.

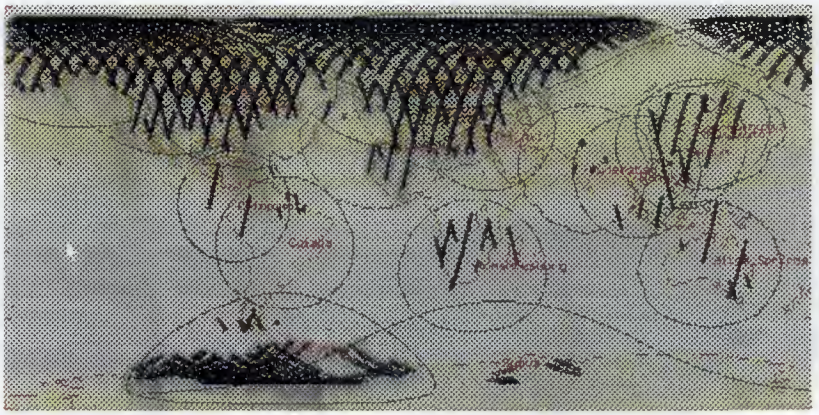

FIGURE 23. DESC ERS-1 cover map for 2nd Ice phase.

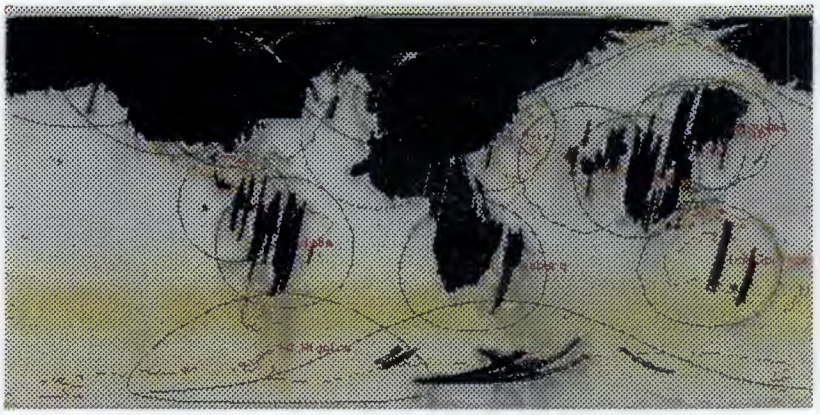

FIGURE 24. DESC ERS-1 cover map for Geodetic phase, 10 April to 1 August 1994.

5.1 Commissioning Phase.

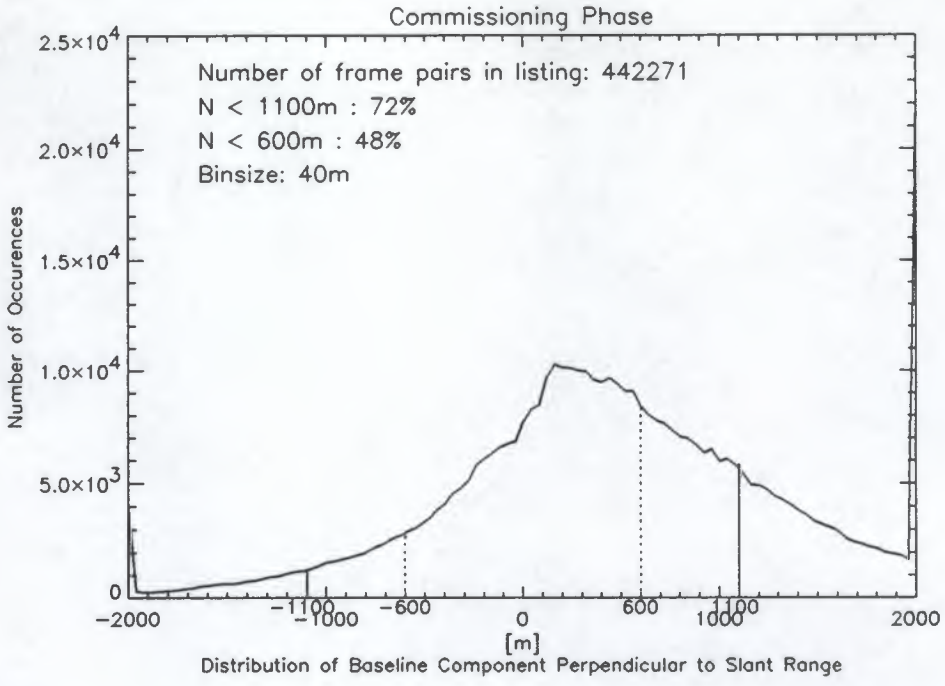

FIGURE 25. Baseline distribution for acquisitions in the Commissioning phase. Binsize 40m.

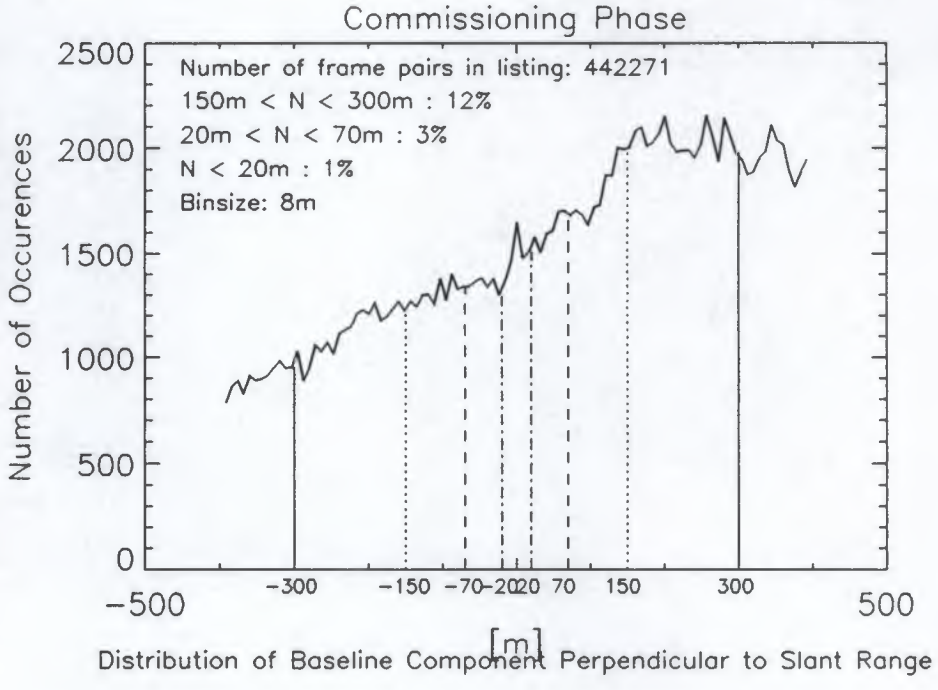

FIGURE 26. Baseline distribution for acquisitions in Commissioning Phase. Extract containing baselines smaller than 400m, binsize 8m.

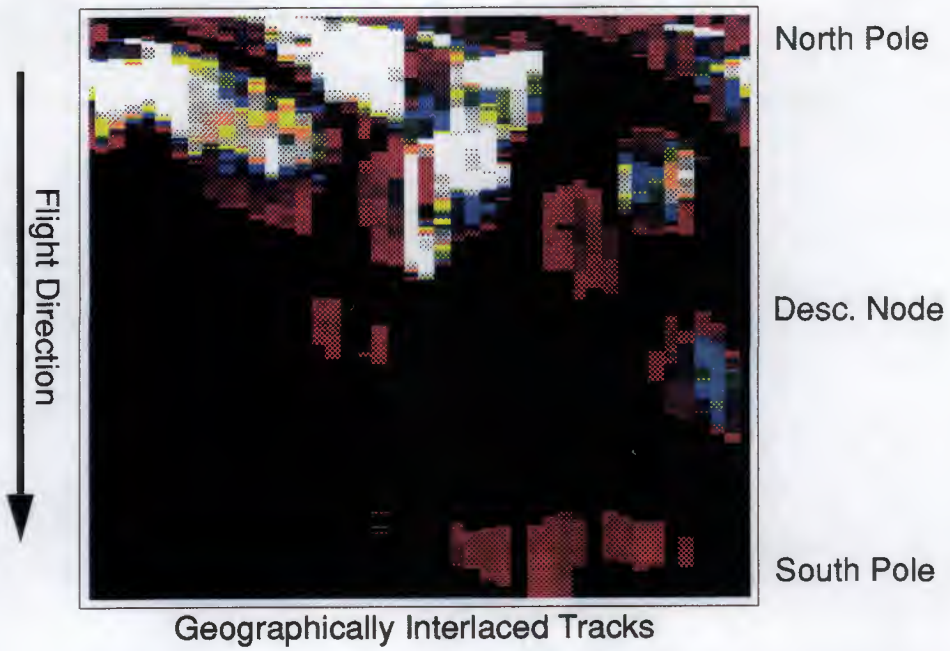

FIGURE 27. Commissioning phase acquisitions as seen by the full INSAR Baseline Listing (=acquisition surface for Commissioning Phase).
Maximum number of pairs = 903, average number of pairs over acquisition area = 10.19.

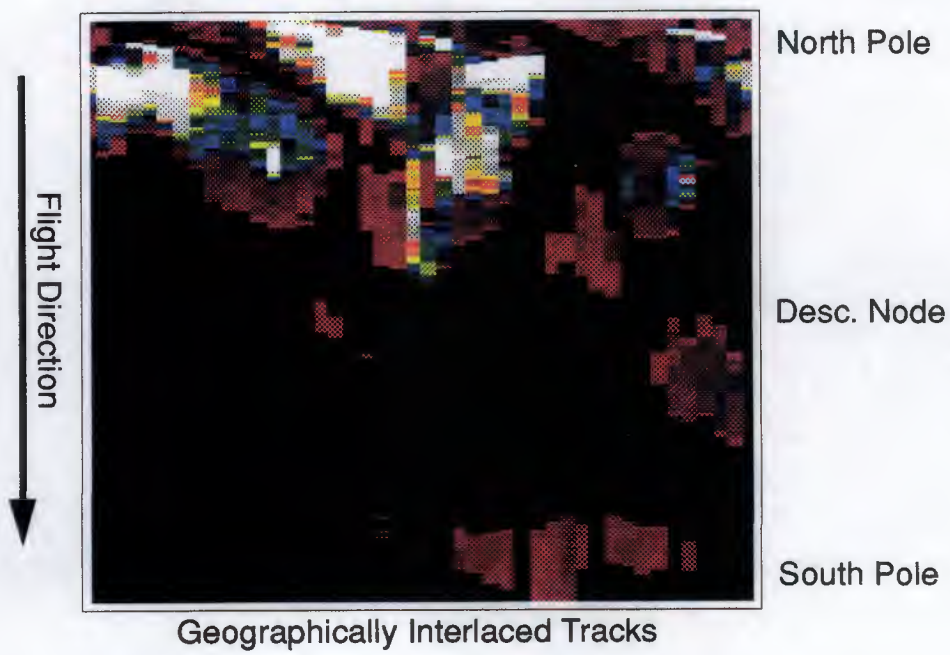

FIGURE 28. Commissioning phase acquisitions as seen by the INSAR Baseline Listing, filtered for |Bperp|<1100m. 97.50% of the acquisition surface covered.
Maximum number of pairs = 678, average number of pairs over acquisition area = 7.34.

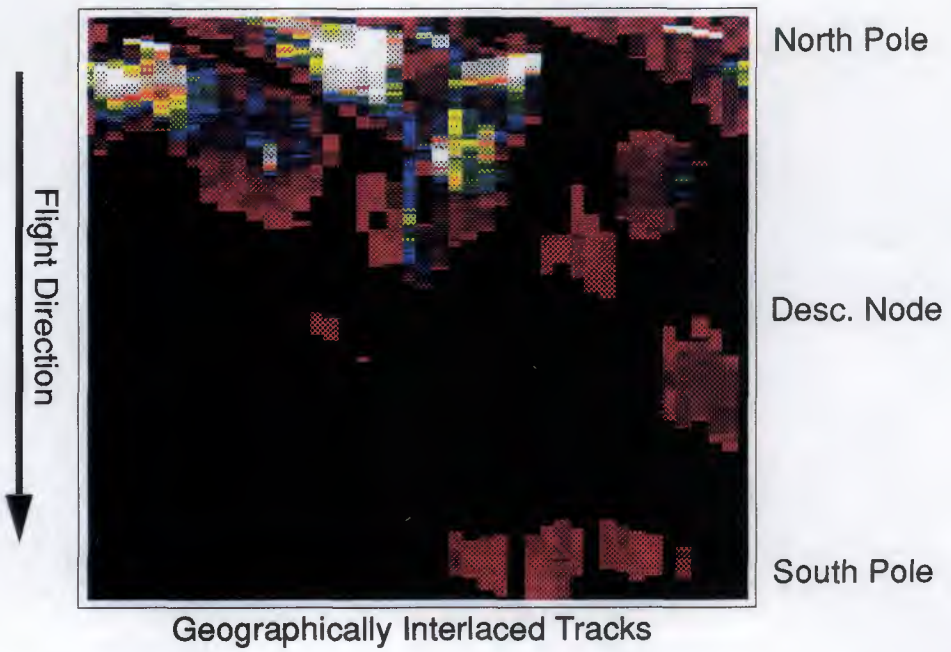

FIGURE 29. Commissioning phase acquisitions as seen by the INSAR Baseline Listing, filtered for |Bperp|<600m. 94.67% of the acquisition surface covered. Maximum number of pairs = 417, average number of pairs over acquisition area = 4.99.

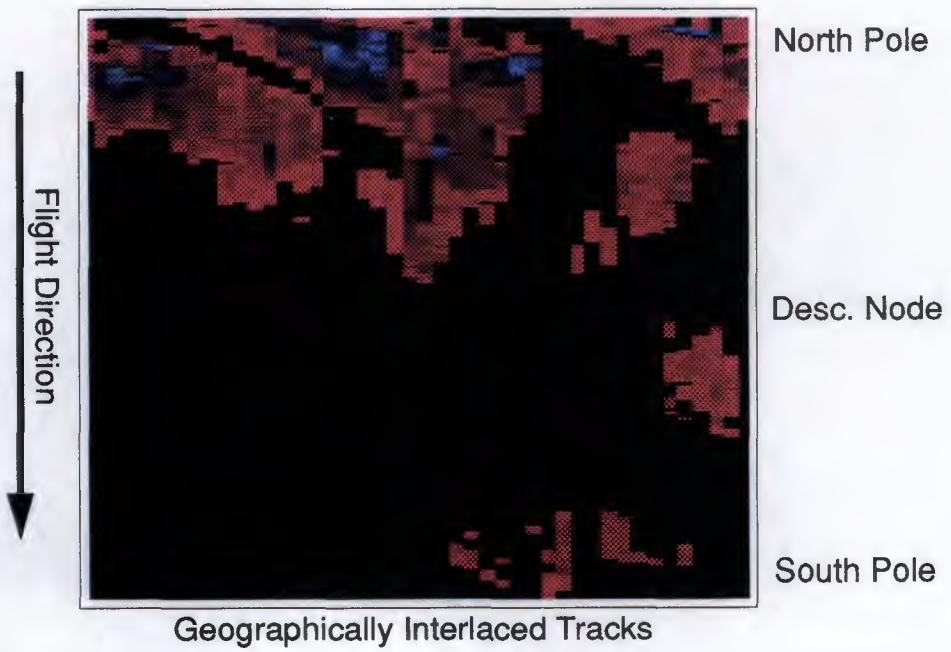

FIGURE 30. Commissioning phase acquisitions as seen by the INSAR Baseline Listing, filtered for 150m< |Bperp|<300m. 82.01% of the acquisition surface covered. Maximum number of pairs = 106, average number of pairs over acquisition area = 1.36.

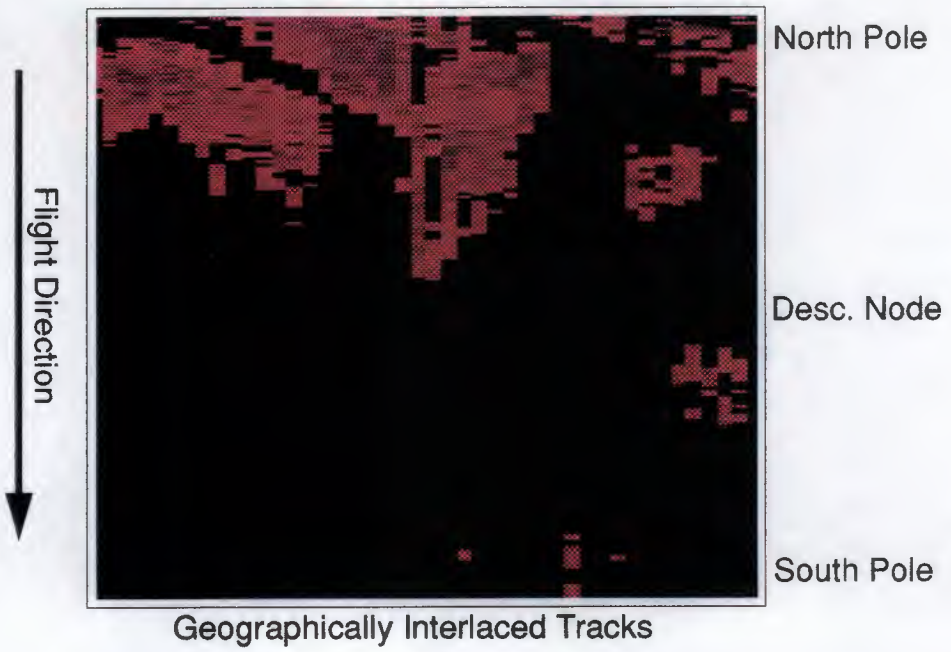

FIGURE 31. Commissioning phase acquisitions as seen by the INSAR Baseline Listing, filtered for 30m< |Bperp|<70m. 66.63% of the acquisition surface covered. Maximum number of pairs = 43, average number of pairs over acquisition area = 0.42.

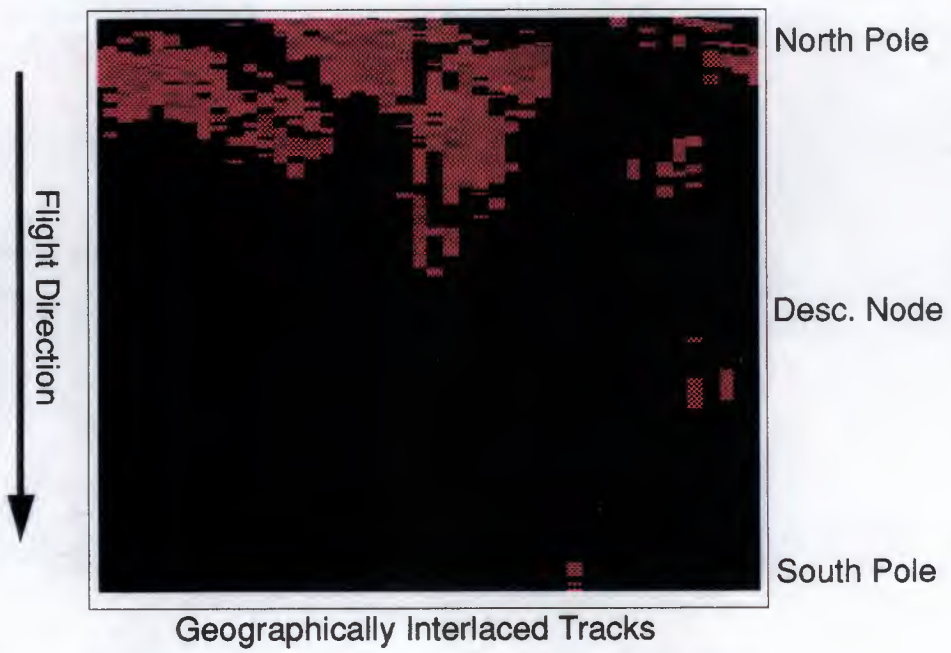

FIGURE 32. Commissioning phase acquisitions as seen by the INSAR Baseline Listing, filtered for |Bperp|<20m. 54.56% of the acquisition surface covered. Maximum number of pairs = 24, average number of pairs over acquisition area = 0.21.

5.2 1st Ice Phase.

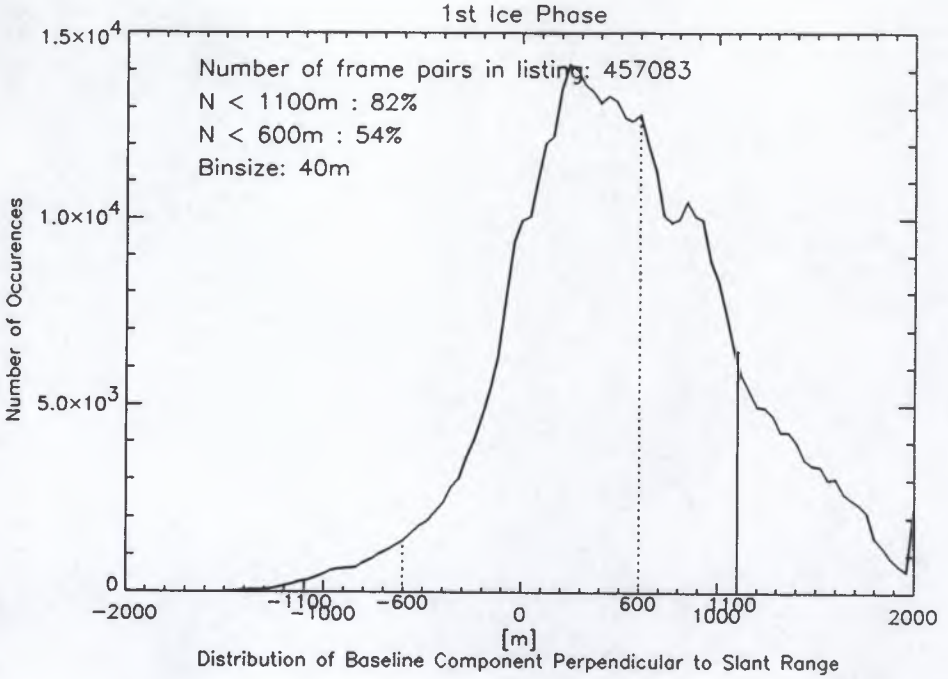

FIGURE 33. Baseline distribution for acquisitions in the 1st Ice phase. Binsize 40m.

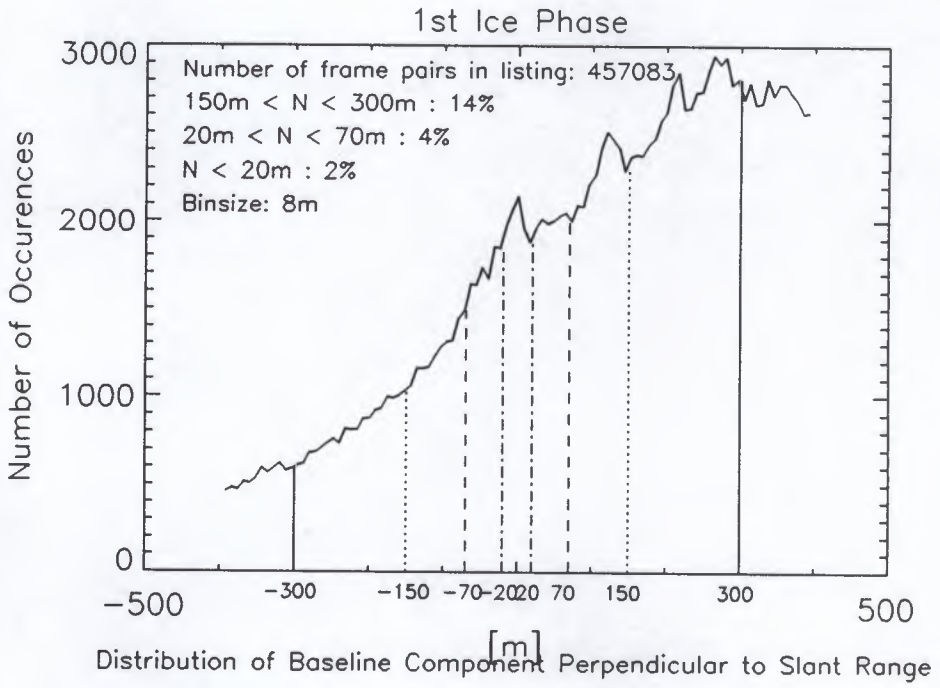

FIGURE 34. Baseline distribution for acquisitions in 1st Ice phase. Extract containing baselines smaller than 400m, binsize 8m.

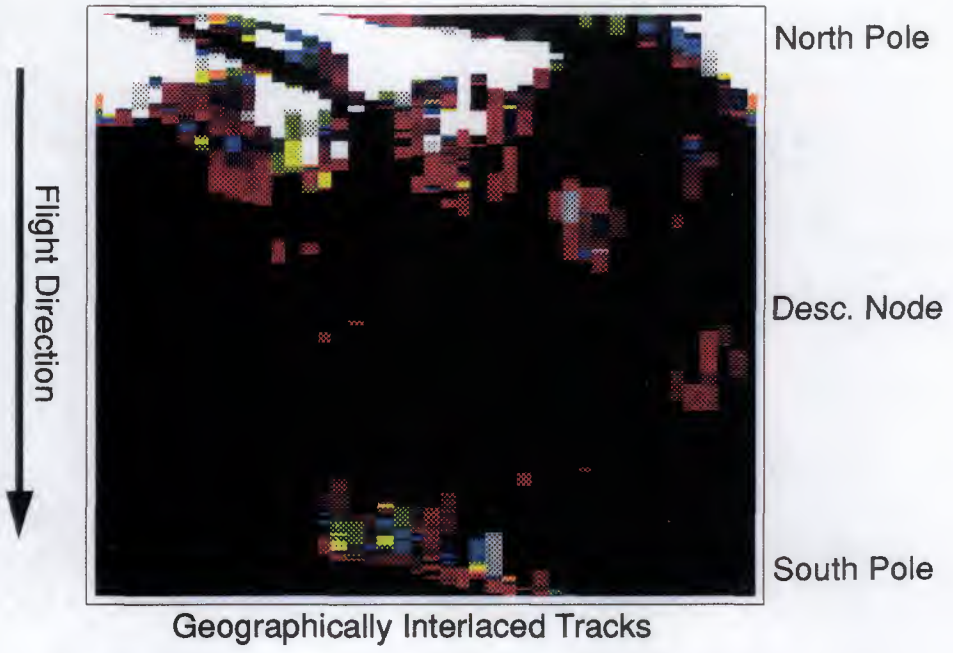

FIGURE 35. 1st Ice phase acquisitions as seen by the full INSAR Baseline Listing (=acquisition surface for 1st Ice Phase).
Maximum number of pairs = 496, average number of pairs over acquisition area = 34.94.

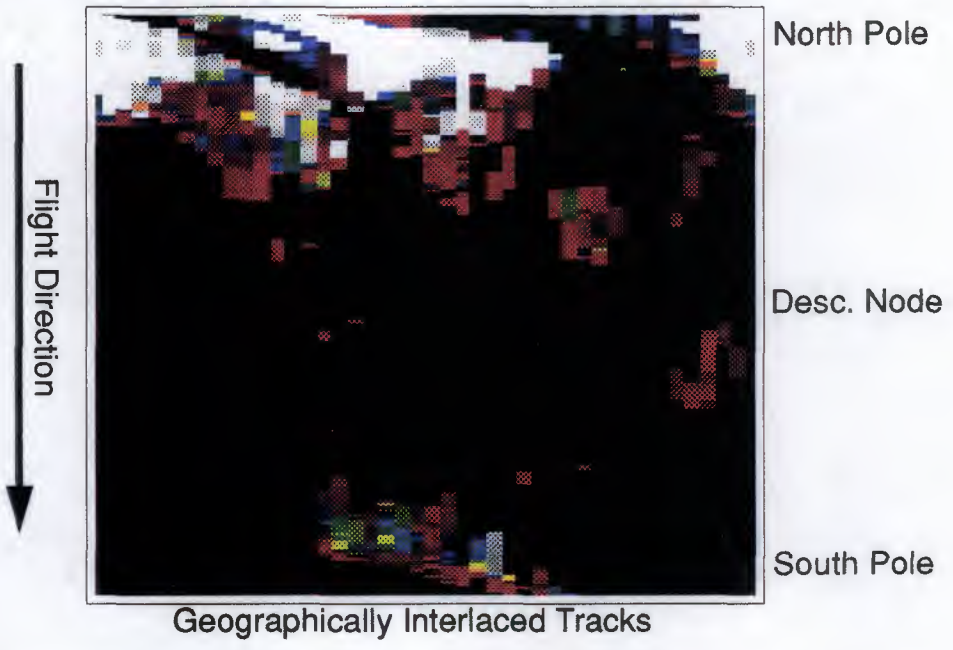

FIGURE 36. 1st Ice phase acquisitions as seen by the INSAR Baseline Listing, filtered for |Bperp|<1100m. 96.21% of the acquisition surface covered.
Maximum number of pairs = 407, average number of pairs over acquisition area = 29.89.

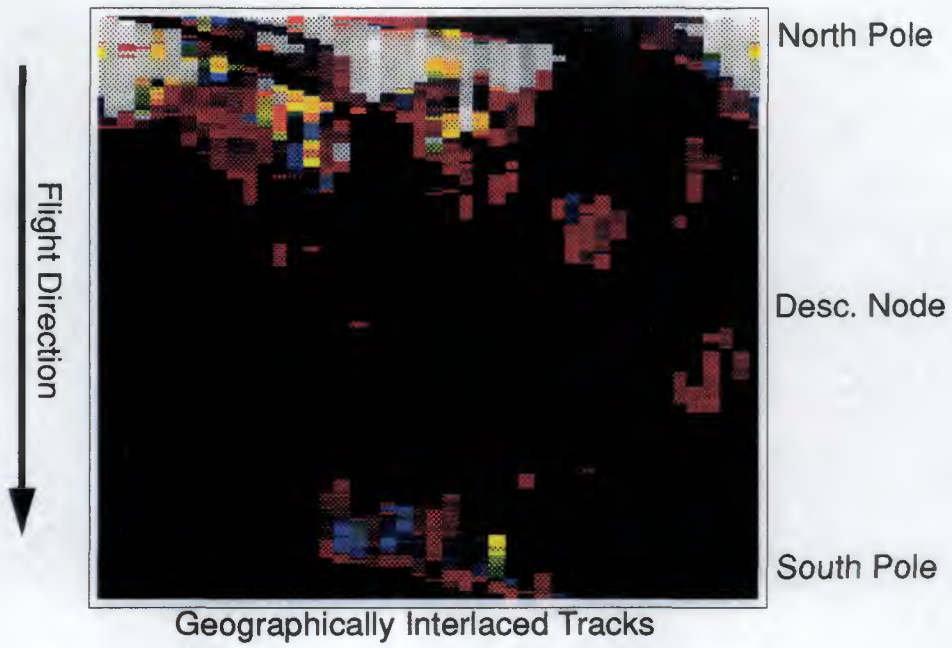

FIGURE 37. 1st Ice phase acquisitions as seen by the INSAR Baseline Listing, filtered for |Bperp|<600m. 91.22% of the acquisition surface covered. Maximum number of pairs = 297, average number of pairs over acquisition area = 19.78.

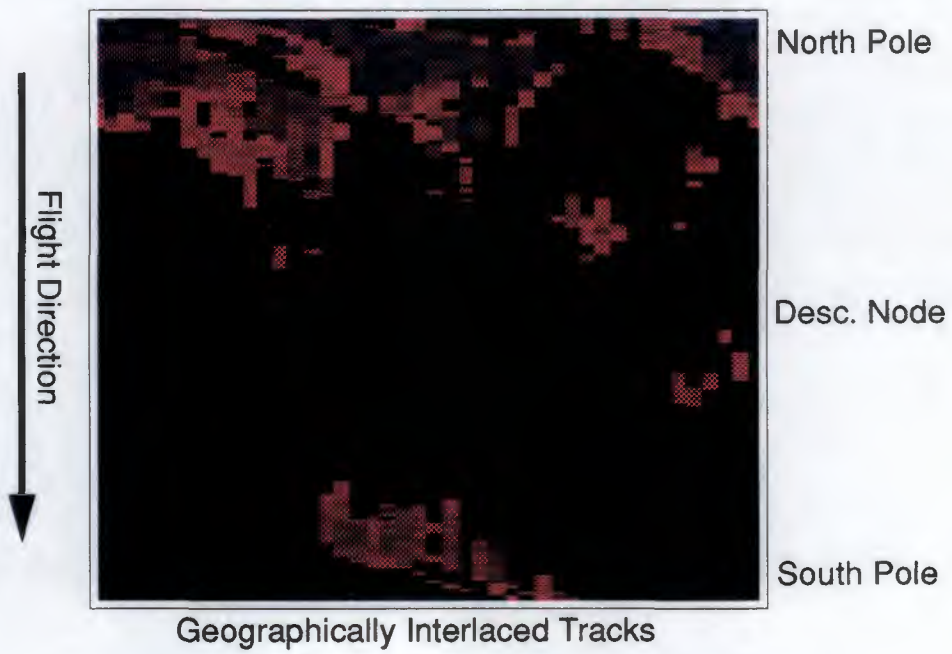

FIGURE 38. 1st Ice phase acquisitions as seen by the INSAR Baseline Listing, filtered for 150m< |Bperp|<300m. 80.73% of the acquisition surface covered. Maximum number of pairs = 81, average number of pairs over acquisition area = 5.10.

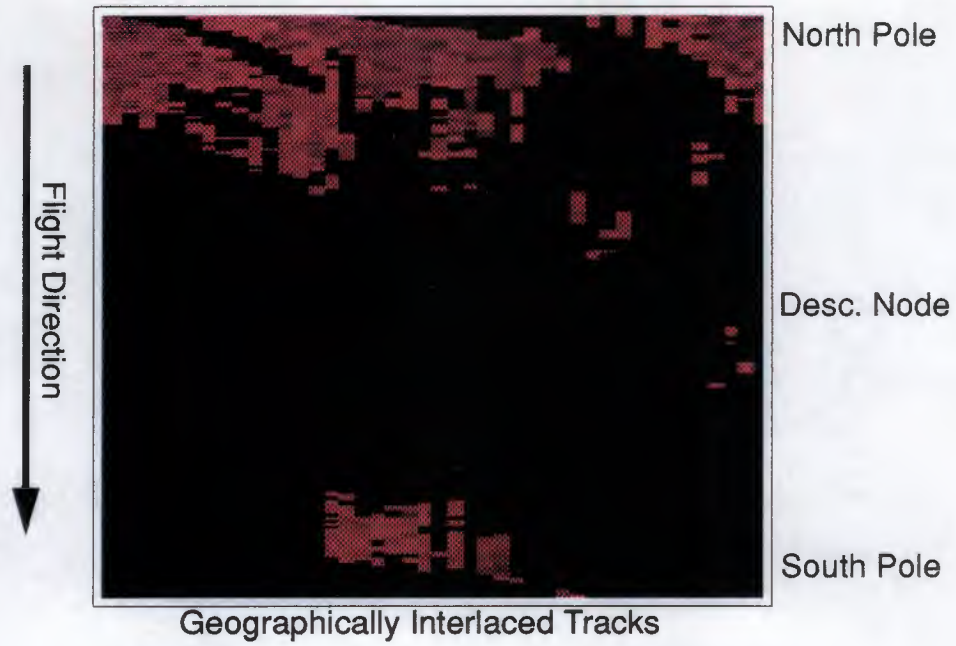

FIGURE 39. 1st Ice phase acquisitions as seen by the INSAR Baseline Listing, filtered for 30m< |Bperp|<70m. 69.03% of the acquisition surface covered. Maximum number of pairs = 37, average number of pairs over acquisition area = 1.69.

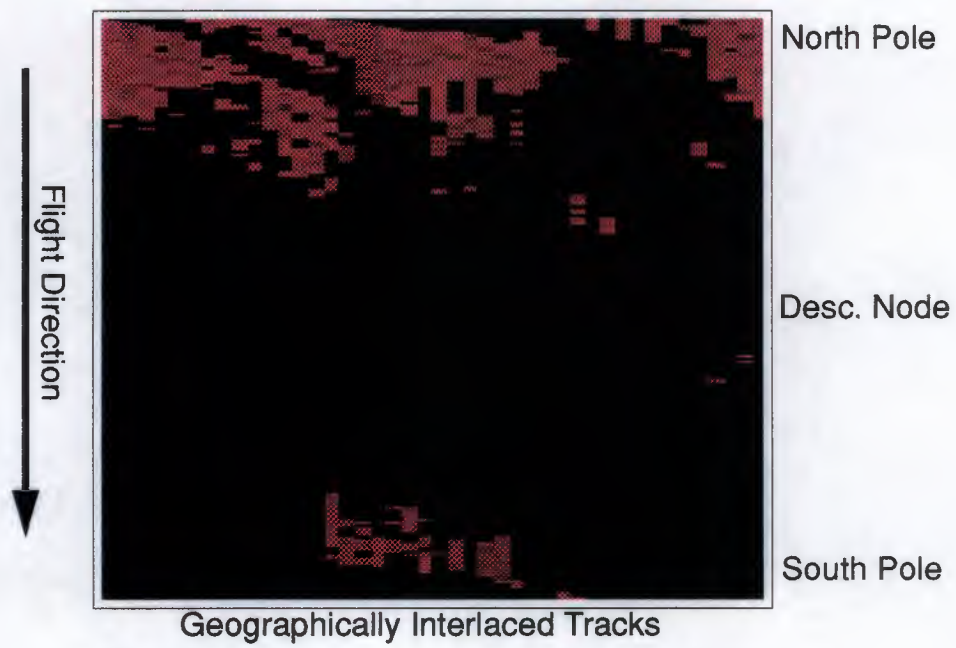

FIGURE 40. 1st Ice phase acquisitions as seen by the INSAR Baseline Listing, filtered for |Bperp|<20m. 62.15% of the acquisition surface covered. Maximum number of pairs =25, average number of pairs over acquisition area = 0.91.

5.3 Multidisciplinary Phase.

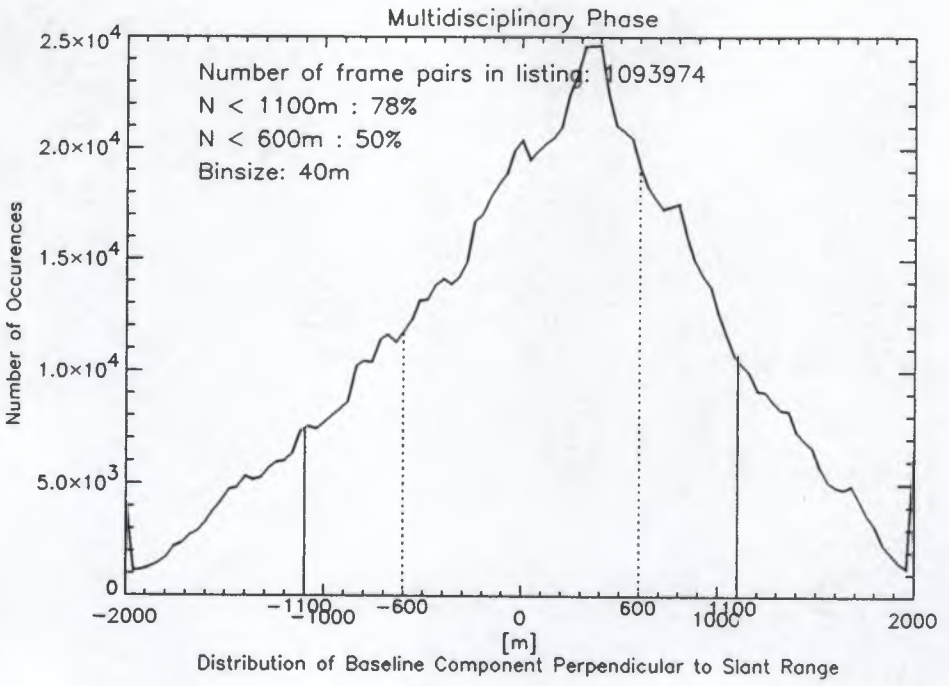

FIGURE 41. Baseline distribution for acquisitions in the Multidisciplinary phase. Binsize = 40m.

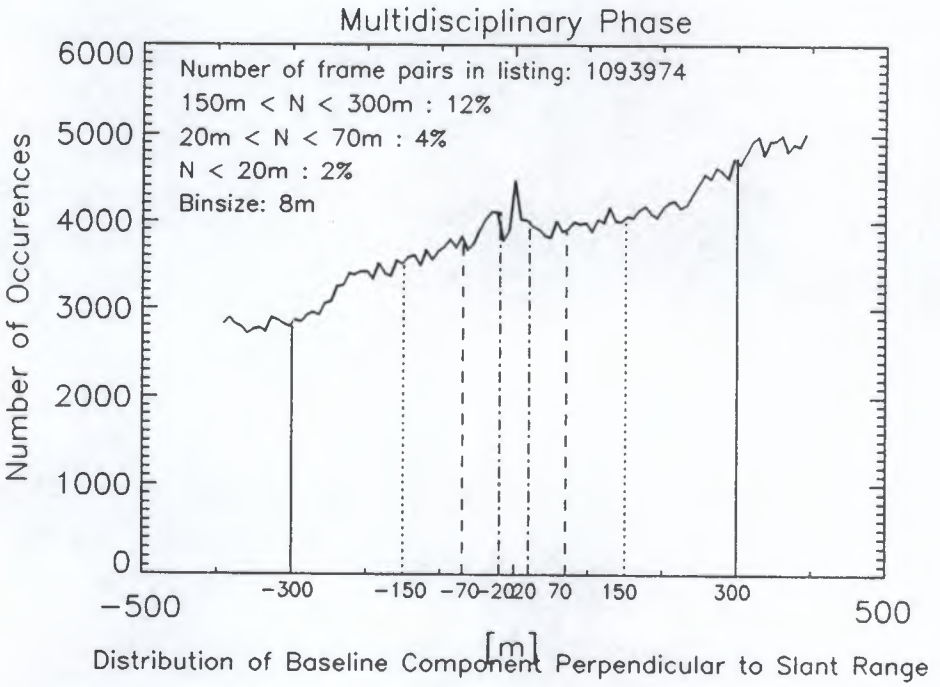

FIGURE 42. Baseline distribution for acquisitions in Multidisciplinary phase. Extract containing baselines smaller than 400m, binsize 8m.

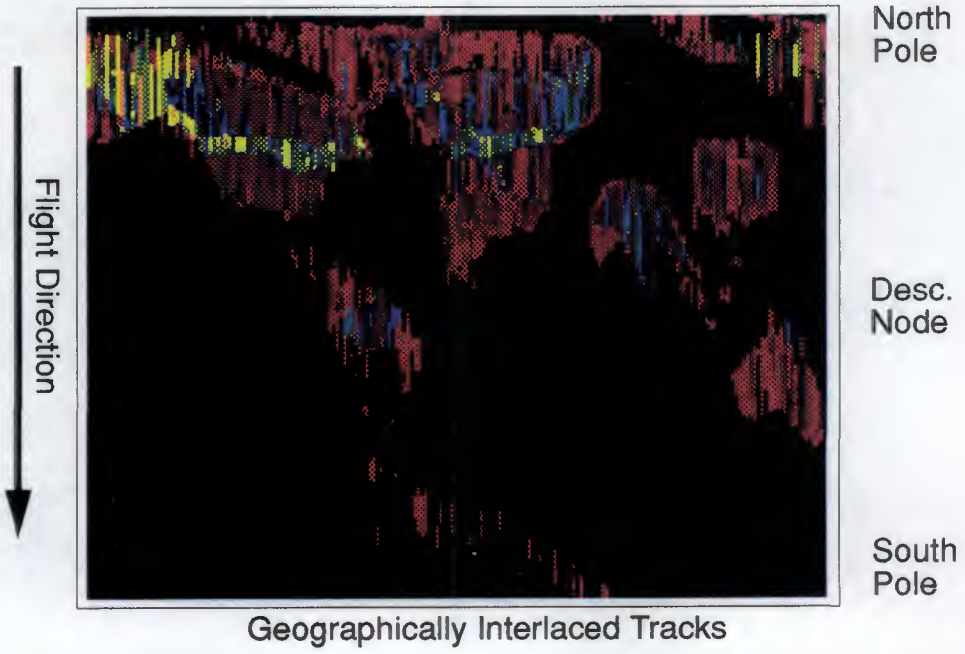

FIGURE 43. Multidisciplinary phase acquisitions as seen by the full INSAR Baseline Listing (=acquisition surface of Multidisciplinary Phase).
Maximum number of pairs=153, average number of pairs over acquisition area = 3.23.

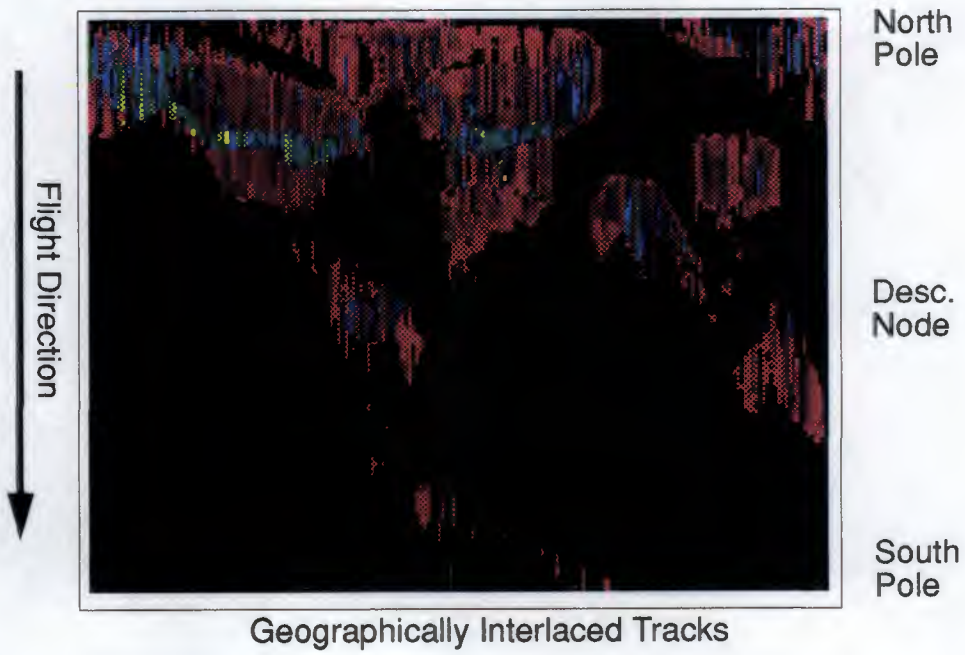

FIGURE 44. Multidisciplinary phase acquisitions as seen by the INSAR Baseline Listing, filtered for |Bperp|<1100m. 95.02% of the acquisition surface covered.
Maximum number of pairs=142, average number of pairs over acquisition area = 2.53.

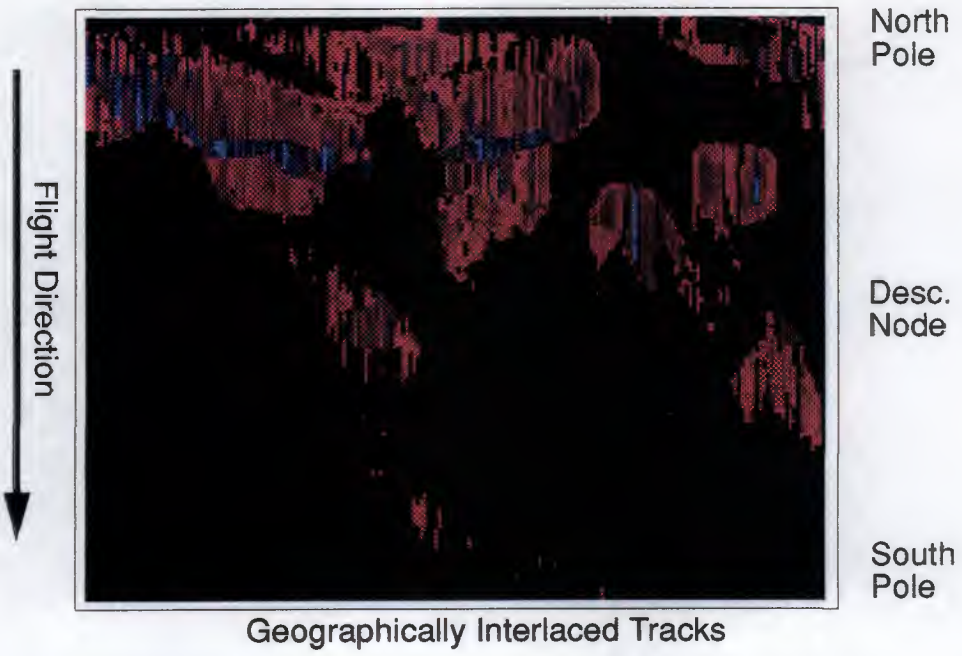

FIGURE 45. Multidisciplinary phase acquisitions as seen by the INSAR Baseline Listing, filtered for |Bperp|<600m. 88.34% of the acquisition surface covered. Maximum number of pairs=115, average number of pairs over acquisition area = 1.62.

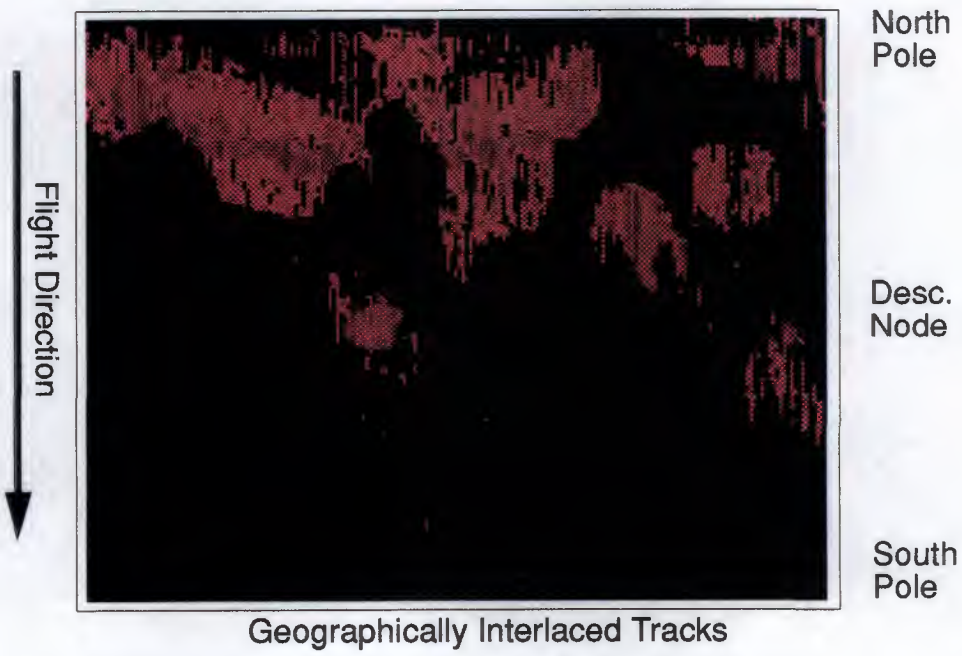

FIGURE 46. Multidisciplinary phase acquisitions as seen by the INSAR Baseline Listing, filtered for 150m< |Bperp|<300m. 65.14% of the acquisition surface covered. Maximum number of pairs=36, average number of pairs over acquisition area = 0.41.

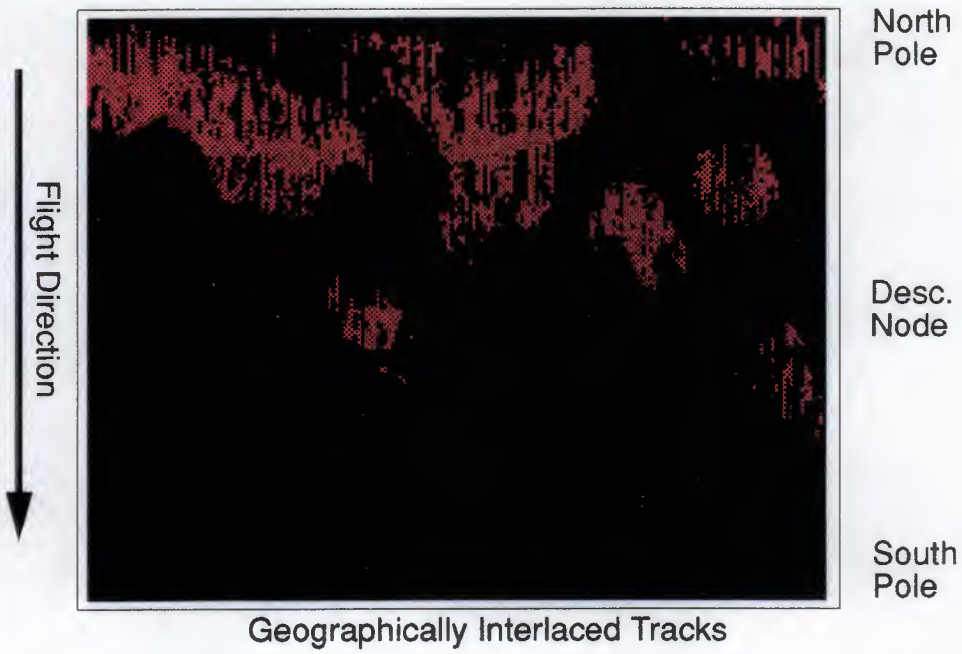

FIGURE 47. Multidisciplinary phase acquisitions as seen by the INSAR Baseline Listing, filtered for 30m< |Bperp|<70m. 44.15% of the acquisition surface covered. Maximum number of pairs=15, average number of pairs over acquisition area = 0.13.

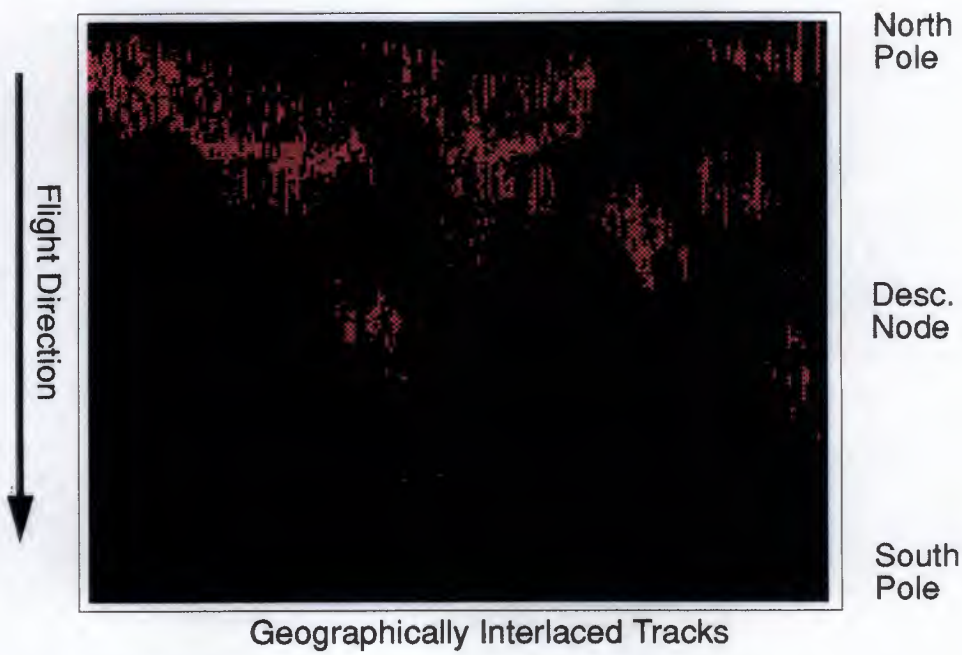

FIGURE 48. Multidisciplinary phase acquisitions as seen by the INSAR Baseline Listing, filtered for |Bperp|<20m. 44.15% of the acquisition surface covered. Maximum number of pairs=12, average number of pairs over acquisition area = 0.07.

5.4 2nd Ice Phase.

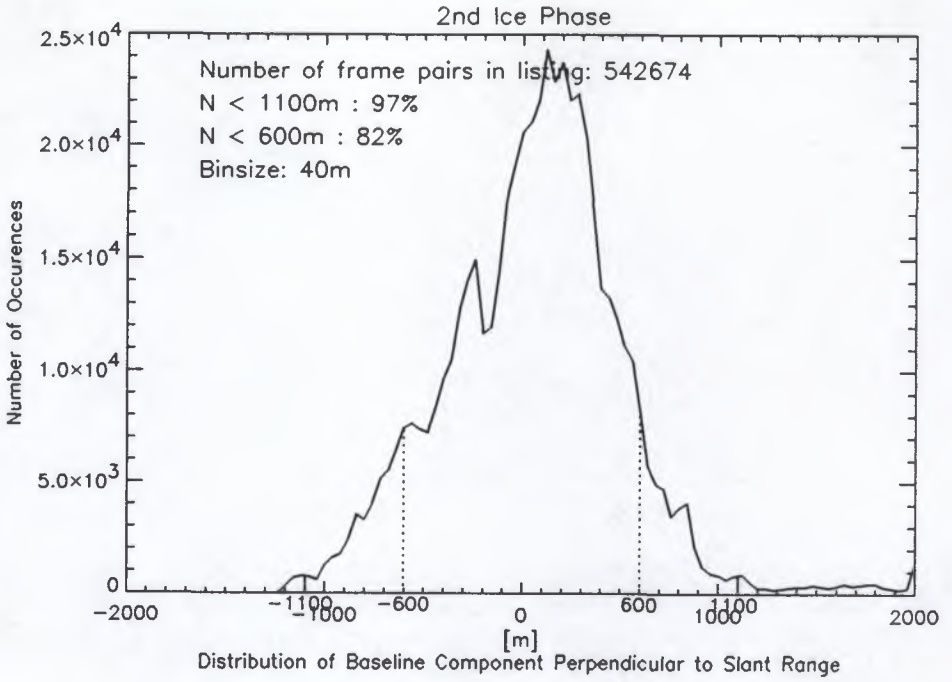

FIGURE 49. Baseline distribution for acquisitions in the 2nd Ice phase. Binsize 40m.

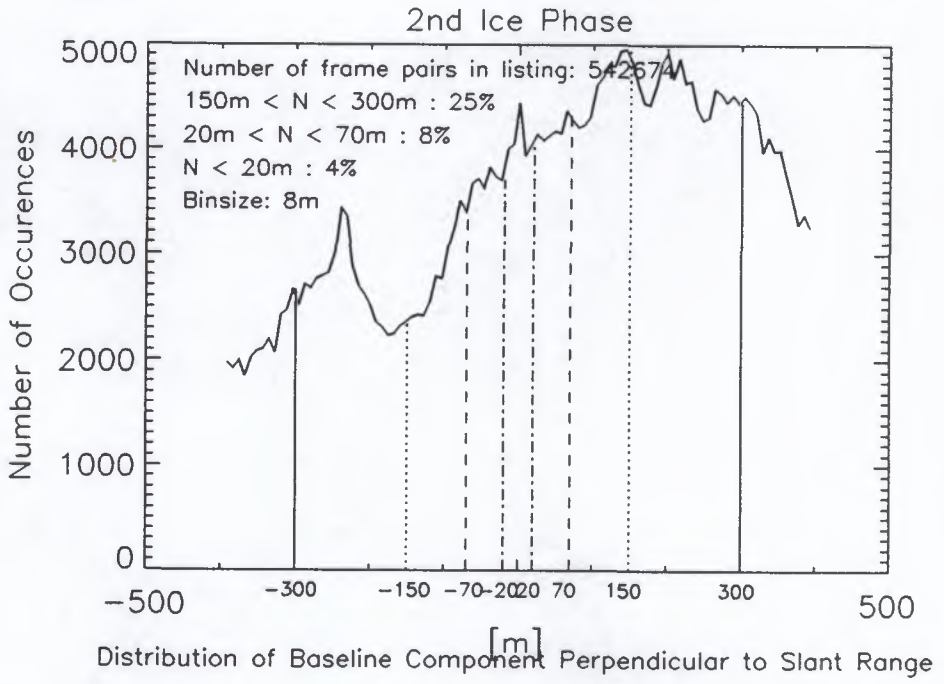

FIGURE 50. Baseline distribution for acquisitions in 2nd Ice Phase. Extract containing baselines smaller than 400m, binsize 8m.

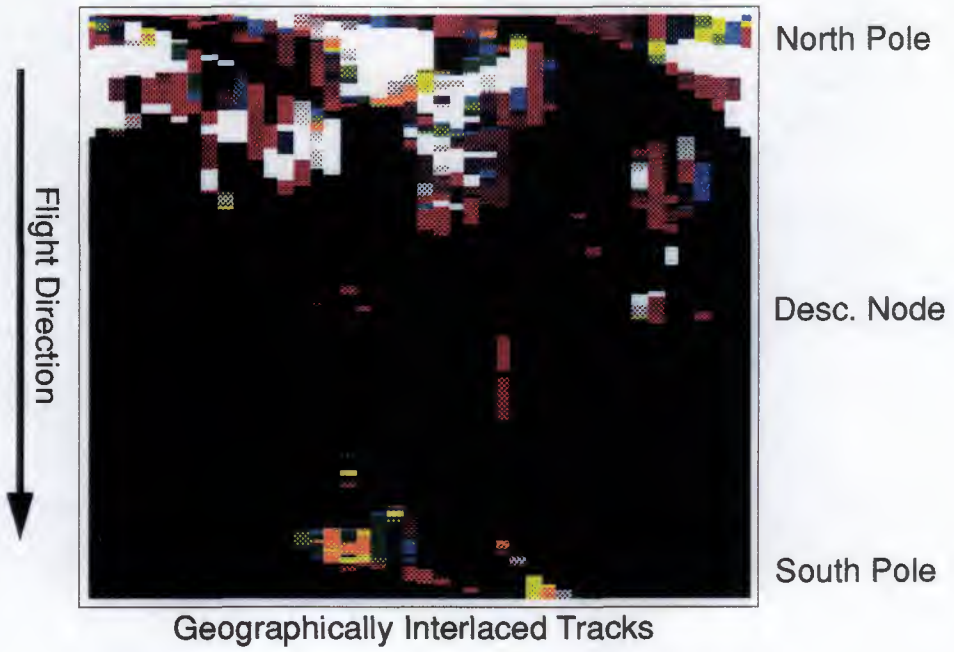

FIGURE 51. 2nd Ice phase acquisitions as seen by the full INSAR Baseline Listing (=acquisition surface for 2nd Ice Phase).
Maximum number of pairs = 561, average number of pairs over acquisition area = 31.75.

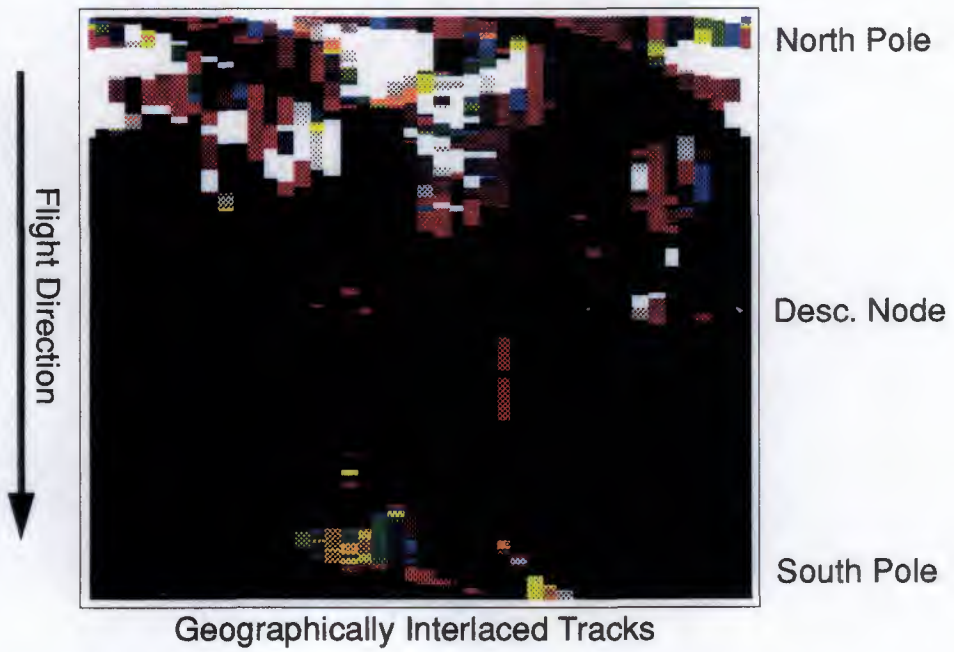

FIGURE 52. 2nd Ice phase acquisitions as seen by the INSAR Baseline Listing, filtered for |Bperp|<1100m. 98.14% of the acquisition surface covered.
Maximum number of pairs = 561, average number of pairs over acquisition area = 31.48.

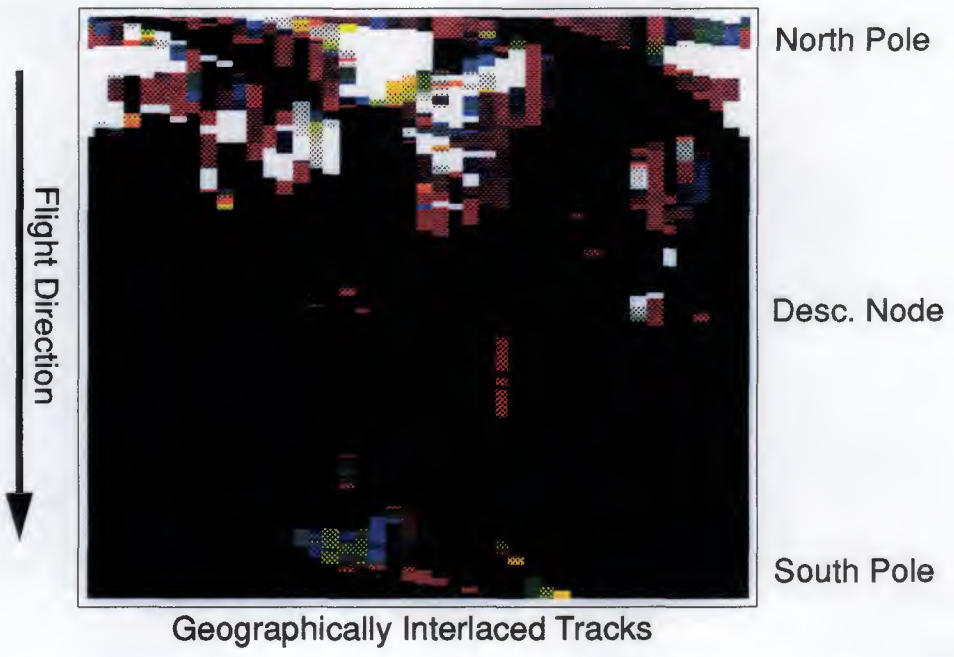

FIGURE 53. 2nd Ice phase acquisitions as seen by the INSAR Baseline Listing, filtered for |Bperp|<600m. 97.57% of the acquisition surface covered.
Maximum number of pairs = 530, average number of pairs over acquisition area = 26.72.

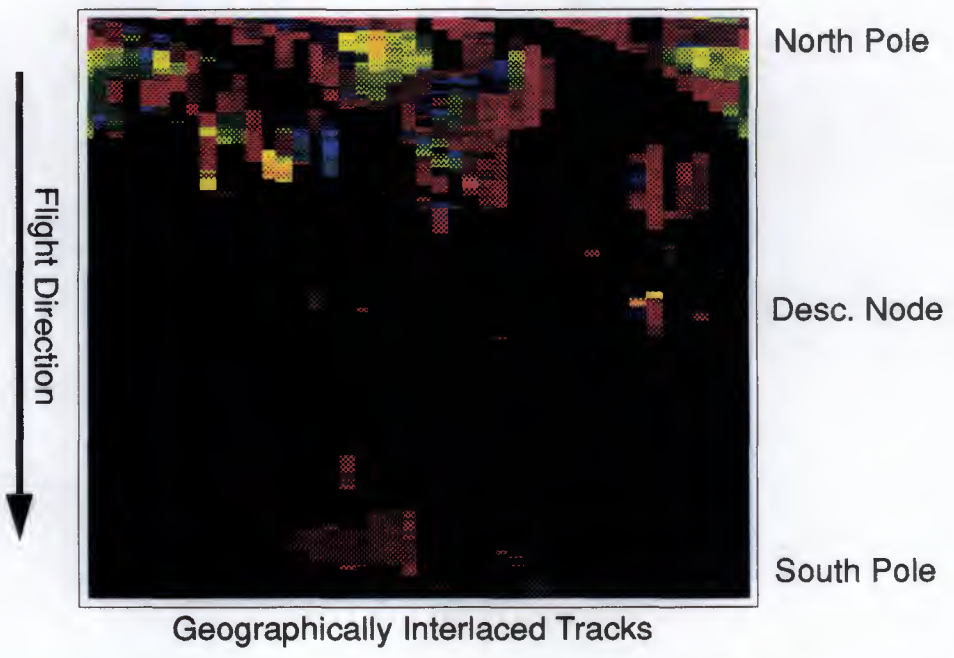

FIGURE 54. 2nd Ice phase acquisitions as seen by the INSAR Baseline Listing, filtered for 150m< |Bperp|<300m. 84.72% of the acquisition surface covered.
Maximum number of pairs = 170, average number of pairs over acquisition area = 8.22.

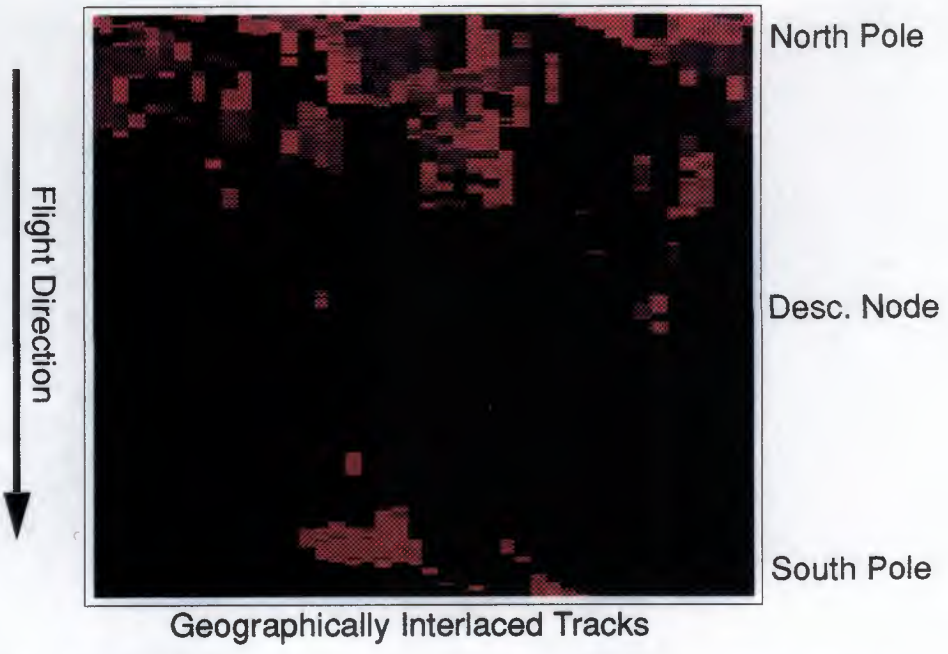

FIGURE 55. 2nd Ice phase acquisitions as seen by the INSAR Baseline Listing, filtered for 30m< |Bperp|<70m. 76.39% of the acquisition surface covered.
Maximum number of pairs = 63, average number of pairs over acquisition area = 2.58.

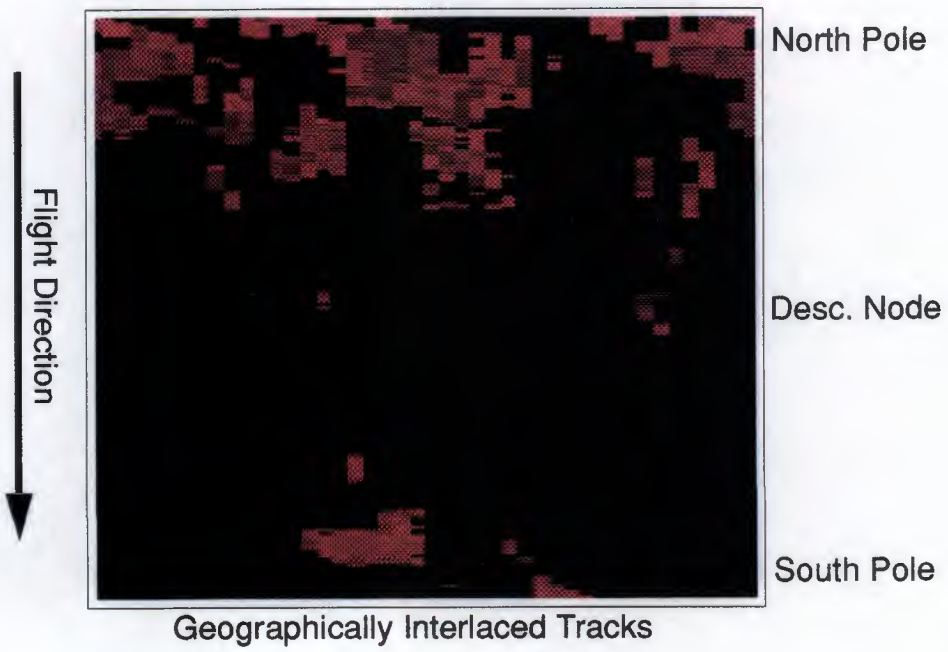

FIGURE 56. 2nd Ice phase acquisitions as seen by the INSAR Baseline Listing, filtered for |Bperp|<20m. 69.81% of the acquisition surface covered.
Maximum number of pairs = 35, average number of pairs over acquisition area = 1.45.

5.5 1st to 2nd Ice Phase.

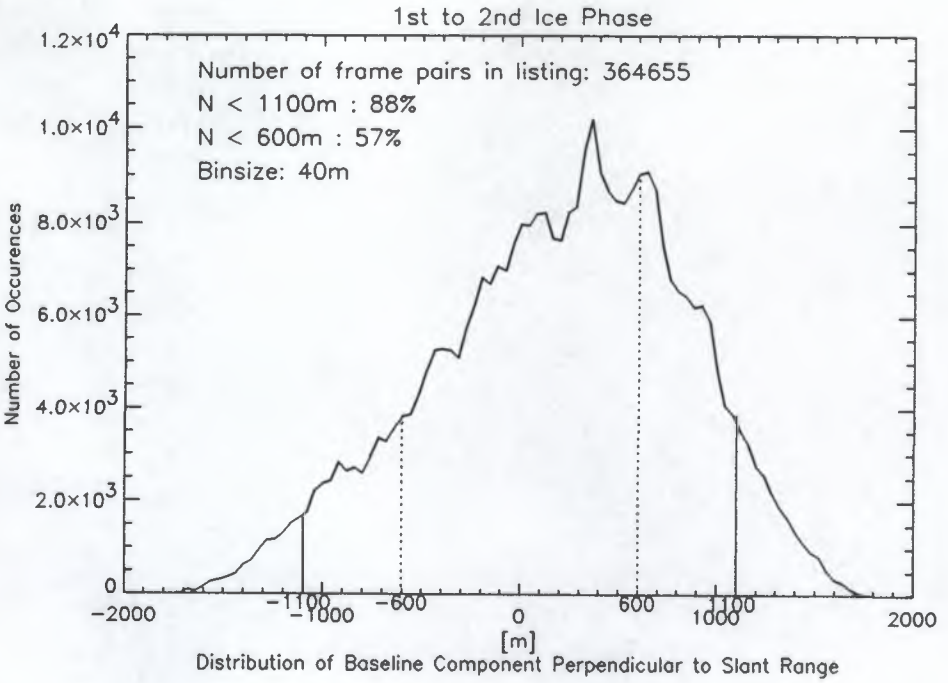

FIGURE 57. Baseline distribution for acquisitions in the 1st to 2nd Ice phase. Binsize 40m.

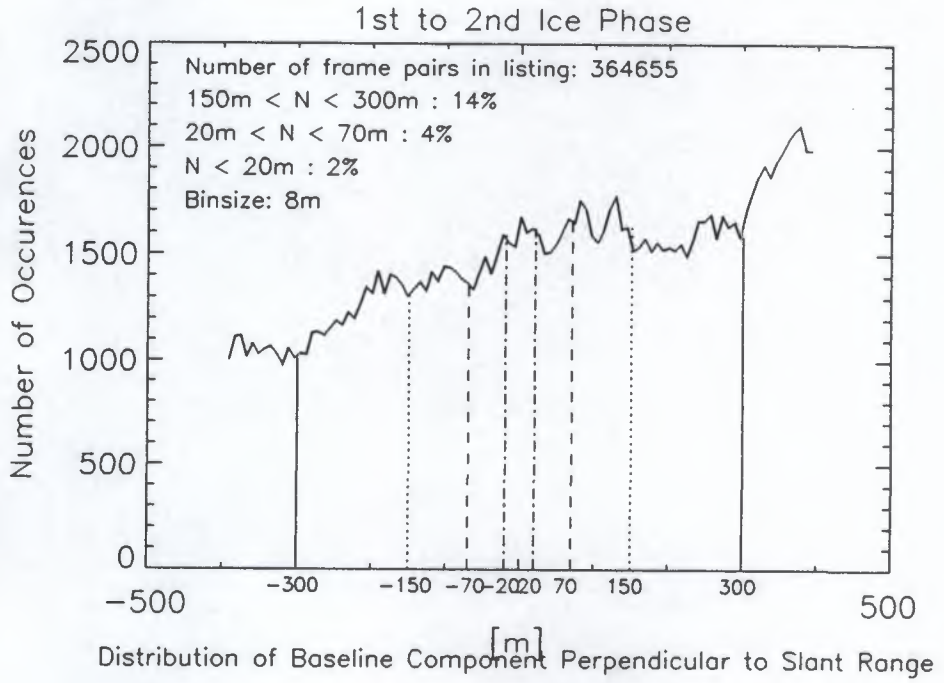

FIGURE 58. Baseline distribution for acquisitions in 1st to 2nd Ice phase. Extract containing baselines smaller than 400m, binsize 8m.

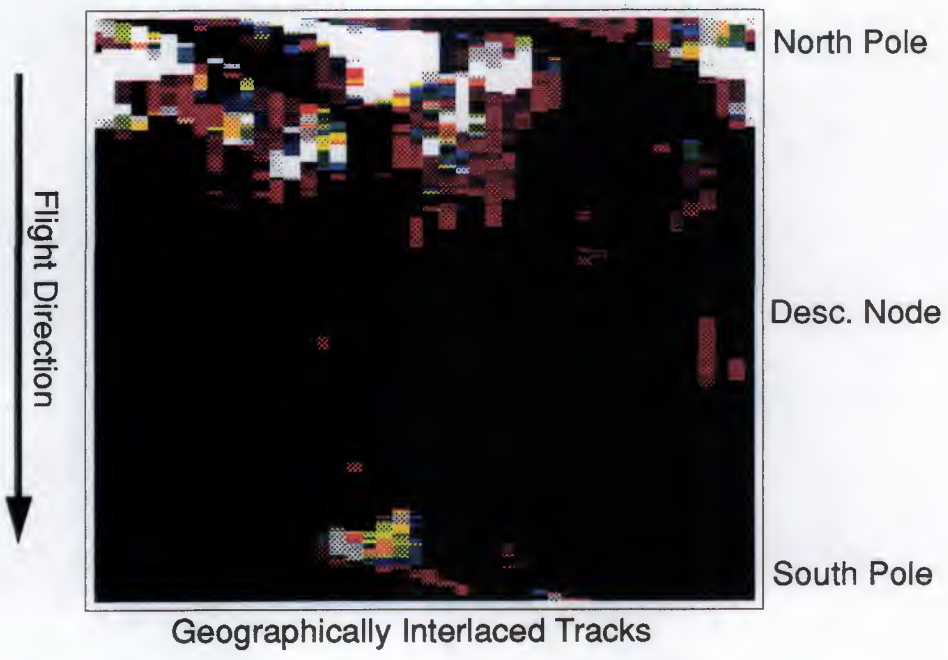

FIGURE 59. 1st to 2nd Ice phase acquisitions as seen by the full INSAR Baseline Listing (=acquisition surface for 1st to 2nd Ice Phase).
Maximum number of pairs = 589, average number of pairs over acquisition area = 23.27.

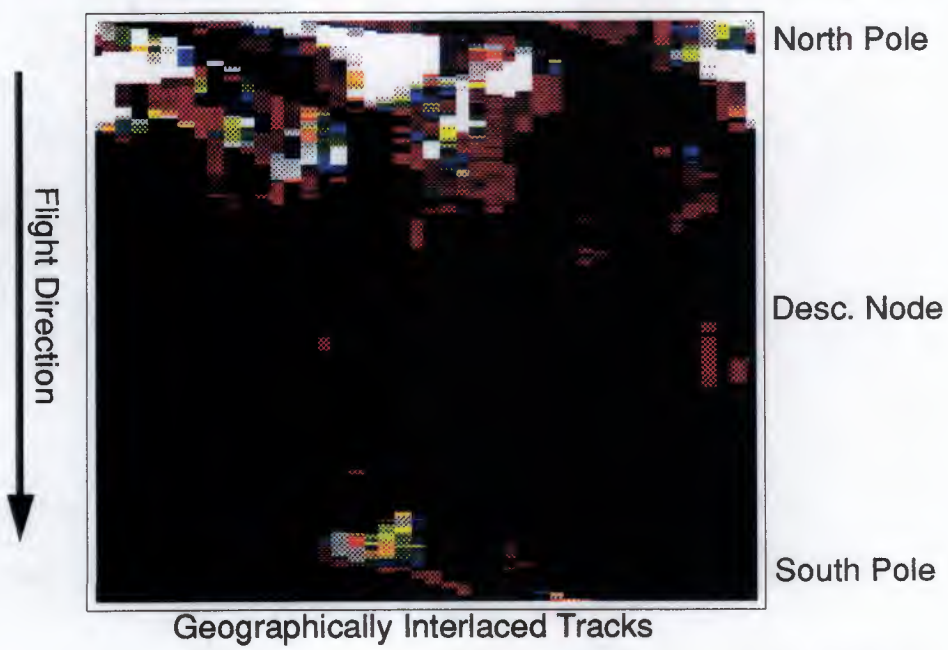

FIGURE 60. 1st to 2nd Ice phase acquisitions as seen by the INSAR Baseline Listing, filtered for |Bperp|<1100m. 99.82% of the acquisition surface covered.
Maximum number of pairs =527, average number of pairs over acquisition area = 21.50.

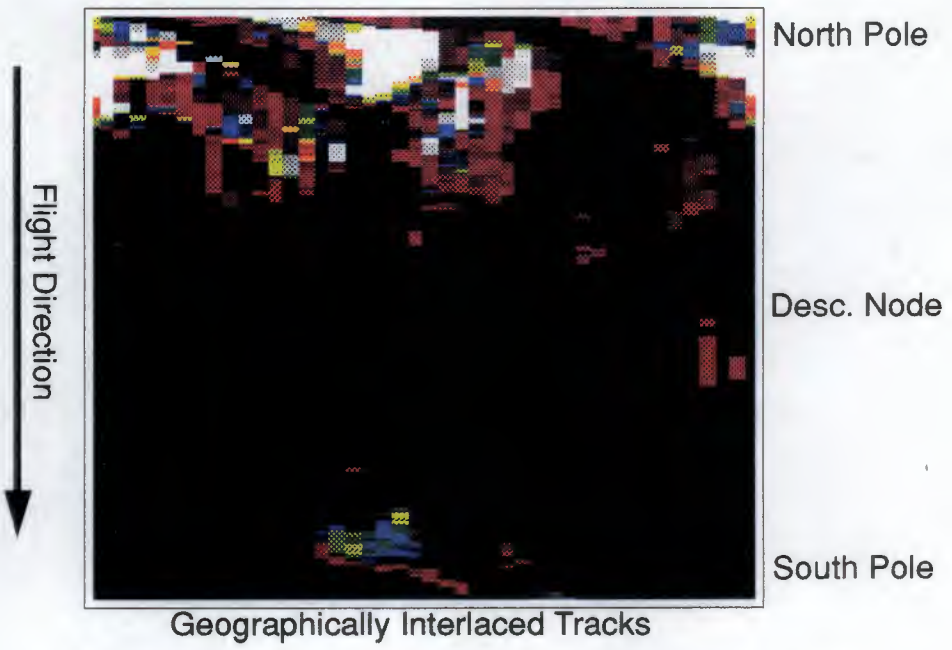

FIGURE 61. 1st to 2nd Ice phase acquisitions as seen by the INSAR Baseline Listing, filtered for |Bperp|<600m. 98.04% of the acquisition surface covered. Maximum number of pairs = 386, average number of pairs over acquisition area = 14.47.

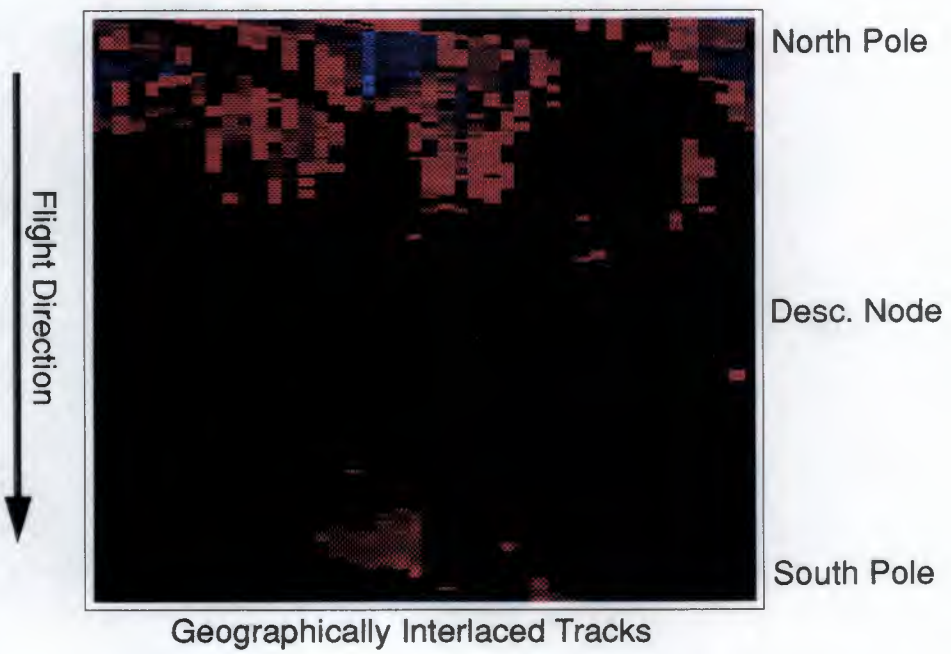

FIGURE 62. 1st to 2nd Ice phase acquisitions as seen by the INSAR Baseline Listing, filtered for 150m< |Bperp|<300m. 83.13% of the acquisition surface covered. Maximum number of pairs = 118, average number of pairs over acquisition area =3.52.

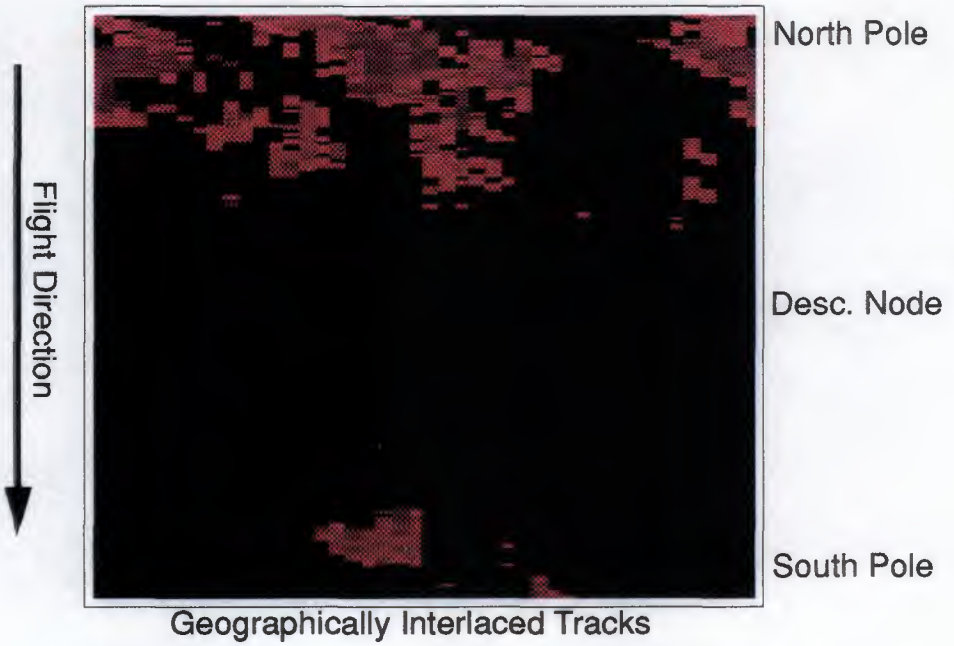

FIGURE 63. 1st to 2nd Ice phase acquisitions as seen by the INSAR Baseline Listing, filtered for 30m< |Bperp|<70m. 66.23% of the acquisition surface covered. Maximum number of pairs = 45, average number of pairs over acquisition area = 1.26.

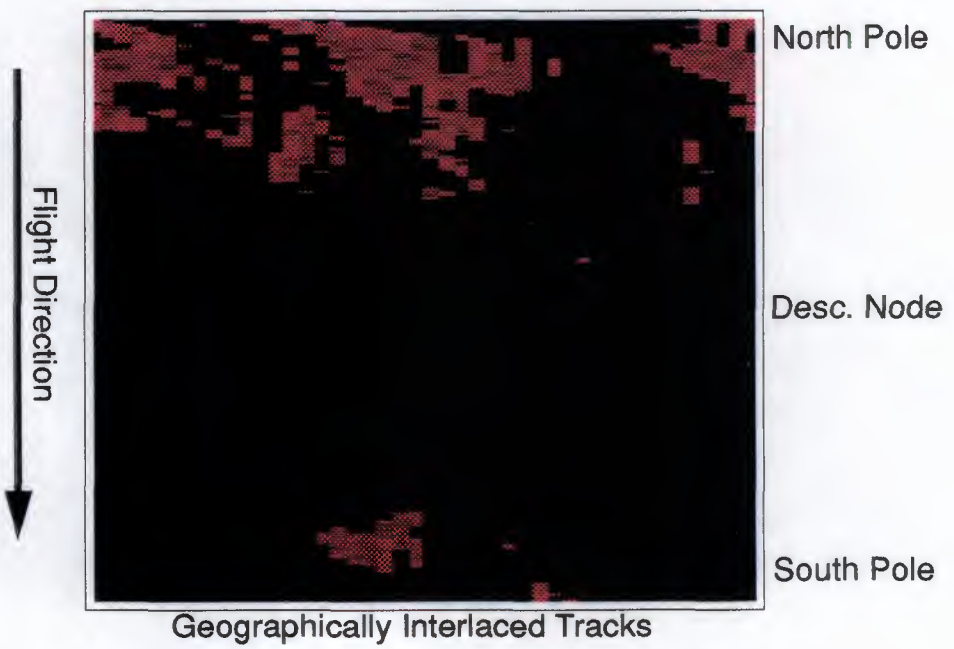

FIGURE 64. 1st to 2nd Ice phase acquisitions as seen by the INSAR Baseline Listing, filtered for |Bperp|<20m. 57.22% of the acquisition surface covered. Maximum number of pairs =25, average number of pairs over acquisition area = 0.67.

5.6 Geodetic Phase (First Four Months)

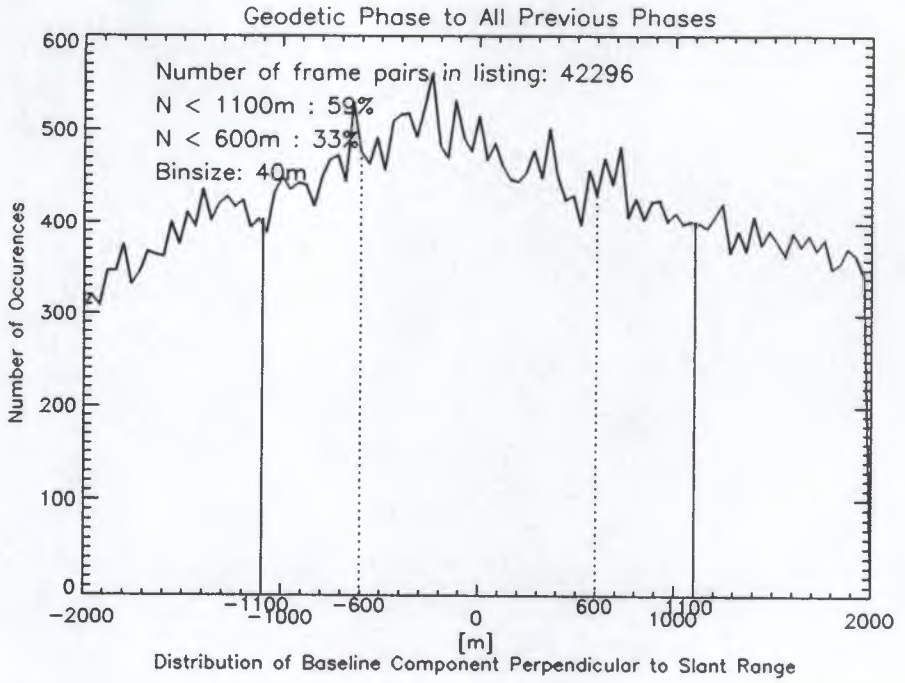

FIGURE 65. Baseline distribution for cross phase acquisitions between the Geodetic phase and all other phases. Binsize 40m.

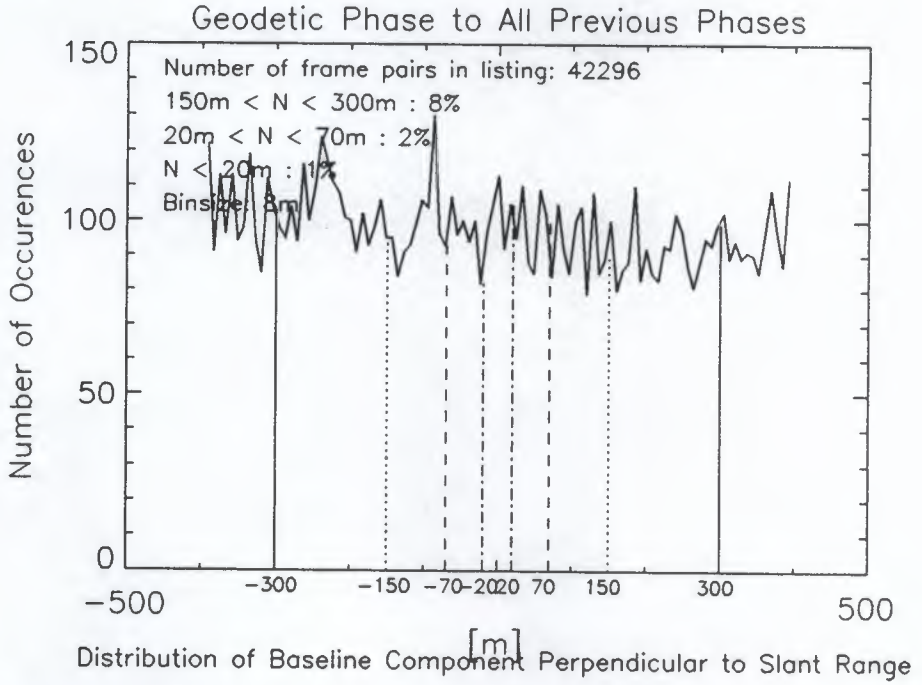

FIGURE 66. Baseline distribution for cross phase acquisitions between the Geodetic phase and all other phases. Extract containing baselines smaller than 400m, binsize 8m.

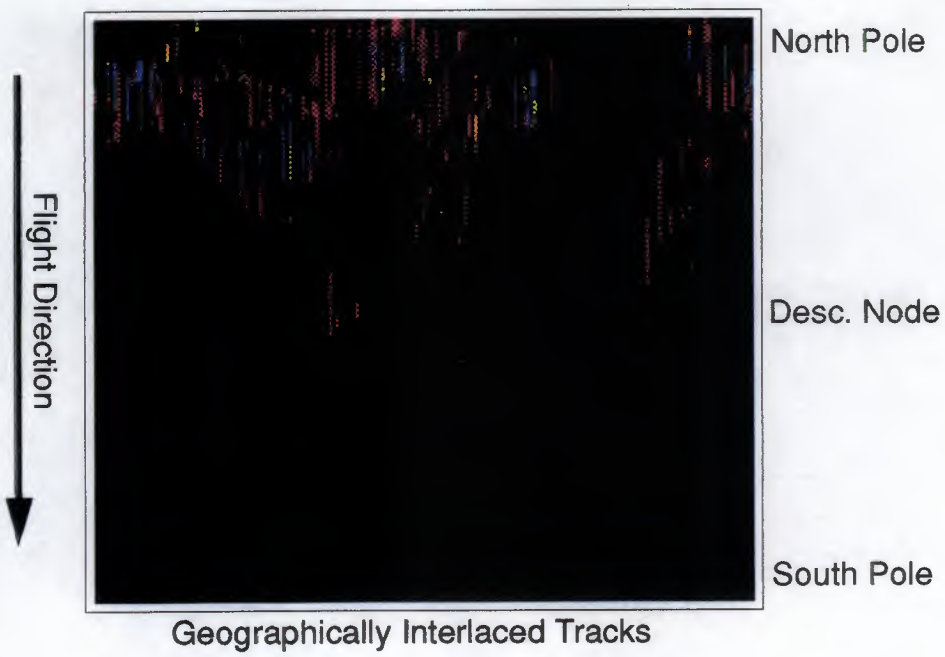

FIGURE 67. Geodeticphase acquisitions as seen by the full INSAR Baseline Listing (=acquisition surface for Geodetic Phase). Maximum number of pairs = 49.

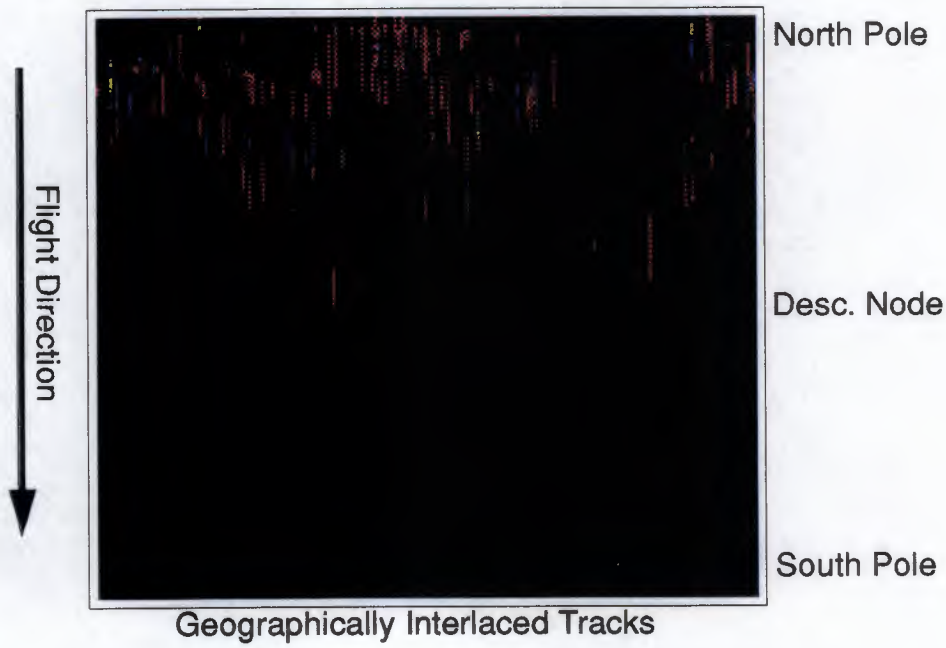

FIGURE 68. Geodetic phase acquisitions as seen by the INSAR Baseline Listing, filtered for |Bperp|<1100m. 78.8% of the acquisition surface covered. Maximum number of pairs =37.

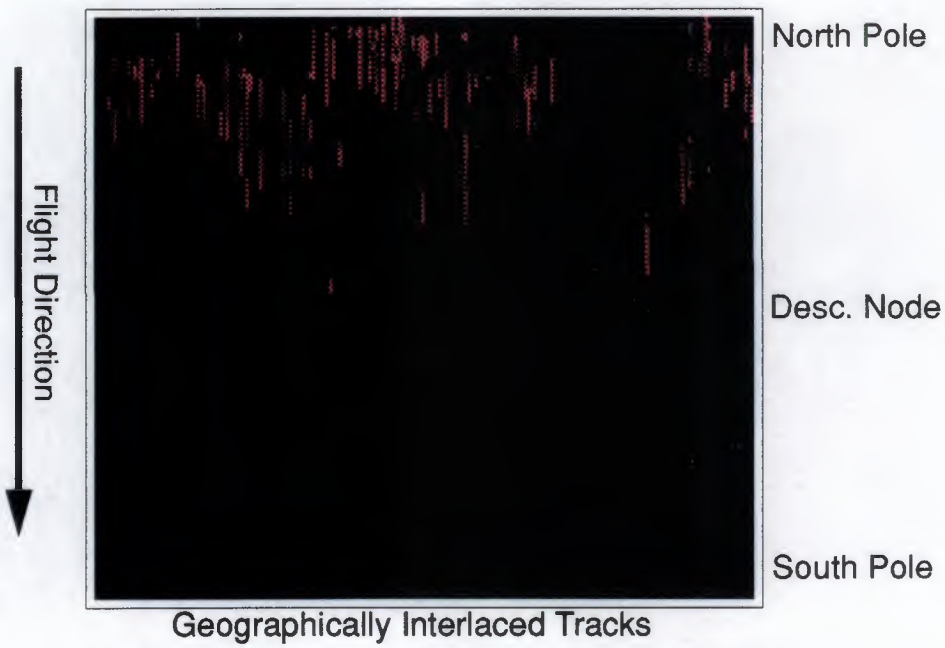

FIGURE 69. Geodetic phase acquisitions as seen by the INSAR Baseline Listing, filtered for |Bperp|<600m. 61.0% of the acquisition surface covered. Maximum number of pairs = 23.

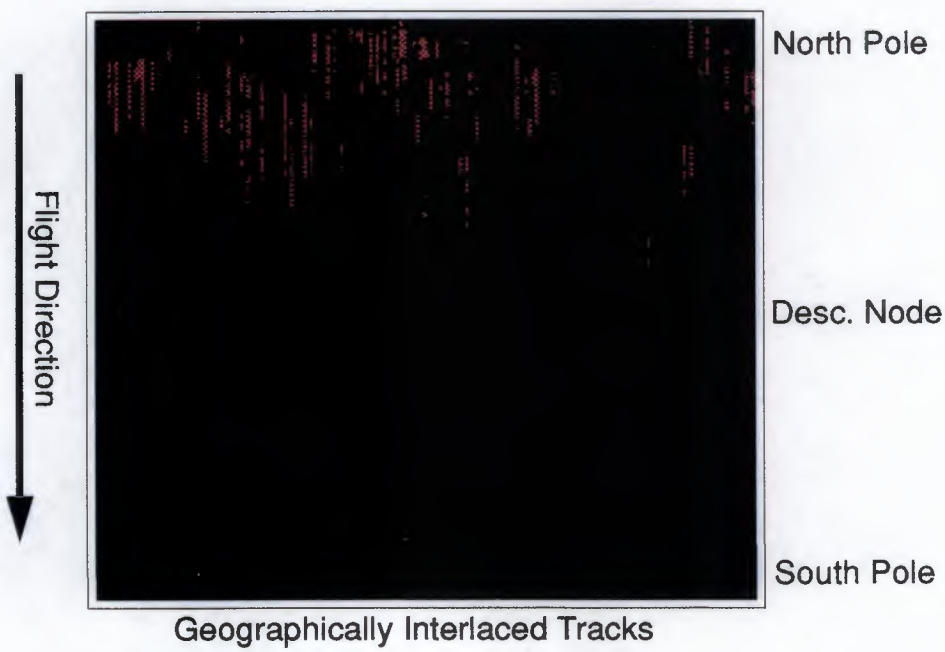

FIGURE 70. Geodetic phase acquisitions as seen by the INSAR Baseline Listing, filtered for 150m< |Bperp|<300m. 34.7% of the acquisition surface covered. Maximum number of pairs = 9.

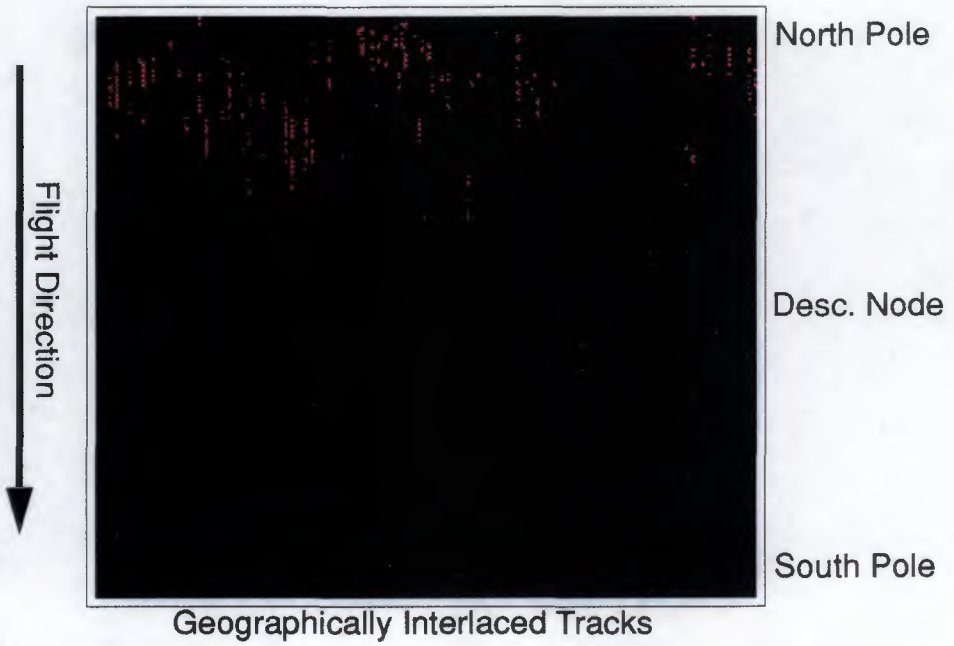

FIGURE 71. Geodetic phase acquisitions as seen by the INSAR Baseline Listing, filtered for 30m< |Bperp|<70m. 15.6% of the acquisition surface covered. Maximum number of pairs = 5.

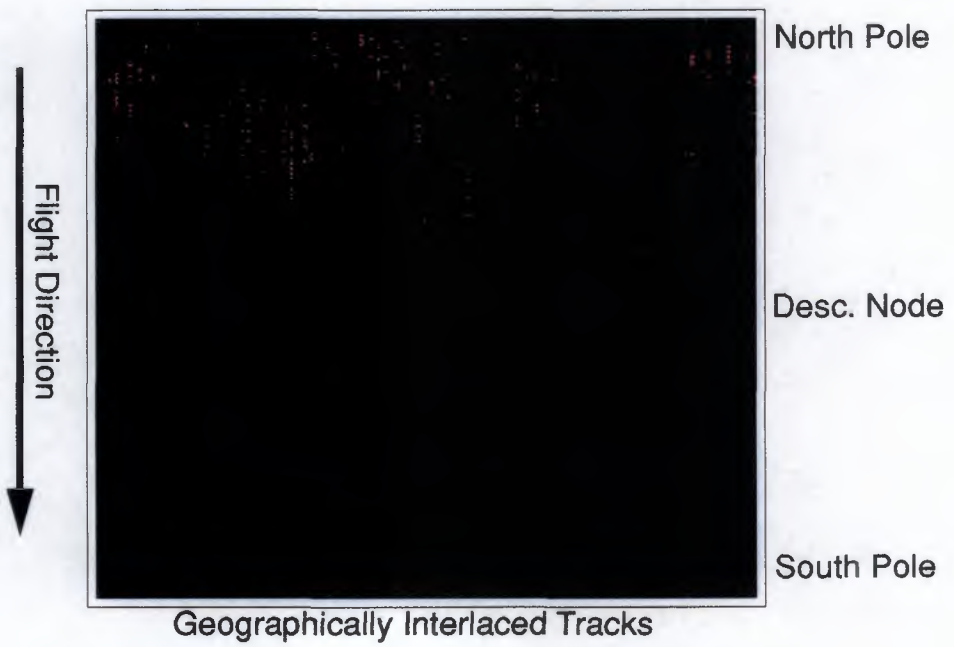

FIGURE 72. Geodetic phase acquisitions as seen by the INSAR Baseline Listing, filtered for |Bperp|<20m. 8.9% of the acquisition surface covered. Maximum number of pairs =4.

6.0 Conclusions.

6.1 INSAR Baseline Accuracy.

Several verification tests of the INSAR Baseline algorithm have been performed using independent methods and the results compared with the theoretical accuracy of the algorithm. These tests have established confidence in the algorithm and in its implementation. The results are summarised in Table 13.

The algorithm is implemented with internal consistency checks based on orbit propagation in forward and reverse direction so as to ensure that the closest point of approach between any two orbits is identified to within ± 1m along track.

By comparing baselines for interferometric pairs separated by multiple repeat cycles with the cumulative baselines for all intervening pairs, an error bound of 5m has been established for the algorithm. If an orbit with frames at midnight had been tested we would have got a higher error-bound due to inconsistencies between some of the restituted orbit files.

The difference between the theoretical 3-sigma error estimate (25m) and the found 5m absolute error bound, indicates that the algorithm performs better than our simple error analysis. This may be explained by correlated error sources on repeat orbits.

Baselines derived with this algorithm have been compared with those derived by independent workers using both orbit propagation and SAR data analysis for 12 sites worldwide. The results are consistent when considering the uncertainty of along track positioning of the measurement points. The results indicate that this error bound is dominated by random effects. The highest errors were found in this test, which then gives the upper estimate of the error bound.

This level of accuracy is sufficient for the proposed use of the INSAR Baseline Listing, which is to identify suitable INSAR acquisition pairs.

For Surface Motion Detection applications the frame based algorithm is accurate enough to identify image pairs where the baseline is of the order of a few meters. The exact location of the nearest point of approach of the two orbits will not be possible with the established accuracy. To obtain such accuracy Precise orbit files and two baseline estimations per frame should be applied.

The INSAR Baseline algorithm has been applied to the whole of the ESR-1 Commissioning phase, the 1st and 2nd Ice phase as well as the whole Multidisciplinary phase and the first few months of the Geodetic phase.

The resulting listings are available on-line and partly in printed version.

Members of ERS Fringe Group (coordinated by ESA/ESRIN) have been testing the INSAR Baseline Listing, either by using it for identification of image pairs or for comparison with their own baseline estimations.

TABLE 13. INSAR Baseline accuracy tests and results.

Test Title	Test Description	Accuracy
2.2 Theoretical worst case accuracy.	2*3σ for the two restituted orbits plus maximum error of the orbit propagator	**|B| < 25m** 3-sigma rms
3.1 Observed internal consistency of the algorithm.	Shifting of baselines into common reference system.	**|Bperp| < 5m** absolute error, (random + systematic)
3.2 Observed external consistency with precision orbit propagator.	Comparison between the algorithm and ESOC derived data with correction of along track displacement between the two datasets.	**|B| < 6m** absolute error, (random + systematic)
3.3 Observed external consistency by study of orbit inclination drift.	The inclination drift phenomena is verified to be observed and measured accurately by the INSAR Baseline Listing.	No error bound on B *
3.4 Observed agreement with baseline values derived by INSAR scientists.	Baselines found by frequency analysis of the images have been scaled to correct for nominal parameter values. Orbit derived data have been compared directly.	**|Bperp| < 9m** absolute error, (random only) **|Bperp| < 10m** absolute error, (random + systematic)
3.5 Observed restituted orbit inconsistencies	Found by two way propagation at all day changes in the ERS-1 mission phases.	**|Bperp|<7m**

* The inclination drift study gives no absolute error bound on B, but establishes confidence in the data indirectly by the observation of physically known phenomena.

6.2 Interferometric Opportunity with the ERS Missions.

Present status:

The statistics generated from the INSAR Baseline Listing have shown that there exists a large archive of ERS-1 SAR data suitable for interferometric applications. The results are listed below in table 11.

TABLE 14. Present INSAR potential.

Application	Baseline regime	Measured performance*		
		% A,B,C[1]	% D[2]	% E[3]
Practical INSAR limit:	$B_{perp} < 600$ m	50 - 57	85	36
Digital Terrain Models:	150m < B_{perp} < 300m	13 - 15	26	9
Surface Change Detection:	30m < B_{perp} < 70m	4 - 5	9	3
Surface Feature Movement:	$B_{perp} < 5$m **	2 - 3	4	1

1) 1 km deadband orbit maintenance strategy.
2) Orbit maintenance strategy with increased inclination manoeuvre frequency.
3) Cross phase baselines only (6 to 12 km radial component and higher baseline change ratio).

* Percentage of all identified acquisition pair combinations.
** For practical reasons a 20m limit was applied in the statistical survey.

Further potential:

It has been demonstrated that SAR interferometric applications require a precise set of orbital criteria to be met. The frequency with which ERS-1 satisfies these has been studied.

Analysis of the ERS-1 baseline statistics has shown spatial and temporal trends in the baseline distributions which are correlated with external factors influencing the orbit. Examples of such factors are: solar activity, solar and lunar gravitational effects, and orbit manoeuvres. The analysis of the baseline statistics gives a useful insight into the impact of any particular orbital maintenance strategy upon interferometric applications.

The orbit maintenance strategy for the 2nd Ice phase of ERS-1 takes this into account in order to yield even higher probability of obtaining interferometric pairs than in preceding phases of the mission.

The significant increase of good baselines in the 2nd Ice phase is a strong argument for increasing the inclination manoeuvre frequency also for future ERS operations.

7.0 References.

1 M. Giani, C. Prati, F. Rocca, ESA Contract no. 8928/90/F/BZ, "Study on SAR Interferometry and its Applications"

2 M. Rosengren, ESA/ESOC/FCSD/OAD/STB, "ERS-1 - An Earth Observer that Exactly Follows Its Chosen Path", ESA bulletin number 72, November 1.

3 M. Rosengren, ESA/ESOC/FCSD/OAD/STB, "The Orbit Control Of ERS-1, AAS 93-308".

4 G. Aa. Solaas, ESA/ESRIN/DPE/OM, "SAR Interferometry Orbit Listing, Volume 1 to 3".

5 "TechnicalNote on ERS-1 CUS Data Product Identifier, ER-TN-EPO-GU-1003-1.1 Issue 1, Rev. 1", 05 May 1989.

8.0 Annex I: INSAR Baseline Comparison.

As explained in section 3.4 two different approaches to the INSAR Baseline estimation are currently used.

Method 1:

Analysis of orbital data by orbit propagation techniques similar to the ones used for the INSAR Baseline Listing.

Method 2:

Measurement of the frequency spectrum shift of the two complex SAR images used to create the interferogram. The shift can be related to the baseline through a known formula (see equation 1).

Further down we present the numbers that were referred to in section 3.4. The INSAR Baseline Listing contents have been compared with INSAR Baselines supplied by scientists in the INSAR user community (FRINGE group).

Where two numbers are given in any column the number in **bold** identifies the number related to the frame based algorithm. Where only one number is given in an ESRIN column this identifies the UTC based algorithm.

8.1 Method 1: Orbit Determined Baselines.

8.1.1 Institute: University of Zürich, Site: BONN.

Lat: 50.75 N, Lon: 7.0 E

In the following measurements the timing marks of minute 36 (37 for reference orbit = 3287 and 3545) was used. The satellite position was within the following boundaries: 49.9 - 50.3 latitude and 11.0 - 11.3 longitude. Bonn is situated at 50.75 latitude and 7 longitude, which is so close to the timing point that we use the given values without interpolation.

Orbits		B Across ESRIN Zurich		B Radial ESRIN Zurich		B ⊥ Slant Range ESRIN Zurich		Δ
3459	3502	-450	-456	7	7	-420 **-423**	-420	0 **-3**
3459	3545	-970	-983	-41	-42	-924 **-932**	-927	3 **-5**
3459	3674	161	159	-45	-46	135 **134**	131	4 **3**
3502	3545	-521	-527	-47	-49	-505 **-508**	-507	2 **-1**
3502	3674	613	615	-51	-52	557 **558**	551	6 **7**
3545	3674	1138	1142	-3	-4	1065 **1067**	1057	8 **10**

8.1.2 Institute: University of Zurich, Site: LOETSCHENTAL.

Lat: 63.8 N, Lon: 20.3 W

Minute 12: Lat: 40.5 N, Lon: 5.4 E Bl: 137 P_SR: -28
Minute 13: Lat: 45.7 N, Lon: 3.9 E Bl: 142 P_SR: -4
Minute 14: Lat: 49.2 N, Lon: 2.5 E Bl: 147 P_SR: 10

The big difference in position forces us to use interpolation.
With linear approach and 0.5 interval we obtain the following results:

Orbits	B Across ESRIN	B Radial ESRIN	B ⊥ Slant Range ESRIN	ZÜRICH	DELTA
3086 3129	-53m	134m	0m	5m	5m

8.1.3 Institute: JPL, Site: TOOLIK LAKE.

Lat: 68.7 N, Lon: 150.9 W

1st pair:

Minute 30: Lat: 68.1 N, Lon: 2.4 E Bl: 381 P_SR: 375
Minute 31: Lat: 69.0 N, Lon: 140.4 W Bl: 106 P_SR: 50
Minute 32: Lat: 65.7 N, Lon: 144.1 W Bl: 110 P_SR: 18

2nd pair:

Minute 30: Lat: 68.2 N, Lon: 2.5 E Bl: 46 P_SR: -42
Minute 31: Lat: 68.9 N, Lon: 140.5 W Bl: 227 P_SR: 196
Minute 32: Lat: 65.6 N, Lon: 144.2 W Bl: 247 P_SR: 215

The small difference in position enables direct use of the minute 34 values.

Orbits	Acr.	Rad.	Baseline ESRIN	Zebker	Δ	B ⊥ Slant Range ESRIN	Zebker	Δ
943 1029	14	105	106	106	0	50	40	10
1029 1072	224	-37	227	233	-6	196	201	-5

8.1.4 Institute: JPL, Site: MANLEY HOT SPRINGS.

Lat: 64.9 N, Lon: 149.3 W

Minute 18: Lat: 60.3 N, Lon: 154.2 W Bl: 232 P_SR: 208
Minute 19: Lat: 63.7 N, Lon: 156.9 W Bl: 196 P_SR: 174
Minute 20: Lat: 67.1 N, Lon: 160.3 W Bl: 160 P_SR: 139

The small difference in position enables direct use of the minute 19 values.

Orbits	B Acr.	B Rad.	Baseline ESRIN	Zebker	Δ	B ⊥ Slant Range ESRIN	Zebker	Δ
982 935	194	-23	196	178	18	-45	-45	0

8.1.5 Institute: JPL, Site: MT. KATMAI.

Lat: 58.3 N, Lon: 155.0 W

1st pair:

Minute 33: Lat: 62.3 N, Lon: 147.2 W Bl: 123 P_SR: -13
Minute 34: Lat: 58.9 N, Lon: 149.6 W Bl: 144 P_SR: -45
Minute 35: Lat: 55.4 N, Lon: 151.6 W Bl: 169 P_SR: -77

2nd pair:

Minute 33: Lat: 61.8 N, Lon: 147.5 W Bl: 97 P_SR: 60
Minute 34: Lat: 58.4 N, Lon: 149.9 W Bl: 99 P_SR: 63
Minute 35: Lat: 55.0 N, Lon: 151.9 W Bl: 101 P_SR: 65

The small difference in position enables direct use of the minute 34 values.

Orbits	B Acr.	B Rad.	Baseline ESRIN	Zebker	Δ	B ⊥ Slant Range ESRIN	Zebker	Δ
943 1029	14	105	144	144	0	-45	-45	0
1459 1502	86	-49	99	99	0	63	62	1

8.1.6 Institute: JPL, Site: SHISHALDIN VOLCANO.

Lat: 64.9 N, Lon: 149.3 W

Minute 14: Lat: 49.3 N, Lon: 166.9 W Bl: 88 P_SR: -82
Minute 15: Lat: 52.8 N, Lon: 169.5 W Bl: 62 P_SR: -56
Minute 16: Lat: 56.3 N, Lon: 170.3 W Bl: 36 P_SR: -31
Minute 17: Lat: 59.7 N, Lon: 172.4 W Bl: -9 P_SR: -5

The big difference in position forces us to use interpolation. With linear approach and 0.5 interval we obtain the following results:

Orbits	B Acr.	B Rad.	Baseline ESRIN	Zebker	Δ	B ⊥ Slant Range ESRIN	Zebker	Δ
2670 2713	48	3	49	49	0	-44	-44	0

8.1.7 Institute: JPL, Site: PISGAH LAVA FLOW.

Lat: 64.9 N, Lon: 149.3 W

Minute 40: Lat: 36.6 N, Lon: 169.5 W Bl: 94 P_SR: -67
Minute 41: Lat: 33.1 N, Lon: 170.3 W Bl: 129 P_SR: -103

The big difference in position forces us to use interpolation. With linear approach and 0.3 interval we obtain the following results:

Orbits	B Acr.	B Rad.	Baseline ESRIN	Zebker	Δ	B ⊥ Slant Range ESRIN	Zebker	Δ
5783 6284	-110	35	115	113	2	91	90	1

8.2 Method 2: Image Derived Baselines.

8.2.1 Institute: POLIMI, Site: BONN.

Lat: 50.75 N, Lon: 7.0 E

Direct use of minute 36 and 37, without interpolation.

Orbits	B Across ESRIN	B Radial ESRIN	B ⊥ Slant Range ESRIN	POLIMI	Δ(1.189)
3287 3330	766	-9	714 **716**	601	0 **-1**
3287 3373	1488	-4	1394 **1397**	1174	-1 **-4**
3287 3416	1748	-3	1638 **1641**	1382	-5 **-9**
3287 3459	1534	1	1438 **1442**	1214	-5 **-7**
3287 3502	1081	8	1016 **1018**	853	1 **0**
3287 3545	558	-39	509 **509**	427	1 **0**
3287 3588	1490	-45	1381 **1383**	1153	10 **6**
3287 3631	1813	-45	1684 **1687**	1418	-2 **-6**
3287 3674	1694	-43	1573 **1576**	1322	1 **-2**
3330 3373	722	5	678 **681**	573	-3 **-3**
3330 3416	981	6	922 **926**	781	-6 **-6**
3330 3459	767	11	723 **726**	613	-5 **-5**
3330 3502	315	18	301 **302**	258	-5 **-6**
3330 3545	-205	-29	-203 **-206**	-171	0 **-1**
3330 3588	724	-35	666 **667**	559	1 **0**
3330 3631	1047	-35	969 **971**	817	-2 **-4**
3330 3674	928	-33	858 **860**	721	0 **0**
3373 3416	259	1	244 **245**	208	-3 **-3**
3373 3459	45	6	45 **45**	39	-1 **-1**
3373 3502	-405	13	-375 **-378**	-318	3 **1**
3373 3545	-925	-34	-879 **-887**	-739	0 **-4**
3373 3588	3	-40	-10 **-13**	-12	4 **1**
3373 3631	325	-40	290 **290**	246	-2 **-3**
3373 3674	206	-38	180 **179**	150	1 **0**
3416 3459	-213	5	-198 **-199**	-168	1 **1**
3416 3502	-664	12	-618 **-623**	-523	3 **1**
3416 3545	-1183	-36	-1122 **-1132**	-949	6 **1**
3416 3588	-255	-41	-254 **-258**	-222	9 **7**
3416 3631	66	-41	47 **45**	36	4 **2**
3416 3674	-52	-39	-63 **-65**	-57	4 **3**
3459 3502	-450	7	-420 **-423**	-354	0 **0**
3459 3545	-970	-41	-924 **-932**	-781	4 **0**

3459 3588	-42	-46	-55 **-58**	-51	5 **2**
3459 3631	280	-47	246 **245**	204	3 **1**
3459 3674	161	-45	135 **134**	110	4 **2**
3502 3545	-521	-47	-505 **-508**	-427	2 **1**
3502 3588	409	-53	365 **365**	306	1 **-9**
3502 3631	732	-53	667 **669**	559	2 **1**
3502 3674	613	-51	557 **558**	469	0 **-1**
3545 3588	933	-5	873 **874**	728	7 **4**
3545 3631	1257	-5	1176 **1178**	985	4 **1**
3545 3674	1138	-3	1065 **1067**	889	7 **5**
3588 3631	323	0	303 **304**	258	-3 **-4**
3588 3674	204	2	192 **193**	162	0 **0**
3631 3674	-118	2	-110 **-110**	-93	0 **1**

8.2.2 Institute: CTH, Sweden, Site: UMEÄ.

Lat:63.8 N, Lon:20.3 W

Minute 31:	Lat: 69.4 N,	Lon: 33.7 E	Bl: 78	P_SR: 71
Minute 32:	Lat: 65.7 N,	Lon: 29.9 E	Bl: 57	P_SR: 51
Minute 33:	Lat: 62.4 N,	Lon: 26.8 E	Bl: 35	P_SR: 31
Minute 33:	Lat: 59.5 N,	Lon: 23.6 E	Bl: 13	P_SR: 10

The along track disalignment of the UTC minute positions forces us to use interpolation to derive the baseline at the right latitude.
With linear interpolation and 0.5 minute interval we obtain the following results:

Orbits	B Across ESRIN	B Radial ESRIN	B ⊥ Slant Range ESRIN Ulander Δ(1.083)		
3086 3129	46m	-4m	41m **39m**	33m	5m **2m**
3086 3172	-283m	-43m	-281m **-288m**	-260m	0m **0m**
3086 3215	-210m	-64m	-219m **-226m**	-212m	10m **8m**
3086 3258	-301m	-37m	-295m **-303m**	-270m	-2m **-4m**
3129 3172	-329m	-38m	-322m **-327m**	-290m	-7m **-6m**
3129 3215	-256m	-59m	-261m **-365m**	-245m	4m **5m**
3129 3258	-348m	-32m	-337m **-342m**	-303m	-8m **-7m**
3172 3215	74m	-20m	62m **62m**	51m	-6m **5m**
3172 3258	-18m	6m	-14m **-14m**	-12m	-1m **0m**
3215 3258	-91m	27m	-76m **-76m**	-62m	-8m **-7m**
3645 3688	-163m	5m	-152m	-140m	12m

- the last pair is disconnected from the prior orbits, and has therefore not been scaled.

8.2.3 Institute: CNES, Site: ETNA.

Lat: 37.5 N, Lon: 15.0 E

1st pair:

Minute 10:	Lat: 34.2 N	Lon: 12.7 E	BL: 198	P_SR: 191
Minute 11:	Lat: 37.8 N	Lon: 11.6 E	BL: 220	P_SR: 212

The small differences in latitude enables direct use of the minute 11 values. Because of missing lines in the raw data the image derived baselines may be of varying quality.

	Orbits	Radius, Theta	B Across, B Radial	B Δ Acr., B Δ Rad.
CNES	5785 8290	230m 10.4°	226m 41m	
ESRIN		220m 5.2°	219m 20m	7m 21m
CNES	6286 6787	220m 185.8°	-219m -22m	
ESRIN		189m 180.0°	-189m 0m	-30m -22m
CNES	6286 8791	496m ?°	496m -55m	Supposed -6.4°
ESRIN		467m -6.4°	464m -52m	32m -3m
CNES	6787 8290	233m -171.0°	-217m -34m	
ESRIN		218m -177.1°	-218m -11	1m -23m
CNES	7288 8791	8791	564m -?°	Supposed -175.5°
ESRIN		-516m -41m	-516m -41m	-46m -3m

8.2.4 Institute: CNES, Site: SPITSBERG (SVALBARD).

Lat: 79 N, Lon: 13.0 E

This is to far north to use the latitude as an indication of the local interpolation to be performed. We therefore make use of the frame number supplied by CNES, which leads to minute 22.5. Uncertainty in the along track positioning is here of importance since the baseline is changing rapidly.

	Orbits	Radius, Theta	B Across, B Radial	B Δ Acr., B Δ Rad.
CNES	899 985	175m - 193m -?°	174m 18m *	Supposed 6.0°
ESRIN		198m 6.0°	197m 21m	-22m -2m
CNES	985 1114	204m - 141m ?°	139m -19m *	Supposed -7.8°
ESRIN		184m -7.8°	182m -25m	-42m 6m

- worst case estimate in the given baseline range (best estimate gives near zero error).

8.2.5 Institute: CNES, Site: LOS ANGELES.

Lat: 34.0 N, Lon: 118 W

1st pair:

Minute 40:	Lat: 38.5 N,	Lon: 113.5 W	BL: 177	P_SR: 136
Minute 41:	Lat: 35.0 N,	Lon: 112.4 W	BL: 153	P_SR: 107

2nd pair:

Minute 40:	Lat: 39.3 N,	Lon: 113.7 W	BL: 496	P_SR: 450
Minute 41:	Lat: 35.7 N,	Lon: 112.6 W	BL: 501	P_SR: 455

The difference in latitude indicates extrapolation by 0.3 in the first case and by 0.5 in the second case.

	Orbits	Radius, Theta	B Across, B Radial	B Δ Acr., B Δ Rad.
CNES	4051 5554	141m -24.7°	128m -59m	
ESRIN		146m -27.4°	129m -67m	-1m 8m
CNES	5053 5554	497m -2.6°	497m -22m	
ESRIN		503m -4.3°	502m -38m	-5m 16m

8.2.6 Institute: CNES, Site: UKRAINE.

Minute 12:	Lat: 40.5 N,	Lon: 30.9 E,	BL: 98m	P_SR= -87m
Minute 13:	Lat: 44.0 N,	Lon: 29.9 E,	BL: 82m	P_SR= -71m
Minute 14:	Lat: 47.5 N,	Lon: 28.3 E,	BL: 65m	P_SR= -55m
Minute 15:	Lat: 51.0 N,	Lon: 26.8 E,	BL: 48m	P_SR= -39m
Minute 16:	Lat: 54.5 N,	Lon: 25.1 E,	BL: 31m	P_SR= -23m
Minute 17:	Lat: 58.0 N,	Lon: 23.2 E,	BL: 15m	P_SR= -7m
Minute 18:	Lat: 61.4 N,	Lon: 20.8 E,	BL: 10m	P_SR= 8m

The frame information given by CNES indicates the use of minute 13, 15 and 17.

1014 1100	Frame	Radius, Theta	B Across, B Radial	B Δ Acr., B Δ Rad.
CNES	927	70m 171°	-69m 11m	
ESRIN		82m 172°	-80m 11m	11m 0m
CNES	1082	42m 169°	-47m 8m	
ESRIN		48m 168°	-46m 10m	1m -2m
CNES	1237	15m 160°	-14m 5m	
ESRIN		15m 129°	-11m 9m	3m -4m